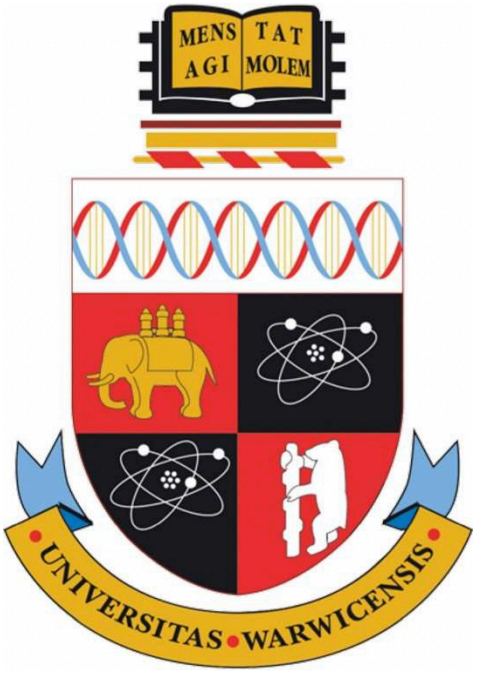

Experimental investigation on the impact of temperature during creep and stress relaxation behaviour of London clay

By

Bradley James Sheridan

A thesis submitted to the University of Warwick in fulfilment of the requirements for the degree of

Doctor of Philosophy
in
Urban Science

University of Warwick
Warwick Institute for the Science of Cities
June 2022

Table of Contents

List of Figures

List of Tables

List of symbols and acronyms

α	C_{ae}/C_c ratio
α_i	Creep coefficient
α_1	Coefficients depending on the thermal sensibility of the soil
α_2	Coefficients depending on the thermal sensibility of the soil
β	Instantaneous change in normalised void ratio
B	Skempton B value
C_α	Secondary consolidation coefficient
C_{ae}	Secondary consolidation
$C_{\alpha\varepsilon}$	Secondary consolidation in terms of strain
C_c	Compression index
C_r	Reloading index
C_s	Swelling index
C_v	coefficient of consolidation
C_c^*	Incremental compression index
Δe	Change in void ratio
$\Delta\varepsilon$	Change in strain
$\Delta\sigma$	Relaxed stresses
$\Delta\sigma_v$	Vertical net stress
Δu_d	Excess pore-water pressure accounted for possible dilation
ΔT	Temperature change
ε_a	Axial strain
ε	Strain
ξ	Residual stress ratio
ε_V^P	Plastic volumetric strain
ε_r	Pre-relaxation strain level
ε_v	Strain rate
e	Void ratio
e_{100}^*	Void ratio at 100kPa
e_{1000}^*	Void ratio at 1000kPa
e_0	Initial void ratio
e_1	Hypothetical void ratio
e_g	Void ratio corresponding to the preconsolidation
e_p	Void ratio 24 hours after the end of loading in creep tests
G_s	Specific gravity of the solids
γ	Model parameter which depends on the soil type
I_P	Plasticity index
k_0	Coefficient of lateral earth pressure at rest
κ_T	Elastic coefficient at room temperature
λ	Cam-clay compression coefficient
m	Slope of the line in $\log\dot{\varepsilon} - \log t$ space
m_c	Slope of the compression curve
P_c	Preconsolidation
P_c'	Preconsolidation stress at the current room temperature
P_{c0}'	Preconsolidation stress at the initial temperature

$\mathrm{PP_{ratio}}$	Excess pore water pressure against total strain
$\mathrm{R_\alpha}$	Coefficient of stress relaxation
$\sigma'_{\mathrm{c}}(\mathrm{T})$	Preconsolidation stress at room temperature
$\sigma'_{\mathrm{c}}(\mathrm{T_0})$	Preconsolidation stress at tested temperatures
σ_{pCRS}	CRS preconsolidation
σ_{pMSL}	MSL preconsolidation
σ_{p}	Apparent preconsolidation stress
σ'_{p}	Preconsolidation stress
σ_{s}	Residual total vertical stress
σ_{v}	Total stress
σ_{vnet}	Vertical net stress
σ'_{v}	Vertical effective stress
σ_y	Yield Stress
σ_0	Pre-relaxation total vertical stress
$\mathrm{s_{AEV}}$	Suction at air entry value
$\mathrm{s_o}$	Initial suction
t	Time
T	Temperature
$\mathrm{T_0}$	Initial temperature
u_a	Pore air pressure
u_w	Pore water pressure
u_{exc}	Excess pore-water pressure
$\mathrm{w_L}$	Liquid limit
$\mathrm{w_P}$	Plastic limit
$\mathrm{w_o}$	Water content
1D	One dimensional
ASTM	American society for testing and materials
CRS	Constant rate of strain
EOP	End of primary consolidation
HCT	High capacity tensiometers
IL	Incremental loading
IPCC	Intergovernmental Panel on Climate Change
LC	London clay
LCF	London clay formation
LPT	Linear potentiometric transducer
LVDT	Linear vertical displacement transducer
MSCRS	Multistage compression relaxation test
MSL	Multi-staged loading
NCL	Normal compression line
PSD	Particle size distribution
PWPT	Pore-water pressure transducer
SS-CRS	Single-stage compression relaxation tests
SWRC	Soil water retention curve
THM	Thermo-hydro-mechanical
VCL	Virgin compression line
WDXRF	Wavelength Dispersive X-Ray Fluorescence
XRF	X-Ray Fluorescence

Acknowledgements

Firstly, I would like to thank my supervisor, Dr Mohammad Rezania, for his encouragement and guidance throughout this PhD over the last four years. Throughout the troubles, you were on hand to provide the best solutions available. Secondly, I would like to thank Dr Meghdad Bagheri, who allowed me to use the facilities at Coventry University and was always on hand to have an insightful discussion and answer any difficult questions I may have. Thirdly, I would like to thank all the technical staff at Warwick University who provided endless amounts of support.

The financial support from the Engineering and Physical Sciences Research Council (EPSRC) is greatly acknowledged.

I want to thank all my colleagues in WISC cohort 4, who made the PhD an enjoyable time, with special thanks to Elisa Baioni, who was there whenever I needed any support. I am truly grateful to you.

My most special recognition goes to my Parents, Brother and Sister for their encouragement, patience and belief in me. Without their unconditional support, I would not have been able to complete the PhD.

Lastly, I would like to thank my Grandparents for their unconditional support and belief in me, to which this thesis is dedicated.

Declaration

I hereby declare that this dissertation is original work and has not been submitted for a degree or diploma or other qualification at any other university.

Bradley Sheridan

June 2022.

List of Publications

Journal Papers:

Sheridan et al (2022) – Temperature effect on creep and stress relaxation of clays – Under Review in Scientific Journal.

Sheridan et al (2023) – Creep and consolidation of Unsaturated Bank Station London Clay – Internal Review

COVID-19 Impact Statement

During the PhD project, the experimental programme was severely impacted due to the lockdown of the laboratory.

Due to the impact, it meant that the experimental had to be altered and trimmed down to accommodate the remaining time. The experimental program that was unable to be completed is as follows:

- Additional thermal MSL testing to further strengthen the results.
- Thermal creep testing across the 4 temperature intervals and two stress levels.
- Thermal unsaturated testing across the 4 temperature intervals and the vertical stress range of 10 – 1280 kPa.
- Thermal MSCRS testing at 0.01 mm/min strain rate.
- Thermal unsaturated CRS SS-CRS and MSCRS tests.

Abstract

The ever-growing climate problem has created a drive to ensure a sustainable future can be achieved by meeting the net zero carbon emissions requirement by 2050. Within the UK there has been an increase in record temperatures being experienced particularly since the turn of the millennium. The UK is now experiencing temperatures which are rising above 40°C and are set to continue over the next century. Therefore, it is crucial to understand why thermo-mechanical behaviour of clays is understood, as the increase in temperature causes an increase number of geomechanical problems. In addition, the temperature fluctuations surrounding energy geo-structures (ground source heating & thermo-piles) must be understood.

The study aims to assess the impact of temperature, ranging between 20 and 55 °C, on the time- and rate-dependent behaviour of London Clay. As the London clay unit lies within the warmest part of the UK and within a high urban development, it is vital we understand the impact temperature can play on this geological unit.

The thesis reports an extensive experimental program on the primary and secondary consolidation, stress relaxation, and rate-dependency. A series of conventional multi-staged loading (MSL) oedometer tests, and temperature-controlled constant rate of strain (CRS) oedometer tests were carried out on saturated and unsaturated reconstituted London clay (unit B) specimens, collected from the Bank Station project upgrade in London, UK.

The results demonstrate that temperature and suction play a pivotal role in the time- and rate-dependent behaviour of the reconstituted Bank Station London clay specimens. The main findings from the experimental program are as follows;

- An increase in temperature results in a linear decrease in apparent pre-consolidation stress (σ_p) values and in an increase in secondary consolidation ($C_{\alpha e}$) and $C_{\alpha e}/C_c$ values, especially at higher stresses. The compression index (C_c) and swelling index (C_s) parameters are less sensitive to temperature variations.
- A coupled effect of temperature and strain rate on 1D compression response was identified. At a constant temperature, the higher the strain rate, the higher the σ_p. Similarly, at a constant strain rate, the higher the temperature, the lower the σ_p.
- The dependence on stress, temperature and suction observed in the Bank Station London clay specimens rejects the hypothesis of a constant α assumed by Mesri et al. (1994).
- The coefficient of stress relaxation (R_α) values appears to be temperature- and strain rate-dependent. Furthermore, the study demonstrates that the $R_\alpha = \alpha$ relationship can be applied to the set of vertical stress and temperature appraised in the present work.

Chapter One – Introduction

1.1. Motivation

Increase in global temperatures due to exponential rises in anthropogenic (industrial) activities over the past 100+ years, which have involved unsustainable consumption rates of fossil fuels and consequently generated significant amounts of greenhouse gas emissions (e.g., CO2, SO2), it is crucial to understand the influence of global warming and its impact on sustainable development so that geotechnical engineers know the effects on the thermal and mechanical behaviour of the ground. It is particularly vital to understand the behaviour of clayey soils that are susceptible to shrinkage and swelling.

Increasing knowledge in energy geotechnics is necessary for pursuing a more stable and sustainable energy source (ground source heating & thermo-piles). As currently geothermal energy within the UK delivers less than 0.3% of the UK's annual heat demand. With an increase in the knowledge on the effects of temperature on the thermo-mechanical behaviour of soils, it will allow the UK to 'tap in' and produce even greater heat delivery to the UK's market. Indeed, the influence of the natural temperature on the geothermal structures is more significant, the latter being located in the shallow subsurface where the seasonal fluctuations in temperature alter the heat storage during different seasons. Based on the upward trend of the temperature fluctuations, the Intergovernmental Panel on Climate Change (IPCC) has stated that by 2080, a 5°C rise in temperature and a much drier summer with a 22% drop in rainfall are expected in cities, especially London (Arkell and Darch (2006); Murphy et al. (2010); Lowe et al. (2018)).

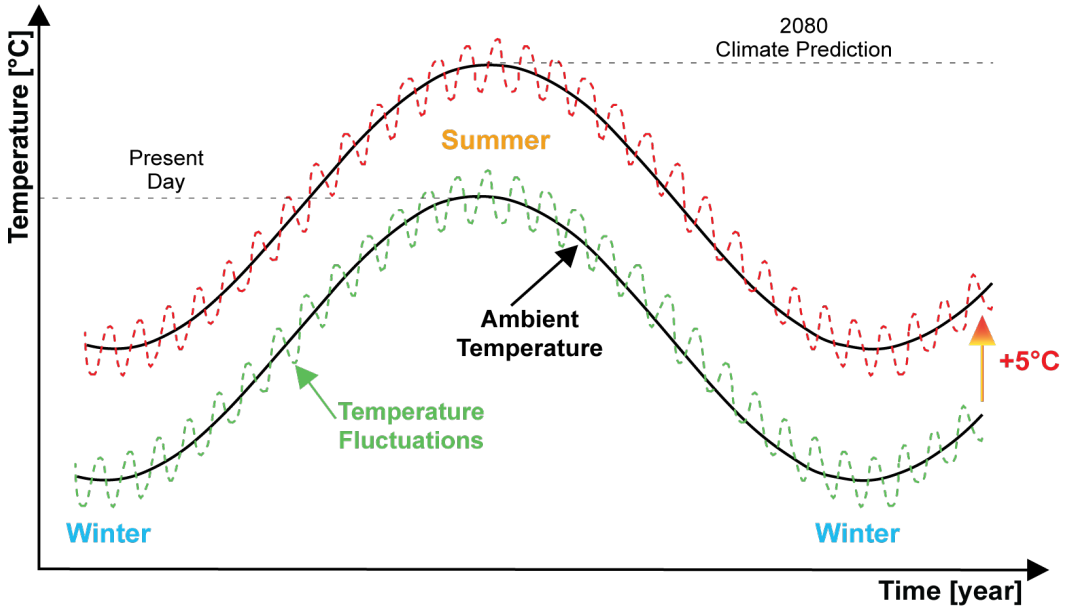

Figure 1.1 - Comparison between the current climatic temperatures and the climatic predictions by UKCP18.

Climate influence on shallow deposits can alter the hydro-mechanical properties and state variables, particularly in clay-rich deposits such as the London clay, which is susceptible to volume change due to water content variations. Alterations in climate make these clay-rich deposits a vast problem for near-surface infrastructure and buildings due to the high probability of volumetric strains (i.e. shrink-swell) (Harrison et al. (2012); Harrison et al. (2020)). It is, therefore, necessary to study the impact of these stresses on the resilience of hydro-mechanical properties, especially stress relaxation and compressibility, of reconstituted stiff clay specimens.

Experimental work has been undertaken on the time-dependent behaviour of clays when subjected to thermal alterations specifically for deep waste repository applications, where stiff clays (e.g., Boom Clay) have been used as the barrier medium (Delage et al., 2000, Sultan et al., 2002, Cui et al., 2009). These studies address the failure mechanism of clay through experimental investigations at high temperatures (> 70°C) (Hueckel and Pellegrini, 1992). However, only a limited number of creep behaviour studies at temperature ranges below 50°C have been conducted (Li et al. (2018); Jarad et al. (2019); Kaddouri et al. (2019); Lahoori et al. (2021)) and these are characteristic of shallow energy structures, such as geothermal piles and shallow depth waste repositories. Thus, the dependency of creep behaviour on small temperature changes around geo-structures remains poorly understood.

The construction of geo-structures (thermo-piles) is performed by multiple stages of loading, with the soil being subjected to varying effects of strain at each stage. The strain encountered at each stage can be determined to analyse the creep behaviour within the structure and their response to assess the impact of strain rate on the performance of the structures and how they perform under differing climatic conditions. Furthermore, during the construction phases, the soil body contains a decreasing stress body over time at a slow strain rate which can be determined as stress relaxation. The stress relaxation in this statement is related to the construction phase reaching the required requirements of the construction build (e.g., short-term undrained behaviour in an open excavation prior to the completion of the structure). The relationship between creep and stress relaxation under varying strain rates and thermal conditions is limited.

The limited information regarding the thermo-mechanical behaviour of stiff clays in the creep and relaxation phase is poorly understood. The present study is geared to improve the knowledge of the effects of temperature alterations on the viscous response of clays, such as London clay, and to provide a better understanding of the construction and maintenance of geo-structures subjected to climate change improvement in understanding temperature alterations on the viscous response of clays such as London clay. This will create a better understanding of the construction and maintenance of geo-structures subjected to climate change. As a result of this research study, it would hope to provide commercial prospects which would help to reduce costs on infrastructure that are affected by ground movement due to temperature variations.

1.2. Aims and Objectives

The main aim of this study is to investigate the influence of temperature (between 20 to 55°C) on time- and rate-dependent behaviour of stiff overconsolidated (reconstituted) London Clay. In addition, the effect of suction on time- and rate-

dependent behaviour is analysed. To achieve these aims, the following objectives required fulfilment:

- To investigate the effect of soil suction on the primary and secondary consolidation of reconstituted London clay in oedometric conditions;
- To examine effect of temperature on the primary and secondary consolidation of reconstituted London clay in oedometric conditions;
- To investigate the coupled effects of temperature and strain rate on the stress-strain response of reconstituted London clay;
- To examine the coupled effects of temperature and strain rate on the one-dimensional (1D) stress relaxation behaviour of reconstituted London clay.

1.3. Thesis Layout

Chapter *One* – Introduces the conducted research program.

Chapter *Two* – Presents a literature review of the general background on thermal behaviour of soils from experimental studies, as well as a review of previous experimental work on London clay specimens focusing on the effects of temperature and suction on primary consolidation, creep, stress relaxation, and the rate-dependency behaviour.

Chapter Three – Presents the experimental methodology, and the calibration and verification of the testing equipment. Also, a detailed description of the soil employed in the experimental tests is provided.

Chapter Four – Is spilt into two sections and discusses: (1) the outcome of primary and secondary consolidation of reconstituted London clay, in saturated and unsaturated states. The influence of suction on the time-dependent stress-strain behaviour is examined. (2) presents the outcome of primary and secondary

consolidation of reconstituted London clay under a saturated state. The time-dependent and stress-strain behaviour under thermal conditions is here analysed.

Chapter *Five* – Investigates the coupled effects of temperature and stress rate on stress-strain and viscous behaviour of clays. The coupled effects of temperature and strain rate on the stress-strain response of reconstituted London clay is examined in CRS compression and relaxation tests.

Chapter Six – Provides a discussion on the compressibility behaviour of oedometer tests; the influence of temperature on creep and stress relaxation behaviour; and discusses the applications of the research.

Chapter *Severn* – Summaries the main experimental findings from this study and provides recommendations for future research.

Chapter Two – Literature Review

2.1. Introduction

This literature review aims to provide information regarding experimental studies completed on the London clay formation (LCF) in a saturated and unsaturated state, with aspects linking to the time- and rate-dependent behaviour of clays. The literature presented in this thesis is structured into two main sections: 1) an overview of published literature concerning the thermo-mechanical behaviour of soils, and 2) an overview of laboratory and experimental work on saturated and unsaturated clays, with particular attention devoted to the results and findings on London clay specimens.

Firstly, a brief overview of the UK's ground source heating market was reviewed. In 2008, the UK government introduced the Climate Change Act which aimed for 80% greenhouse gas reduction by 2050. However, the goal of this act in recent years has been updated by the UK government to achieve a 100% reduction in greenhouse gas emissions by introducing the NetZero strategy. The UK today contains roughly 43,700 ground source heating pumps according to the International Energy Agency. These along with the other 'sustainable' energy sources (e.g., deep geothermal and mine geothermal schemes) within the UK generate around 1,330 GWh per year, which only makes up 0.3% of the UK's annual heat demand. To meet the demands of the NetZero strategy by 2050 the UK's Climate Change Committee predicts that 20% of UK heat must come from 'sustainable' energy sources, such as ground source heat pumps (Committee on Climate Change, 2019).

In order to achieve the goals, the UK government intend to install 600,000 ground source heating pumps each year by 2028 (UK Government, 2020). However, the high installation rate of ground source heating pumps can result in temperature changes within the subsurface and may cause environmental effects. For example, the installation of these energy geo-structures can allow for local temperature changes of 4 to 10°C (Casasso and Sethi, 2019). The local temperature change in the

subsurface may raise many problems within a highly densely populated urban area such as London. As an increase of ground source heating pumps within small proximity of each other may result in alteration of the thermo-mechanical behaviour of the subsurface (i.e., London Clay Formation). Hence, it is vital to understand how the London Clay formation behaves due to an increase in temperature.

2.2. Thermo-Mechanical Behaviour of Soils

The influence of temperature on the thermo-mechanical behaviour of soils plays a crucial role in understanding its impact on the ability to create a sustainable and efficient design model for geotechnical engineers. Construction activities in either deep (e.g., radioactive waste repositories) or shallow excavations (e.g., geothermal resources) subject soils to temperatures that are different to what they have had in the past (Bourne-Webb et al., 2009, Loveridge and Powrie, 2013, Favero, 2016, Li et al., 2018, Kaddouri et al., 2019, Lahoori et al., 2021). Hence, many laboratory-based experimental thermal studies have been conducted use temperatures that are different to the temperatures for the soils when they are in situ (Campanella and Mitchell, 1968).

During the temperature change of saturated clays, the main two components that alter are the pore-fluid and the soil particle. When clay is subject to heating, there is generally an increase in excess pore pressure due to the difference in the thermal expansion coefficient of the pore-fluid and particle matter within the clays (Li, 2019). The amount of pore pressure change is dependent on the hydraulic conductivity, drainage condition and the rate of heating. Within clays, they contain a structure and fabric defined by particle alignment, compaction, inter-particle bonding such as face-to-face, whose nature are dependent on age and geological mode of formation and are easily influenced by environmental change. The alteration of bonding within the clays as a result of environmental changes (i.e., heating) can cause rapid reconfiguration of clay particles and interparticle bonding.

There have been many experimental studies completed on the effect of temperature on soils on various samples. The majority of the testing completed have involved oedometer tests (Towhata et al., 1993; Abuel-Naga et al., 2007; Favero, 2016; Li et al., 2018; Kaddouri et al., 2019; Lahoori et al., 2021), CRS tests (Tidfors and Sällfors, 1989; Moritz, 1995; Marques et al., 2004; Jarad, 2016; Jarad et al., 2019) and triaxial tests (Sultan et al., 2002; Cekerevac and Laloui, 2004; Trani, 2010; Martinez Calonge, 2017) so that the effects of temperature on basic soil parameters (e.g., compression index, swelling index and apparent pre-consolidation stress) can be quantified. The published literature provides conclusive evidence of trends with temperature increase, such as apparent pre-consolidation stress decreasing. However, such observations are contradictory and inconclusive (e.g., temperature affecting the compression index), which indicates that the mechanical behaviour of soils under thermal loading (heating) appears not to be fully understood.

The following topics within this section discuss the previous studies on thermo-mechanical behaviour of soils and how the primary and secondary consolidation are affected by temperature.

2.2.1. Overview of Thermo-Mechanical Laboratory Tests

The majority of the research carried out involving temperature-controlled laboratory tests have used high-temperature ranges to study the capability of stiff, deep clays as potential sites for radioactive waste repositories (Baldi et al., 1988, Favero, 2016) and how temperature affects the behaviour of the clay (Cekerevac and Laloui, 2004)(Table 2.1).

The temperature testing of soils within a laboratory environment is split into two types: drained conditions, which have open water boundaries that allow water to enter or leave the samples when undergoing temperature change (Campanella and Mitchell, 1968, Delage et al., 2000, Sultan et al., 2002, Abuel-Naga et al., 2007, Martinez Calonge, 2017); or undrained conditions, prevent the flow of water in or

out the sample during temperature change (Hueckel and Pellegrini, 1992, Abuel-Naga et al., 2007). In both these types of testing, the pore fluid usually started at room temperature and was kept between the freezing and boiling point of water to avoid a phase change. Most researchers have used a water bath method to ensure that the water temperature could be controlled by either heating the water directly or using an external source (e.g., a water pump) to maintain the target temperature (Figure 2.1).

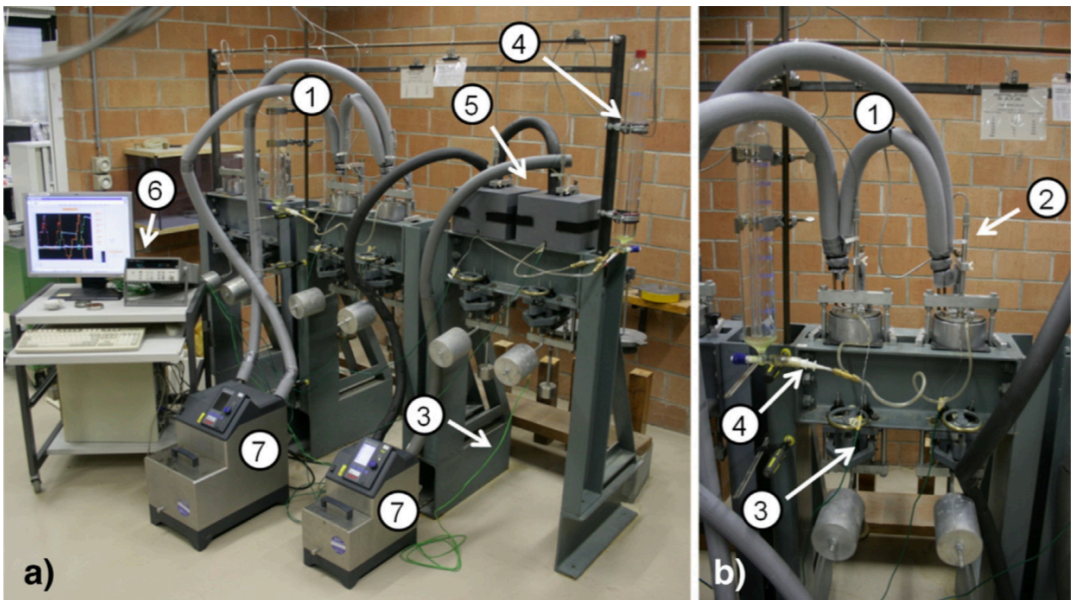

Figure 2.1 - Experimental set up from Di Donna and Laloui (2015). Illustrates an external heating source as the pumps are used to circulate the temperature. 1) Tubes with circulating water at the desired temperature; 2) LVDTs; 3) Thermocouples; 4) Water supplier; 5) Insulation; 6) Data logger; 7) Heater.

From the available studies (see table 2.1), it was observed that during the testing phase of the samples, there is only one variable at a time so that researchers can identify the temperature-dependent response to the soil. The mechanical and thermal loading stages are used separately to identify the influence of temperature on each stage so they can be easily distinguished.

Table 2.1 - Select overview of experimental tests on the thermo-mechanical behaviour of clays.

Researchers	Clay type	Temperature (°C)	Testing equipment
Gupta (1964)	Haney clay	20 - 45	Triaxial
Green (1969)	Bryce clay	5 – 50	Oedometer
Baldi et al. (1988)	Boom clay, Kaolin clay, Pontida clay	20 – 200	Triaxial
Eriksson (1989)	Suphide rich silty clays	5 – 55	Oedometer
Tidfors and Sällfors (1989)	Five Swedish clays (Bäckebol, Upplands, Värnamo, Välen, Gunisle)	25 – 55	CRS & Oedometer
Hueckel and Baldi (1990)	Boom clay, Pasquasia clay, Pontida clay	18 – 115	Triaxial
Burghignoli et al. (1992)	Todi clay, Fiumicino clay, Bologna clay	18 - 54	Triaxial
Towhata et al. (1993)	MC clay, Bentonite	20 – 90	Oedometer
Moritz (1995)	Linköping clay	8 – 70	CRS & Triaxial
De Bruyn and Thimus (1996)	Boom clay	20 – 110	Triaxial
Tanaka et al. (1997)	Illitic clay	28 – 100	Triaxial
Delage et al. (2000)	Boom clay	20 – 100	Triaxial
Burghignoli et al. (2000)	Todi clay, Fumicino clay, Bologna clay	20 – 60	Triaxial
Sultan et al. (2002)	Boom clay	20 – 100	Triaxial
Cekerevac et al. (2002)	CL clay	22 – 90	Triaxial
Marques et al. (2004)	St-Roch-de-l'Achigan clay	10 – 50	CRS, Oedometer & Triaxial
Cekerevac and Laloui (2004)	CM clay	22 – 90	Triaxial
Abuel-Naga et al. (2007)	Bangkok clay	25 – 90	Triaxial
Cui et al. (2009)	Boom clay	25 – 80	Triaxial
Trani (2010)	Bangkok clay	25 – 90	Triaxial
Tsutsumi and Tanaka (2012)	Kasaoka clay, OsakaMa12 clay, Louiseville clay	10 – 50	CRS
Di Donna and Laloui (2015)	Geneva clay	5 – 60	Oedometer
Favero (2016)	Opalinus clay	23.5 – 80	Oedometer
Martinez Calonge (2017)	London clay	20 – 70	Triaxial
Li et al. (2018)	Utby clay	5 – 25	Oedometer
Jarad et al. (2019)	Compacted clayey soil	5 – 70	CRS & Oedometer
Kaddouri et al. (2019)	Compacted clayey soil	5 – 70	Oedometer
Lahoori et al. (2021)	Compacted clayey soil	5 – 50	Oedometer

2.2.2. Effect of Temperature on the Primary Consolidation

The current section discusses the influence of temperature on the primary consolidation (short term) parameters such as compression index (C_c), swelling index (C_s), and apparent preconsolidation stress (σ_p).

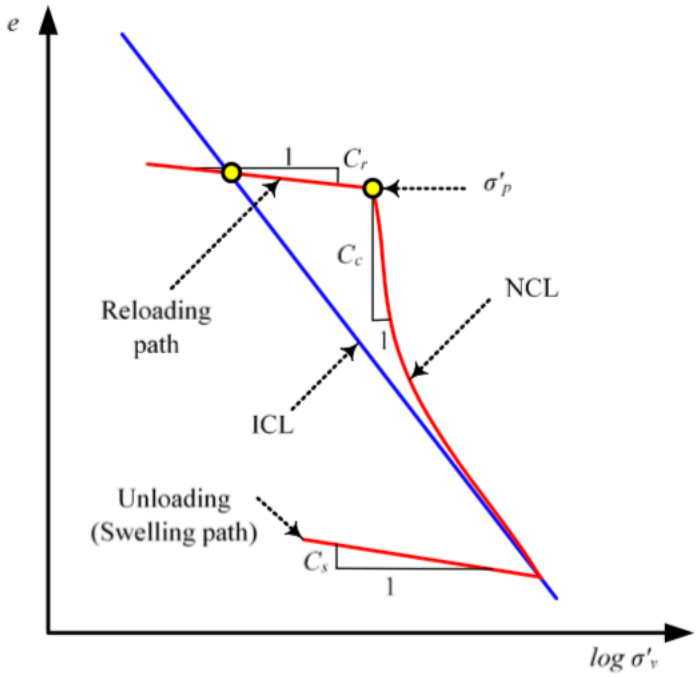

Figure 2.2 - Schematic compression curve (Bagheri, 2018).

Influence of Temperature on the Apparent Preconsolidation Stress

The yield stress (σ_y) or σ_p represents the transition from elastic to plastic behaviour in oedometric conditions and can be termed the pseudo-elastic limit (Shariatmadari and Saeidijam, 2011). The influence of temperature on the σ_p has been investigated by numerous researchers, whereby it has generally proven that as temperature increases, it causes a decrease in σ_p (Sultan et al., 2002, Marques et al., 2004, Laloui et al., 2008, Hong et al., 2013, Jarad, 2016, Kaddouri et al., 2019, Lahoori et al., 2021) due to thermal softening. It was observed in Cekerevac and Laloui (2004) study on saturated reconstituted CM clay that when using a triaxial cell at three different

temperatures (22, 60, 90°C), the σ_p decreases by an average of 4 kPa/10°C as temperature increase. Furthermore, Kaddouri et al. (2019) found that an increase in temperature from 5 to 70°C decreased σ_p linearly by 14.9% (Figure 2.3).

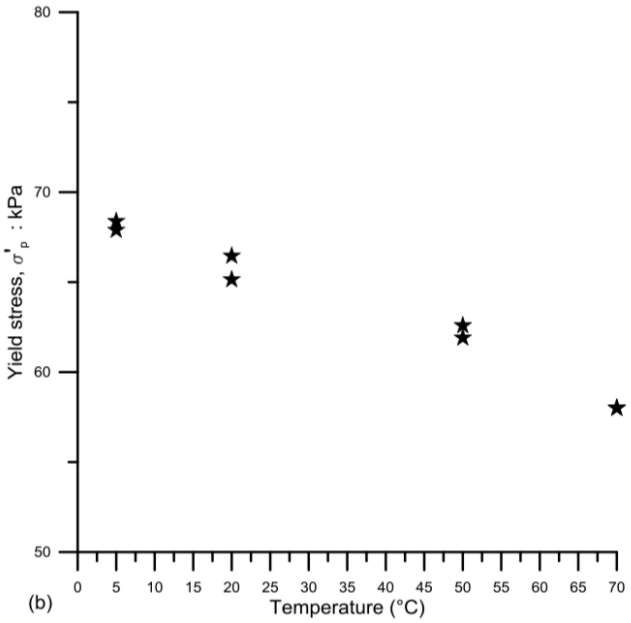

Figure 2.3 - Decrease of the apparent preconsolidation with an increase of temperature during oedometer testing from Kaddouri et al. (2019).

Conversely, very few studies have found temperature to increase the σ_p. For example, Mon et al. (2014) found that when testing Kaolin clay (ASP 100 clays), there was an increase of σ_p by a factor of 2.08 as the temperature increased from 5 to 40°C. They linked the increase in σ_p due to the samples containing a high initial void ratio and suggested that σ_p is dependent on the testing technique. Furthermore, Abuel-Naga et al. (2007) found that the thermal evolution of the soft Bangkok clay appeared to be temperature independent when evaluating the effect of temperature on the σ_p (figure 2.4).

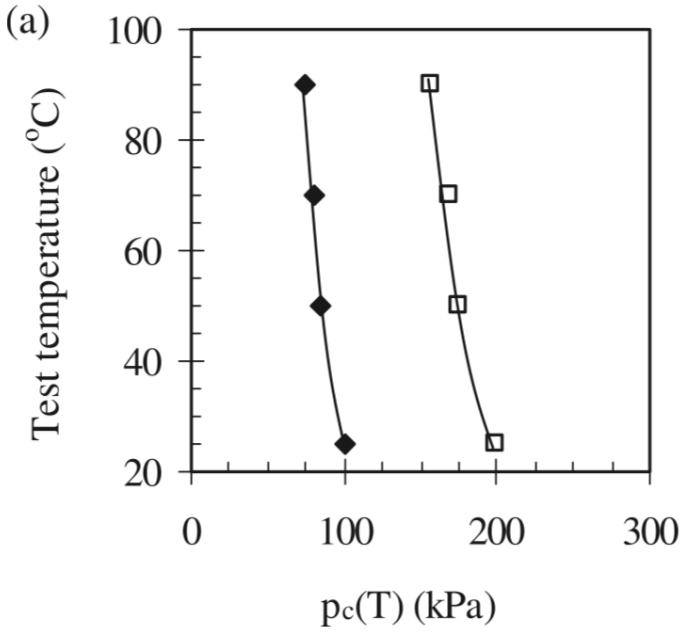

Figure 2.4 – The apparent preconsolidation stress of soft Bangkok clay tested at 100 & 200 kPa ambient pressure by Abuel-Naga et al. (2007).

Several relationships in the literature have been proposed to describe the evolution of apparent preconsolidation as a function of temperature (e.g., Sultan et al. (2002); Cekerevac and Laloui (2004); Abuel-Naga et al. (2005)). The model for defining the evolution of σ_p with temperature was proposed by Hueckel and Baldi (1990), which was an extension of the hardening law of the Cam-clay model, as follows:

$$P_c' = P_{c0}' \exp\left(\frac{1}{\lambda - \kappa_T}\left[e_1 - e_g + (1 + e_0)\varepsilon_V^P\right]\right) + 2(\alpha_1 \Delta T + \alpha_2 |\Delta T| \Delta T) \quad (1)$$

Where P_c' is the preconsolidation stress at the current room temperature T, P_{c0}' is the preconsolidation stress at the initial temperature T_0, ε_V^P is the plastic volumetric strain, ΔT is the temperature change, λ is the Cam-clay compression coefficient, κ_T is the elastic coefficient at room temperature, e_0 is the initial void ratio, e_1 is a hypothetical void ratio defined by P_{c0}' and initial temperature T_0, e_g is the void ratio corresponding to the preconsolidation P_c, α_1 and α_2 are the coefficients depending on the thermal sensibility of the soil (express the decrease of P_c with increasing T). Further extensions of the Cam-clay model have been proposed by Hueckel and Borsetto (1990). Additionally, the relationship between the σ_p and temperature can

be presumed to be either linear (equation 2) (Boudali, 1994) or non-linear (equation 3) (Moritz, 1995, Cekerevac et al., 2002). The temperature-dependency behaviour of soils can be presented by a linear (equation 2) or a non-linear (equation 3) equation which illustrate the relationship between σ_p and temperature:

$$\frac{\sigma_c'(T)}{\sigma_c'(T_0)} = \left[\frac{T_0}{T}\right]^{\alpha} \tag{2}$$

$$\frac{\sigma_c'(T)}{\sigma_c'(T_0)} = 1 - \gamma\left[\log\left(\frac{T}{T_0}\right)\right] \tag{3}$$

Where $\sigma_c'(T)$ and $\sigma_c'(T_0)$ are the preconsolidation stresses at room temperature and tested temperature, α and γ are the model parameters which depend on the soil type respectively.

The relationship between σ_p and temperature during constant rate of strain (CRS) tests follows the trend analysed by conventional oedometer tests, that an increase in temperature causes a decrease in σ_p (Boudali, 1994, Jarad et al., 2019). The experimental work completed on CRS tests illustrates a unique behaviour: the strain rate-preconsolidation stress relationship is temperature dependent, but the slopes of the strain rate-preconsolidation stress relationship at different temperatures are parallel (figure 2.5).

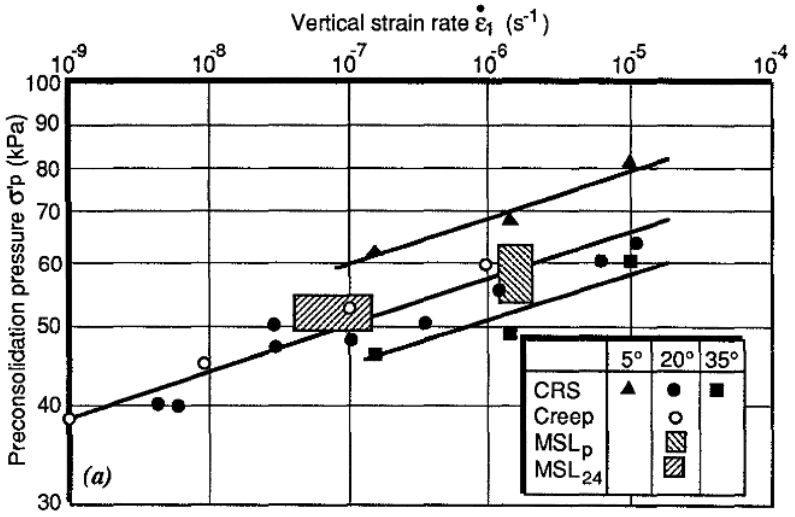

Figure 2.5 - The linear relationship between the strain rate-preconsolidation stress at different temperatures on Berthierville clay (Boudali, 1994).

Boudali (1994), who performed CRS tests on Berthierville clay at different strain rates and temperatures, found the strain rate-preconsolidation stress relationship. Based on the findings found in figure 2.5, Boudali (1994) extended the viscous behaviour model proposed by Leroueil et al. (1985) so that the effect of temperature can be included:

$$\sigma_p' = f(\dot{\varepsilon}_1, T) \tag{4}$$

$$\sigma_v'/\sigma_p'\,(\dot{\varepsilon}_1, T) = g(\varepsilon_1) \tag{5}$$

Further thermo-elasto-viscoplastic constitutive models were generated to represent the behaviour of clays at different temperatures and strain rates. These models include Yashima et al. (1998) and Laloui et al. (2008), who validated the constitutive model by using the experimental data provided on Berthierville clay by Boudali (1994). Similar to the finding of Boudali (1994), Marques et al. (2004) also found a strain rate-preconsolidation stress relationship during CRS tests at different temperatures during the testing of St-Roch-De-l'Achigan clay (figure 2.6). However, it can be seen at a higher temperature and faster strain-rate, the data does not appear to fit a linearly increasing trend (figure 2.6) and appears to sit close to the lower temperature values of σ_p.

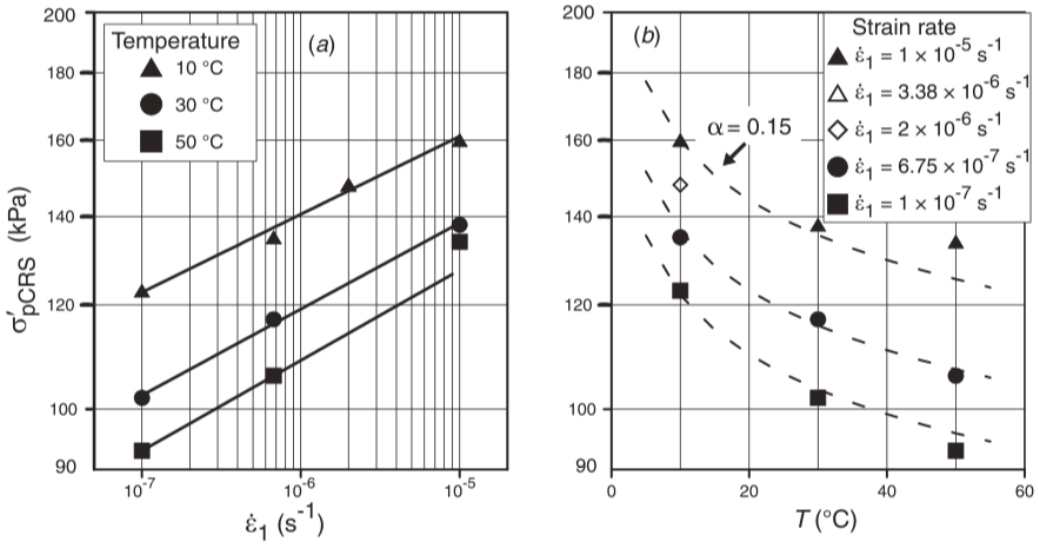

Figure 2.6 - Influence of strain rate and temperature on the preconsolidation stress of St-Roch-de-l'Achigan clay from Marques et al. (2004).

Influence of Temperature on the Compressibility Parameters

Many researchers have studied the effect of temperature on the compressibility parameters (e.g., C_c and C_s), with the observations varying between studies. Understanding the behaviour of the soil plays a crucial role in developing a sufficient engineering model. Most compression tests are completed in drained conditions and illustrate that an increase in temperature causes a shift to the left in the compression curve (figure 2.7) (Baldi et al., 1988, Abuel-Naga et al., 2007, Kaddouri et al., 2019, Lahoori et al., 2021) which indicates thermal softening as the fabric of the pore-structure alter due to water properties being dependent upon temperature. However, it was found by Tsutsumi and Tanaka (2012) and Jarad et al. (2019) during CRS tests that applying a low strain rate on the samples and increasing temperature causes the compression curve to shift to the right slightly as an increase in temperature causes the structure of the clays to be developed more quickly due to the water properties being dependent on temperature, which causes the water layer on the clay particle surfaces to be reduced and create a structure that becomes much more resistant to loading (Tsutsumi and Tanaka, 2012).

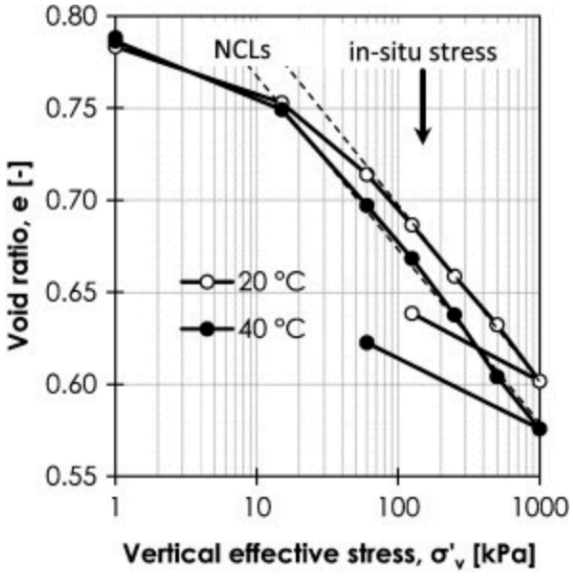

Figure 2.7 - Experimental compression curves from oedometer tests on soil samples obtained near Geneva (Di Donna and Laloui, 2015).

Furthermore, many experimental studies reveal that the compression index (C_c) and swelling index (C_s) experience minimal changes as temperature increases. For example, the study by Lahoori et al. (2021) on compacted clayey soil obtained values of C_c to increase by 0.005 and values of C_s to increase by 0.003 when increasing the temperature from 5 to 50°C. In the study of Abuel-Naga et al. (2007), the C_c was temperature independent, but the C_s was temperature-dependent. However, the study of Trani (2010), on the effect of temperature on soft Bangkok clay, contradicted findings made by Abuel-Naga et al. (2007), which further contradicted observations made by Jarad et al. (2019) indicating that the C_c and C_s would alter slightly with an increase in temperature and variation in strain rate.

2.2.3. Effect of Temperature on Secondary Consolidation Behaviour

Knowledge regarding the influence of temperature on the creep behaviour of soils is still limited, with only a small amount of laboratory results available (Burghignoli et al., 1992, Towhata et al., 1993, Moritz, 1995, Burghignoli et al., 2000, Zhang et al., 2007, Cui et al., 2009, Di Donna and Laloui, 2015, Favero, 2016, Li et al., 2018, Jarad et al., 2019, Kaddouri et al., 2019). Based on the findings in the literature, the consensus is that an increase in temperature causes an increase in creep behaviour.

For example, Li et al. (2018) studied the influence of temperature on intact and reconstituted sensitive Utby clay samples. It was reported that within the temperature range (5 to 25°C) the intact samples were very sensitive to temperature change, as the creep behaviour of the samples increased with temperature, especially at stresses close to σ_p. However, for reconstituted samples, the change in the creep behaviour as temperature increased was not noticeable. Furthermore, the study revealed that the reconstituted samples under high-stress states and increasing temperature did not provide clear and concise evidence of the creep behaviour (figure 2.8).

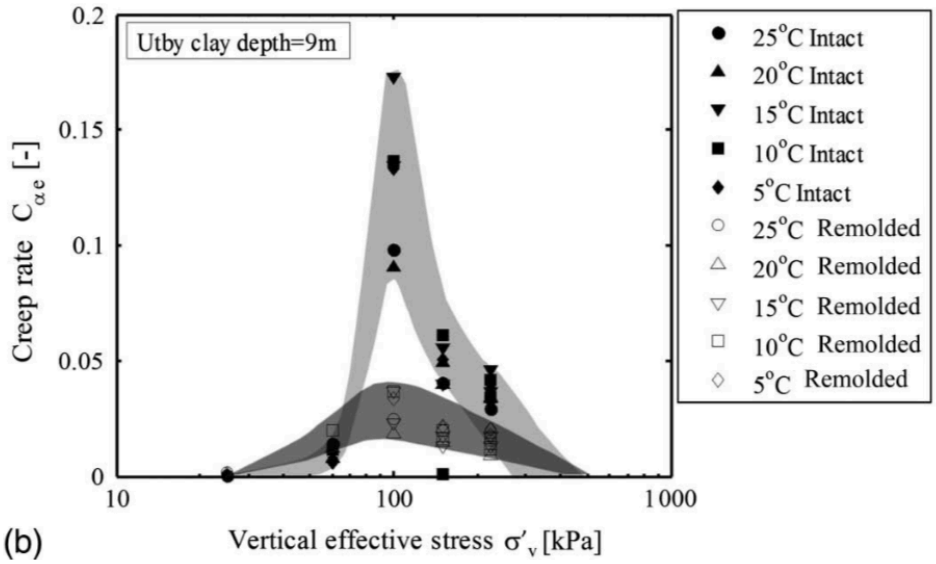

Figure 2.8 - The creep behaviour of intact and reconstituted Utby clay samples extracted from 9m depth analysing the influence of temperature and stress (Li et al., 2018).

Li et al. (2018) stated that the difference in creep behaviour between the intact and reconstituted samples is due to the size of the pores between the aggregates and the bonds between the solid particles, which no longer exist in the reconstituted samples. Similar findings by Green (1969) and Moritz (1995) found that creep behaviour was influenced at lower stresses as temperature increased. However, Kaddouri et al. (2019) found the influence of temperature on the creep behaviour to be greater at higher stresses, as the creep behaviour of the compacted clayey soil increased by 13.6% as temperature increased from 5 to 70°C at the 1280 kPa stress interval (figure 2.9).

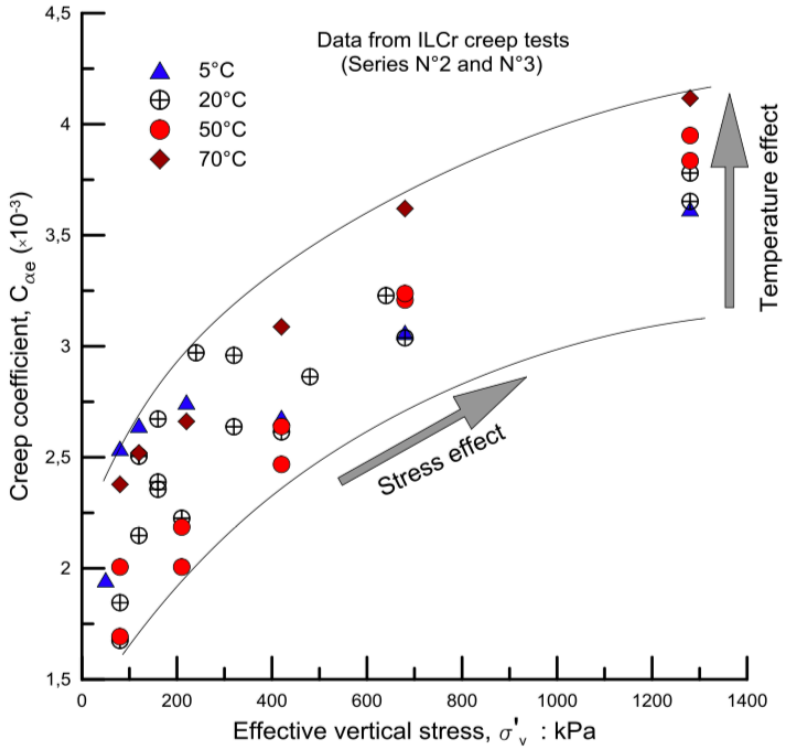

Figure 2.9 - Secondary compression behaviour of compacted clayey soil at different temperatures (Kaddouri et al., 2019).

In the research studies that have found the creep behaviour to be temperature-dependent, creep accelerated at high temperatures due to two mechanisms: 1) reduction of pore-water viscosity, which reduces the frictional resistance between particles, and 2) thermally induced viscosity reduction which results in shrinkage due to the release of pore-water (Zhang et al., 2007). Conversely, research completed by Di Donna and Laloui (2015) found that the creep behaviour for the S3 sample (Geneva clay) appeared to be temperature independent as the temperature increased from 20 to 60°C. Boudali (1994) and Marques et al. (2004) have found the finding of temperature independency in the creep behaviour.

2.3. Laboratory and Experimental Testing on Clays

This part of the literature review will present a brief overview of laboratory tests completed on saturated and unsaturated samples. It will discuss the results of oedometer and CRS testing with references to the London clay Formation.

2.3.1. Oedometer Testing

Many studies within the literature have used conventional oedometer cells to test saturated specimens. However, to test unsaturated specimens, custom-made oedometer cells are usually required to ensure suction can be analysed, as Monroy et al. (2008) and Rezania et al. (2020) used specialised oedometers equipped with HCTs to analyse the suction response of London clay specimens during a series of 1D compressibility tests.

2.3.1.1. Primary Consolidation Behaviour

Investigation of one-dimensional (1D) compressibility is the most common use of oedometers and is completed in both saturated and unsaturated soils and studied through incremental loading (IL) of the specimens. The results are usually plotted in a semi-logarithmic plot with void ratio (e) against the log of vertical effective stress (σ_v') displayed. The linear relationship that the two parameters display when undergoing compression for the first time is to travel along either the normal compression line (NCL) or the virgin compression line (VCL). Reconstituted specimens permanently lie within the virgin compression range. The soils travel along the two lines mentioned during the loading of the soil, which displays a gradient known as the reloading index (C_r) until the σ_p has been reached and begins plastic straining represented by a steep slope (C_c) of the NCL. The soil eventually re-joins the NCL line. When unloading the soil, it displays a recovery line (C_s) due to swelling and recovering some strains. Conversely, highly structured clays may exhibit steeper slopes in unloading due to the destructuration of inter-particle bonds (Mataic, 2016)

However, unsaturated soils are more complex than that saturated soils due to suction. During the soil loading, the suction increases, which causes an increase in σ_p, known as suction hardening; this causes the compression curves of the soils to shift right (Wheeler and Sivakumar, 1995). Suction also influences the shape and location of the curves during unsaturated testing. During loading of the soil, suction

decreases and increases during unloading; this is seen in the study of Rezania et al. (2020).

The soils compressibility during the primary consolidation stage can be defined by a series of indices are generated from the $e - \log \sigma_v'$ plot.

Table 2.2 – Determination of the compression indices.

Indices	Equation
Reloading Index	$C_r = \frac{\Delta e}{\Delta \log(\sigma_v')}$
Compression Index	$C_c = \frac{\Delta e}{\Delta \log(\sigma_v')}$
Swelling (unloading) Index	$C_s = \frac{\Delta e}{\Delta \log(\sigma_v')}$

Soil Structure

The general definitions and influences of soil structure in this section is defined as "structure" which is a very broad term to interpret the mechanical characteristics of clays. Throughout the literature, the mechanical behaviour of soils is strongly affected by the structure. With the structure being general in defining soils, Mitchell (1976) quoted that soil to contain the structure of interparticle bonding and fabric and applied to the general soil group. Furthermore, the definition by Burland (1990) is to narrow the term to a factor to cause a variation of the mechanical behaviour of soils from intrinsic properties. The intrinsic properties of natural clays (undisturbed) and reconstituted clays differ with natural clays adherent to the in-situ properties, whereas reconstituted clays are independent of the natural states. Furthermore, Burland (1990) suggested soil structure should be determined by a parameter known as void index (I_v);

$$I_v = \frac{e - e^*_{100}}{e^*_{100} - e^*_{1000}} = \frac{e - e^*_{100}}{C^*_c} \tag{6}$$

Where e^*_{100} and e^*_{1000} are the void ratios σ'_v = 100 and 1000 kPa respectively.

Burland (1990) further reported the term "structure" coupled with the combination of "fabric", the arrangement of soil particles and pore spaces, and the "bonding", the interparticle forces which are of a frictional nature. As reported in the literature, the overall effect of soil structure on the engineering characteristics is shown to be significant importance. Further, highlighted in this section is the depositional processes of clays associated with the mineralogy.

Mineralogy

Clay minerals are a group of hydrous aluminium phyllosilicates which are defined by a 2D sheet structure that contain particles which are < 4μm in size and are fine-grained. The formation of these minerals is formed commonly by the chemical decomposition of feldspar, and they are a product of chemical weathering. The basic structure of clay minerals is silicon-oxygen tetrahedral and aluminium-hydroxyl octahedrons. Formation of the silica sheet structure is by the combination of tetrahedral units which create an electrically negative charge, whereas, the octahedral units create a sheet structure termed gibbsite that is formed by a neutral electrical charge. By the creation of these chemically bonded sheets, these create layers which illustrate the clay mineral particles. The three main clay groups are Kaolinite, illite, and Montmorillonite, which all display their properties. With the negatively charged surfaces with silica sheets in presence attract polar water molecules within the pore space, and this influences the plasticity of the mineral. Majority of the clay minerals present high specific surfaces due to the "plate-like" shapes, and with this shape, it increases the surface forces on the clay and results in increase incompressibility.

Interparticle Forces

The result of a combination of all the interparticle forces result from "bonding", and these forces are not purely frictional nature. These can be either electrostatic or

electromagnetic nature (Leong et al., 2012), within the water layer of the soil, it displays Van der Waal forces and viscous stresses.

The full geological life of each soil gives rise to a phenom known as physiochemical equilibrium and occurs between each soil particle. Factors that allow for the physiochemical equilibrium is due to mineralogy, electrostatic and magnetic interactions between ion concentration and water chemistry during the deposition of soils. To cause significant changes in the bonding of clays, then either externally induced variations of the above factors or development of chemical reactions will have to take place. Depositional and post-depositional periods cause the interparticle forces to gain more strength and resistance to yielding.

Anisotropy

The depositional conditions of the clays define the equilibrium of particles and contacts which decide the response of stresses and strains within the soil. A dependent process is the particle deposition and compaction as these are via gravity. Therefore, the arrangement and contacts are anisotropic. 'Anisotropic' determines the way that the soil response to differing stress application and direction.

The anisotropy that arises from the geological history of the soil deposits is 'inherent' (Casagrande and Carrillo, 1944; Arthur and Menzies, 1972). The structure of soils give rise to inherent or structural anisotropy which is formed by geological processes, so the fabric within bedded and laminated soils, and interparticle contacts. Furthermore, the geological processes can give rise to 'cross-anisotropy' which is defined by the material properties displaying identical horizontal directions but differ in the vertical direction. Another known fabric anisotropy is 'plastic strain-induced' which is formed by post-depositional engineering work and plastic straining which alter the internal structure of the soils that allow for this anisotropy to develop.

2.3.1.2. Secondary Consolidation Behaviour

During the secondary consolidation of soils, the rearrangement of soil particles is reconfigured such that they become more stable and deform under a constant effective stress state. The soil's viscous properties control the rate of deformation in this stage, as there is an increase in water content, plasticity, and stress level during creep. Creep can be characterised for all soils in a qualitative similar manner irrespectively of the soil structure, degree of saturation, mineralogy and grain size. During experimental compression tests, creep must be performed under constant effective stress. However, obtaining the same effective stress throughout the testing phase is difficult. As a typical example of the difficulties within undrained triaxial creep tests, pore-water pressure changes will cause changes in effective stress. The literature further states that during drained triaxial creep tests, if the load is not corrected for changes in the cross-sectional area of a specimen can alter the effective stress applied.

Creep behaviour can be defined by three stages: primary creep, this stage is mainly associated with the dissipation of excess pore-water pressure, in which, over time, the strain rate decreases rapidly. After the end of primary consolidation (EOP), the soil's deformation decreases at a reduced rate and is termed the secondary creep. The soil skeleton viscosity controls this stage; however, it has been reported by Hicher (1985) that this stage is rarely observed. The final stage is termed tertiary creep. This is characterised by the acceleration of creep strain that eventually leads to failure, termed creep rupture. These three stages of creep behaviour are the deformations associated with the loading stage of the specimens.

Buisman (1936) stated that a semi-logarithmic law could approximate creep strain with time to quantify the observed creep behaviour further. During long term 1D compressibility tests, the relationship between creep strain and the logarithm of time is usually linear; hence after the EOP, a linear line is fitted to display the conventional secondary consolidation coefficient (C_α) or the secondary compression index and is calculated by:

$$C_\alpha = \frac{\Delta e}{\Delta \log t} \tag{7}$$

$$C_{\alpha\varepsilon} = \frac{\Delta \varepsilon}{\Delta \log t} \tag{8}$$

Where C_α and $C_{\alpha\varepsilon}$ are the coefficients of secondary compression in terms of e and ε, respectively, with Δe and $\Delta \varepsilon$ being the changes in void ratio and vertical strain respectively, under constant effective stress, the value of C_α is derived from incremental load 24-hour oedometer tests. It is highly dependent on the current stress level of the preconsolidation stresses. Conversely, several studies have been conducted in the literature relating to the assumption of constant C_α with time, whereas many authors have found that C_α is dependent on many factors. Authors such as Mesri and Castro (1987) and Mesri and Godlewski (1977) found that the ratio C_α / C_c stays approximately constant with the change in effective stress, with the ratio being defined as the slope of the curve in $\log \dot{\varepsilon} - \log \sigma'_p$ space:

$$\alpha = \frac{C_\alpha}{C_c} = \frac{\Delta \log \dot{\varepsilon}}{\Delta \log \sigma'_p} \tag{9}$$

With inorganic clays and silts having a ratio of 0.04±0.01, organic clays and silts have a higher ratio of 0.05±0.01, according to Mesri et al. (1994).

It has also been stated that the relationship between creep strain and the logarithm of time is non-linear with either increases or decreases in gradients, as Mitchell et al. (1997) found this to be true in triaxial creep testing. Though, creep behaviour can obtain a linear relationship between the logarithm of creep rate and logarithm of time (Singh and Mitchell, 1969, Vaid and Campanella, 1977, Tavenas et al., 1978). To characterise the creep behaviour, Singh and Mitchell (1969) introduced the parameter (m) as the slope of the line in $\log \dot{\varepsilon} - \log t$ space, which is defined by:

$$m = -\frac{\Delta \log \dot{\varepsilon}}{\Delta \log t} \tag{10}$$

As for creep in unsaturated soils, this becomes very complex and difficult as there are many influencing factors, and the definition of creep in saturated soils cannot be applied to unsaturated soils due to changing stresses. As there is very limited literature on creep deformations of clay soils, making assumptions about these conditions' influencing factors is complex. However, Rezania et al. (2020) found that during unsaturated conditions, the observed creep behaviour is linked to initial water content and suction values, as when suction increases, it results in a decrease in volumetric creep strain and the water phase within the specimen has been removed, as the tensile forces at the soil-water interface to become more significant. Furthermore, the creep behaviour observed during these conditions shows that the clay particles do not undergo particle rearrangement or orientation. Assumptions state that if specimens with higher initial suction values undergo more significant volume change, the behaviour is controlled via suction stress rather than applied stress.

Throughout the literature, there have been many debates regarding the relationship between the creep and the primary consolidation, which has created huge debates been authors. Several authors have investigated the creep phenomenon in the literature, which has resulted in many questions still to be answered. When discussing historic creep theories regarding consolidation, Ladd et al. (1977) were the first to propose challenges to the theories. Ladd et al. (1977) proposed two hypotheses: A and B. Ladd et al. (1977) characterised hypothesis A as creep being the process that begins at the end of primary consolidation (EOP) and assumes that the relationship between the effective stress and the strain is independent of the length of primary consolidation. Whereas hypothesis B is associated with creep being an independent process related to the excess pore water dissipation and is represented by elasto-viscoplastic constitutive models. The main difference between the two hypotheses is that they are based on different soil thicknesses (one

experimental and one in-situ layer). Degago (2014) illustrated the two hypotheses by showing two curves (Figure 2.10) which show curve A, showing a simple assumption of hypothesis A and curve B, illustrating a higher strain value at the end of excess pore water dissipation developed from a viscous model. Many laboratories and in-situ testing of creep support the validity of hypothesis B. However, research by Mesri (2003) and Mesri and Vardhanabhuti (2006) supports hypothesis A as it is believed that the strain during primary consolidation is caused by a change in time and change in effective stress.

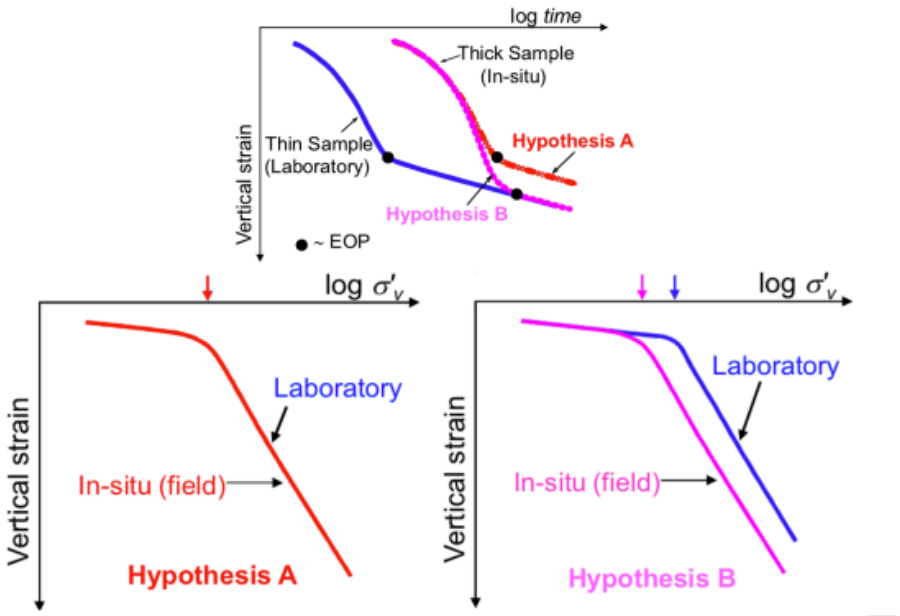

Figure 2.10 - Creep hypothesis from Ladd et al. (1977) explained by Degago (2014).

The following section will briefly discuss the 1D compressibility of reconstituted London clay samples in both saturated and unsaturated states. Both primary and secondary consolidation will be discussed with a greater emphasis on unsaturated specimens due to the lack of experimental studies completed on unsaturated London clay samples within the literature.

2.3.1.1. Previous London Clay Oedometer Tests

The geomechnical behaviour of the London clay formation has been subject to extensive experimental research. Many industrial and academic projects have taken place over time so the compressibility of the formation is well studied (e.g., Heathrow Terminal 5 construction (Gasparre, 2005)). The main interests throughout the literature have been saturated specimens obtained from select locations across the London Basin within the London clay formation. The studies of Gasparre (2005), Nishimura (2006), Sorensen (2006), have studied the Heathrow Terminal 5 site in the west and the east, a study from Bagheri (2018) on the Isle of Sheppey London clay focused on unsaturated specimens.

The study of the LC began in the early 1980s when King (1981) identified the lithological units within the formation with Allenou (2003) and Standing and Burland (2006) illustrating the mechanical responses of the clay with different lithological units. Gasparre (2005) completed a detailed study on LC's characterisation and analysed the compressibility of each subunit in the lithology. The reconstituted specimens' samples were tested from unit C through to A_{3_i}. It was determined by Gassparre and Coop (2008) that the geotechnical parameters such as C_c (0.386) and C_s (0.148) did not show much variance with depth. It was determined that the most influential parameter that affected the geomechanical behaviour of the clay was stresses (>500 kPa), and this was evident in each subunit, as units C and B_2 were more compressible than unit A_3; this was due to the open structure of the clay displayed rather than a packed and orientated layers (Gasparre et al., 2011, Nishimura et al., 2011). Further research found that the structural augments bulk stiffness to reduce the C_s in reconstituted specimens, preferably in natural specimens, and the greater compression applied to the specimens will increase further structural damage. Hight et al. (2011) also found that between the different lithologies, the compressibility behaviour of each sub-unit influences the intrinsic properties and that during compressibility tests, the natural samples display a poor overlay with reconstituted at higher stress levels (Figure 2.11), potentially due to the

strength of the aggregates in natural clay, which are more easily broken down by reconstitution process rather than 1D compressibility.

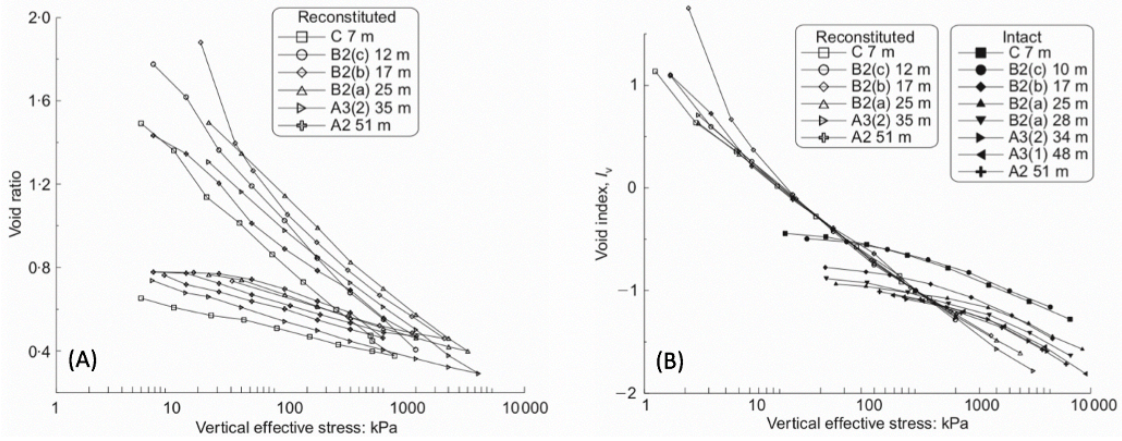

Figure 2.11 - One dimensional compression of LC from Heathrow T5 illustrating the intact and reconstituted samples: (A) in terms of void ratio and (B) in terms of void index (Hight et al., 2011).

It was further found that Sorensen (2006), who studied specimens obtained from unit B_{2_a}, found that the compression index (C_c) displayed a range of 0.41 to 0.51 with λ having a range of 0.178 to 0.221. It was reported by Martinez Calonge (2017) that λ was within the range of Sorensen (2006) at 0.182 and κ to be 0.064, which was the same as Gasparre (2005). The study completed by Bagheri (2018) showed that the saturated Isle of Sheppey LC was very similar to the values reported by both Sorensen (2006) and Gasparre (2005), with C_c and C_s values for the specimen with higher water content (43%) to be 0.408 and 0.133 respectively, where C_c and C_s for the specimen with lower water content (39%) to be 0.383 and 0.125 respectively. It was seen that the compressibility of the specimens from the Isle of Sheppey would increase with greater water content; however, Bagheri (2018) found that the compressibility of the soil was influenced greater by soil structure rather than water content in this study. This statement disagrees with Ma et al. (2018), who stated that the water content value influences clays' compressibility behaviour. Comparing the studies of Gasparre (2005) and Bagheri (2018) shows that the compressibility of the shallower specimens is higher than the deeper specimens, as the specimens from the Isle of Sheppey are more susceptible to compressibility than the Heathrow T5 specimens (Figure 2.12). This supports Gasparre (2005) statement, which stated that shallower specimens would be more susceptible to compressibility. The ability to

characterise and make trends of each reconstituted test performed on LC is difficult due to the geological sub-units, mineralogy and grain size affecting each location (Sorensen, 2006).

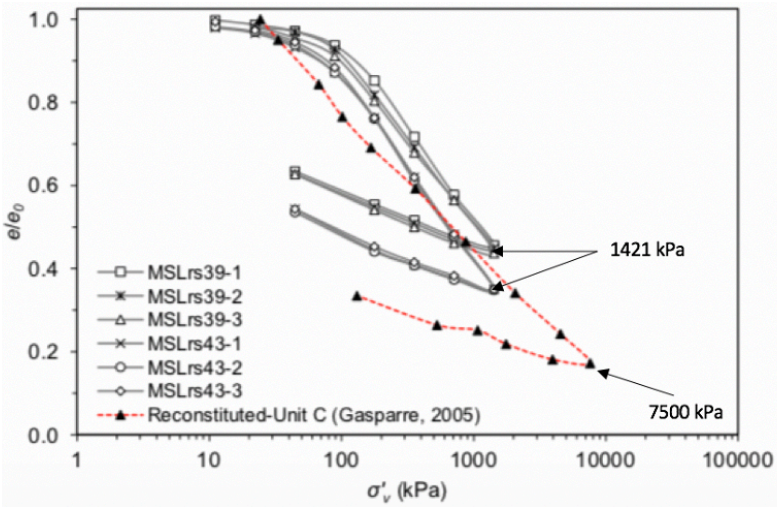

Figure 2.12 - Compression curve of reconstituted specimens from Heathrow T5 (red) and Isle of Sheppey (edited from Bagheri (2018).

Further analysis of LC found that the reconstituted specimens' creep index increase to a peak value of 6-7 times the yield vertical net stress (σ_p') (Rezania et al., 2020). Once the peak was reached, saturated specimens would decrease dramatically. It was observed in the studies (e.g., Bagheri, 2018; Rezania et al., 2020) that in the higher saturated specimens, the creep index (C_{ae}) would experience a sharper increase in the over consolidation region (pre-apparent preconsolidation stress), whereas, in the normal consolidation region (post apparent preconsolidation stress), the rise would be gradual, and these specimens would see a lower peak value (3 – 4) σ_p' before a decrease. The values observed by Bagheri (2018) would lie in the range of 0.012 – 0.013, which is comparable with Sorensen (2006), who obtained an average value of 0.016 for the Heathrow T5 specimens. The study of $\alpha = C_{ae}/C_c$ conducted by Rezania et al. (2020) found that the ratio was too scattered at lower stress levels, but within the higher stresses, it was found that the ratio was less scattered and showed a decreasing trend until obtaining a constant value of 0.024.

There is a lack of 1D compressibility data available in the literature for LC. A general trend seen with the available data is that suction plays a significant role in influencing the parameters C_c and C_s, as Monroy et al. (2008) and Rezania et al. (2020) found that suction affects the shape and location of the compressibility curve (Figure 2.13). Suction also causes the compressibility to decrease, leading to suction hardening due to the increase in yield vertical net stress. Rezania et al. (2020) found that the decrease in C_c and an increase in suction allow the specimens to follow similar trends to the SWRC. However, Monroy et al. (2008) found that with an increase in suction, there was an increase in C_c from 0.349 at 0 kPa suction to 0.723 at suction range 405 – 430 kPa. Both of the studies illustrated that the decrease in C_s coincides with the increase in suction as Monroy et al. (2008) showed as the value went from 0.081 to 0.032. However, this contradicts the statement of Sivakumar (1993), who stated that C_s is independent of suction.

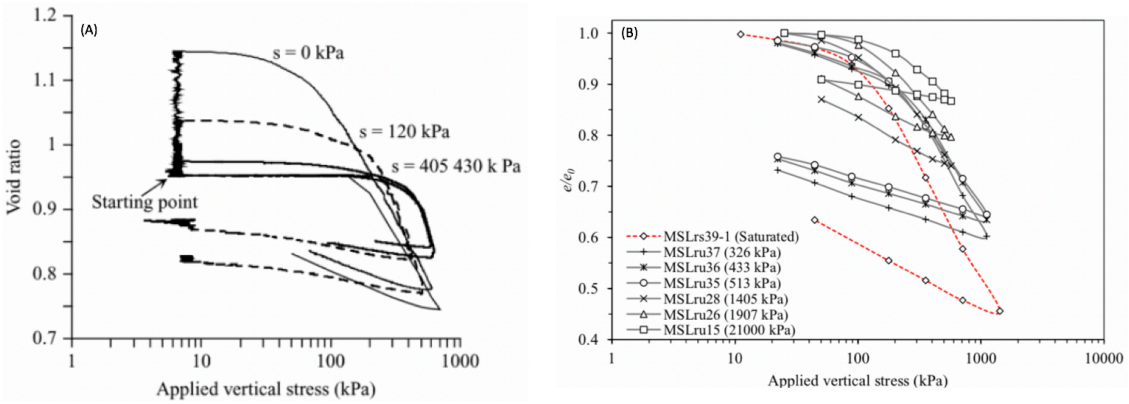

Figure 2.13 - Compression curves of unsaturated oedometer testing on London clay samples. (A) Monroy et al. (2008) and (B) Rezania et al. (2020).

During the 1D tests, it was seen that the pore-water pressure would increase during loading (suction decrease) followed by a pressure equalisation. Whereas during unloading, the pore-water pressure would decrease (suction increase) and show a similar pressure equalisation as in the loading phase. The pressure equalisation that occurs within the specimens happens during the early stages of the test and is potentially due to the change in pore-water pressure, which can be expressed as:

$$\Delta u = \mathrm{B} \times \Delta\sigma_v + \Delta u_d \qquad (11)$$

Where B is the Skempton B value, Δu_d is the excess pore-water pressure accounted for possible dilation, and $\Delta\sigma_v$ is the vertical stress. Rezania et al. (2020) found that the LC's B value was greater than 1.9 for all the tests due to the potential soil paste applied to the HCT at the beginning of the testing sequence.

Within the literature, it has been stated that during compression, the pore-fluid is comprised of air and water. The air bubbles in the pore water fluid will dissolve into solution during consolidation as the air volume will decrease, saturation of the specimen will increase due to a reduction in the void ratio of the specimen (Cuisinier and Laloui, 2004, Koliji, 2008). Rezania et al. (2020) found that with vertical stresses up to 400 kPa, there was an observed linear relationship between the vertical stress applied and suction. However, the trend becomes more variant in stresses higher than 400 kPa. The study also found that with suction < 500 kPa, there are no significant changes to suction responses during the unloading of the specimens.

The creep index study by Bagheri 2018 and Rezania et al., 2020 on unsaturated LC specimens found that they do not display a similar trend to that of saturated samples whereby they do not show an apparent peak value at which C_{ae} begins to decrease. The results from the study of Bagheri (2018) show that the C_{ae} parameter is highly influenced by suction. Furthermore, the secondary consolidation analyses of LC show that the soil suction influences the creep and strain rates during primary creep, as creep strain would increase at a decreasing strain rate. It shows that with constant stress applied, the suction will continue to increase, and the magnitude of strain will decrease. Throughout the tests, it is noticed that the particles within unsaturated specimens do not undergo particle rearrangement due to them containing tensile forces that prohibit this. Furthermore, creep behaviour in LC is seen to be stress-dependent, and the stress increase is more pronounced at the latter stages of the tests (Figure 2.14). However, Bagheri (2018) found that during creep tests with specimens that obtain high initial suction (1405 kPa), the volume change of the specimen is controlled by soil suction rather than the applied stress.

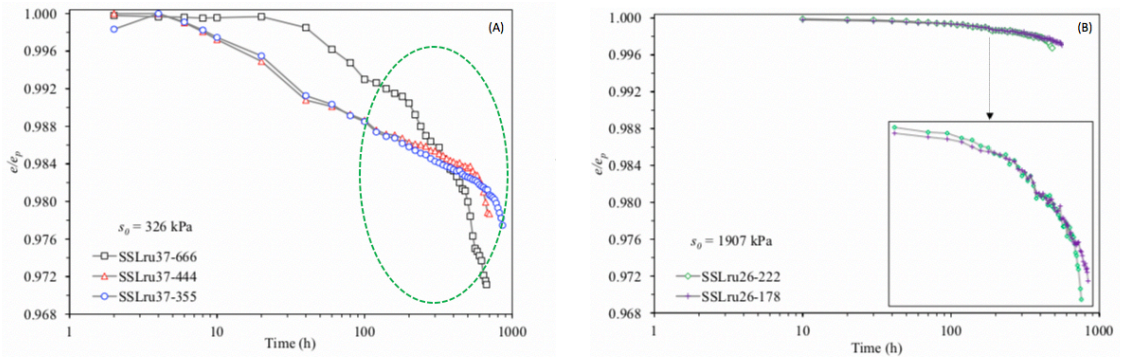

Figure 2.14 - Unsaturated tests from Bagheri (2018) illustrating unsaturated London clay creep tests with (A) showing the stress-dependent samples (low suction) and highlights the increase of stress effects at the latter part of the test (green circle); and (B) showing the suction-dependent specimens (high suction).

From the unsaturated creep tests performed by Bagheri (2018), a simple regression analysis was conducted to develop a creep law of vertical creep strain as a function of constant loading stage duration. The creep law developed from their study is similar to one developed by Priol et al. (2007) and stated that the creep law is to evaluate the effect of suction on the deformation of the specimens and proposed:

$$\frac{e}{e_p} = \beta t^{\alpha_i} \tag{12}$$

Where e is the void ratio, e_p is the void ratio 24 hours after the end of loading in creep tests, β is the instantaneous change in normalised void ratio with respect to e_p, t is time, and α_i is the creep coefficient. From the results illustrated in Bagheri (2018), the creep coefficient varies linearly with suction and that the parameter (α_i) in the long-term creep tests agrees well with the secondary consolidation found in the multistage oedometer tests.

2.3.2. CRS Testing

Constant Rate of Strain (CRS) tests are employed to analyse the effect of strain rate on a soil's 1D consolidation behaviour and are performed by using a constant vertical stress. They were first introduced in the 1960s by Hamilton and Crawford (1960), who proposed to determine the pre-consolidation stress value in a quicker timescale

(rather than using conventional testing techniques), as this point is significant due to irrecoverable (plastic) deformation occurring beyond this point. The standard the CRS tests follow is that of ASTM D4186 (2006), which is for consolidation of soil through this manner. The results of using this testing equipment show that the stress-strain relationship can be analysed along with the pore-water pressures from each specimen.

The advantages of using this testing technique are that the specimens undergo a smooth loading procedure, which reduces disturbance. Continuous results can be recorded, which gives a larger dataset to analyse, and there is a reduction in test time compared with 1D oedometer testing due to appropriate strain rates being used, and finally that permeability coefficients can be obtained from CRS tests (Näätänen et al., 1998). However, the drawback of CRS tests is the inability to measure secondary compression.

Determining the appropriate strain rates is crucial in CRS tests, as either high or low rates can cause irreversible effects on the specimen. During a high strain rate test, the excess pore-water pressure within the sample may become non-uniform and result in variation of effective stress and void ratio across the specimen, which leads to differing deformation rates while testing. However, a slow strain rate test would increase the duration of the test and prevent excess pore-water pressure generation, which is crucial for determining consolidation parameters. The ideal strain rate for CRS tests ranges between 10^{-8} to 10^{-4} mm/s^{-1} (Pereira and De Gennaro, 2010). Hence, the selection of strain rates depends on whether they can control excess pore-water pressure and lie within the boundary for engineering practice.

Throughout the literature, there have been many suggestions when determining the strain rates of CRS tests. However, ASTM D4186 (2006) suggested that the maximum strain rate used for testing should be less than 3 – 15% for the maximum pore-water pressure ratio, which is the ratio of excess pore-water pressure to the applied vertical stress determined by the C_v value. This ratio varies in the literature from 50 – 70% (Smith and Wahls, 1969) to 3 – 20% (Head, 1992). The majority of CRS strain rates

chosen for testing are larger than the strain rates observed in creep phases of conventional oedometer tests. For example, Sorensen (2006) used a strain rate of $2.3 \times 10^{-7}\, s^{-1}$ for conventional oedometer tests and $2.4 \times 10^{-7}\, s^{-1}$ for CRS testing. This results in the compression curves of CRS tests above that of incremental loading oedometer tests. Along with the different compression curves, a fast strain rate in the CRS testing would give rise to an increased pre-consolidation stress value, which leads to a shift in the compression curve to the right (Leroueil, 2006).

Unlike for saturated soils, there is very limited published literature on CRS testing of unsaturated soils. Generally, CRS tests used to study unsaturated soils are similar to saturated soils for understanding the compressive behaviour of the soils in an unsaturated state. However, a procedure to select the correct strain rate has yet to be developed.

To measure the secondary compression during CRS tests, a concept of stress relaxation is introduced, which allows the soil specimens to change in effective stress with time at a zero rate of axial strain. Relaxation tests measure the change of effective stresses with time in either 1D or triaxial conditions. The stress relaxation pattern is similar to creep deformations based on triaxial conditions on drained and undrained clays. The studies' indication shows a linear change in principle stress with the logarithm of time, but no firm conclusion was made regarding the effects of stress prior to the stress-relaxation stage.

Further studies into the stress relaxation stage by Bagheri et al. (2019) during 1D conditions have highlighted that the process of relaxation occurs over three phases (Figure 2.15): (1) fast relaxation, (2) decelerating relaxation, and (3) residual relaxation. The fast relaxation phase is associated with the rapid release of energy within the specimen, and the two other phases are associated with time-dependent particle rearrangement and allow for further energy dissipation over time. It was reported in the study that suction would play a more significant role during the fast and deceleration relaxation, whereby once the soil specimen develops high suction, the rate of relaxation decreases.

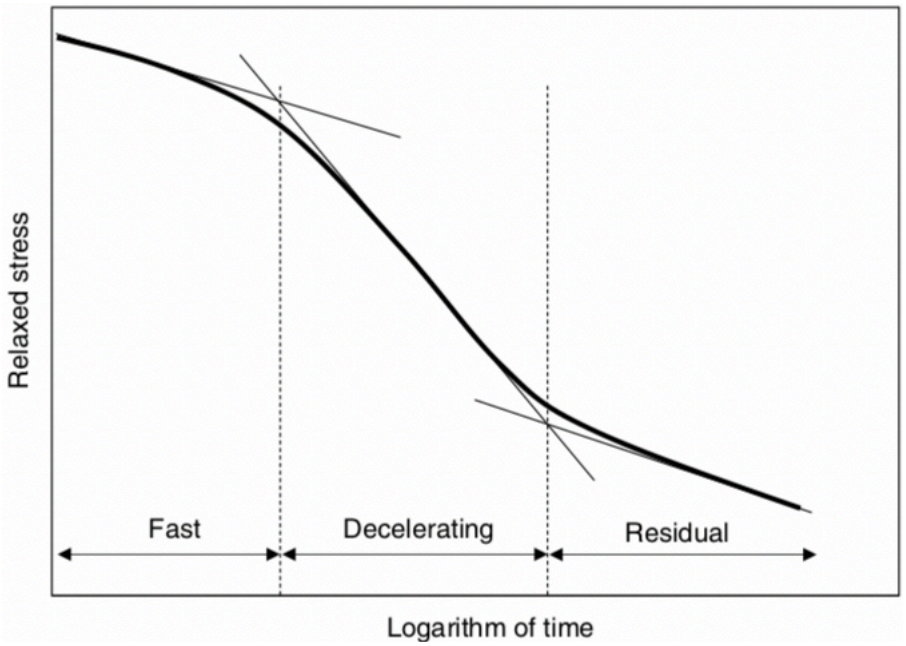

Figure 2.15 - The phases of stress relaxation identified by Bagheri et al. (2019).

Stress relaxation behaviour in soils displays a linear relationship between the vertical effective stress (applied vertical stress in unsaturated soils) and time in $\log \sigma_v' - \log t$ (or $\log \sigma_v - \log t$ in unsaturated soils) space during the relaxation of stresses (Yin et al., 2014). Therefore, the slope of the line can be considered as the stress relaxation coefficient (R_α) and be calculated as:

$$R_\alpha = -\frac{\Delta \log(\sigma_v')}{\Delta \log(t)} \tag{13}$$

To further quantify the stress relaxation parameters for soils, Bagheri et al. (2019) defined the relaxation process using three main parameters, which have been modified from Yin et al. (2014) and Wang et al. (2017) to fit the needs of 1D CRS tests in saturated and unsaturated conditions. The main stress relaxation parameters include: coefficient of stress relaxation (R_α), the residual stress ratio (ξ), and the relaxed stress ($\Delta\sigma$). The values of each parameter are defined by:

$$R_\alpha = -\frac{\Delta \log(\sigma_{vnet})}{\Delta \log(t)} \tag{14}$$

Which R_α is the coefficient of relaxation that is defined as the slope of the plot of σ_{vnet} versus time (t) in $\log \sigma_{vnet} - \log t$ space. The residual stress ratio (ξ) is defined as:

$$\xi = \frac{\sigma_s}{\sigma_0} \qquad (15)$$

Where σ_s is the residual total vertical stress and σ_0 is the pre-relaxation total vertical stress. Finally, the relaxed stress ($\Delta\sigma$) is defined by:

$$\Delta\sigma = \sigma_0 - \sigma_s \qquad (16)$$

2.3.2.1. London Clay CRS Behaviour

The following section will present CRS tests completed on London clay specimens in a saturated and unsaturated nature. With limited work being discussed on the stress relaxation and the rate-dependent behaviour of London clay in an unsaturated state, the only work to date in the literature is Bagheri et al. (2019)

The CRS tests on London clay allow the analysis of the rate dependency, creep, and stress relaxation of both saturated (e.g., Kim and Leroueil (2001); Sorensen et al. (2010); Yin et al. (2014)). However, the time-dependent behaviour of unsaturated clays is minimal due to difficulties (e.g., measuring suction) associated with the experimental program. With that, the only unsaturated data available on the London clay formation was that published by Bagheri et al. (2019).

To date, three strain rates have been used 2.3×10^{-7} (Sorensen, 2006), 2.4×10^{-6}, and 4.8×10^{-7} (Bagheri et al., 2019). Bagheri et al. (2019) found that an increase in strain rate caused the compression curve to shift to the right as stresses increases, which results in higher σ_p' values. When comparing the results of σ_p' from CRS and 1D oedometer tests show CRS tests to produce higher σ_p'.

Furthermore, the influence of strain rate on the compression behaviour of the clays can be seen as the faster strain rate gives rise to a higher σ_p' and a lower C_c value, with the slower strain rate in Bagheri et al. (2019) closely matching the C_c value of the MSL oedometer tests (0.38 and 0.40 for CRS and MSL). This behaviour is more evident in the unsaturated tests, as the higher the strain rate at a given void ratio, the higher the vertical stress. The presence of this behaviour within unsaturated specimens shows that suction plays a greater role in the soil's compression response than the strain rate (Bagheri et al., 2019). The increase in σ_p' with suction shows a linear trend for all strain rates and oedometer tests (Figure 2.16). Within the literature, it is stated that the ratio of σ_p' between CRS and MSL tests has an average value of 1.3 – 1.5 (Cheng and Yin, 2005), and in the study by Bagheri et al. (2019) that the ratio obtained for LC from the Isle of Sheppey for saturated specimens is 1.29, which is close to the average value.

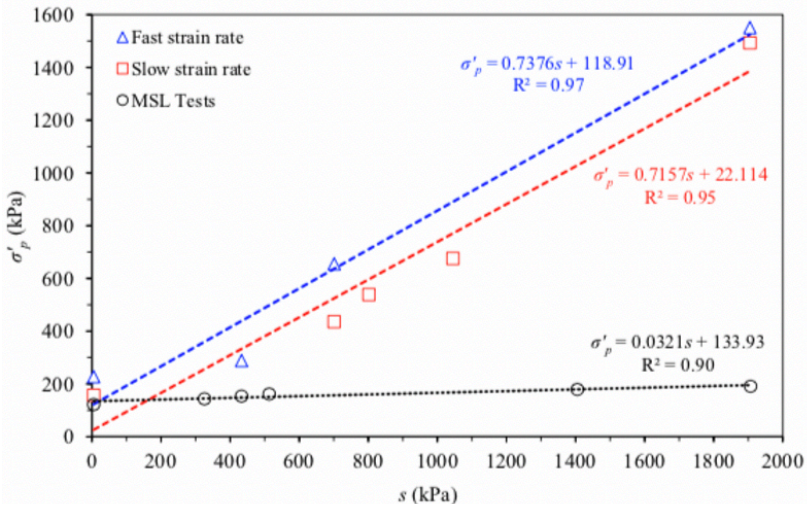

Figure 2.16 - The variation of σ_p' against suction in the Isle of Sheppey London clay CRS and MSL tests (Bagheri et al., 2019).

Once reaching the maximum vertical load applied to the specimens, the relaxation process begins to evaluate the effects of pre-relaxation strain and suction on the relaxation rate of the specimens. Bagheri et al. (2019) discovered that with constant pre-relaxation stress, an increase in suction caused a decrease (relaxed stresses) and increase (stress relaxation ratio) in the relaxation parameters. It was found that the relaxed stress coefficient of the two strain rates would also decrease with an increase

in suction, as the slow strain rate range was 0.019 – 0.011, and the fast strain rate range was 0.029 – 0.017. It was found that the application of $R_\alpha = \alpha$ is accepted by Bagheri et al. (2019) as the ranges obtained from the fast strain fall within the range of α in MSL tests. The relaxed stresses found by Bagheri et al. (2019) are considered reasonable considering the stress-relaxation mechanism as a time-dependent process of particle re-arrangement and gradual change in the configuration of grains, which allow the release of stresses built up in the compression stage. During unsaturated testing, at a constant strain, it is seen that suction has a greater influence on the stress relaxation during the fast and deceleration phase (Figure 2.17); as suction increases, the relaxation rate of the specimens lowers. Both Sorensen (2006) and Bagheri et al. (2019) reported that the slight drainage of water during the saturated tests' relaxation stage did not affect the volume change of the specimen.

Evaluating the pre-relaxation stress levels on unsaturated LC, Bagheri (2018) conducted two tests at an initial suction value of 701 kPa and performed a 24-hour relaxation period once a specific strain value had been reached. It was found that for both strain rates considered, there was an increase in the relaxed stresses with increasing pre-relaxation strain. However, the relaxed stress ratio would increase in the lower pre-relaxation values and then decrease at higher ones. It was seen that an increase in pre-relaxation strain by a factor of 5 would affect the extent of relaxed stresses at each pre-relaxation strain interval, which caused the relaxed stress values to increase by a factor of 2.2 – 3.6. Throughout the testing phase, the specimens' excess pore-water pressure would follow the same trend at the stresses, and during the relaxation period of each interval, there would be complete dissipation. When analysing the relaxation stress levels with time on a log-log scale, it was found that the values would have a linear relationship, and this had been reported in the literature for saturated clays (e.g., Yin et al. (2014)).

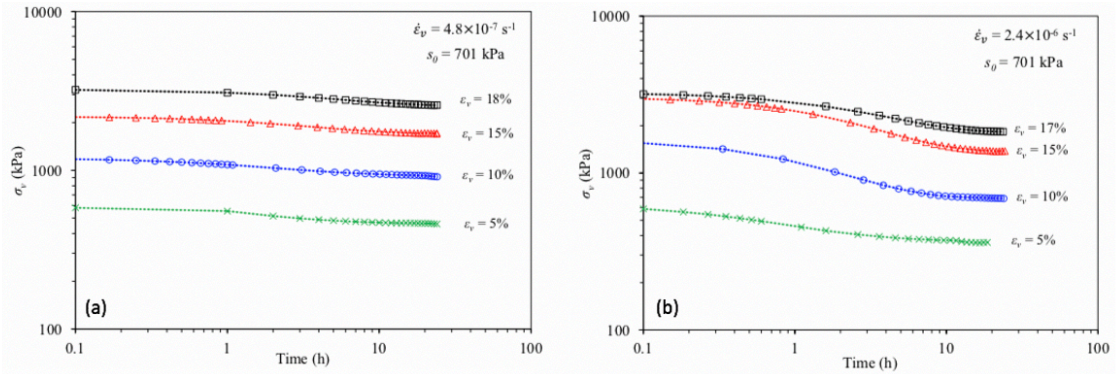

Figure 2.17 - Log-log scale showing the linear relationship between relaxation stresses with time at each pre-relaxation (Bagheri, 2018).

Bagheri et al. (2019) shows that the value of R_α would be between 0.011 – 0.027 for the slow strain rate and 0.025 – 0.035 for the fast strain rate. These values are higher than the single staged compression tests, but the determination of relaxation differs as the single staged compression is a relaxation period of 210 hours, whereas multi-staged compression has a 24-hour relaxation. The R_α values obtained in both tests show that the multi-staged compression would lie within the decelerating phase and single staged compression within the residual phase (Figure 2.17). The study's drawback is the limited amount of data obtained from the multi-staged compression tests to make a full conclusion on the R_α value, which would help determine a more accurate value of the time-dependent parameter.

2.4. Summary

Based on the literature review, it can be seen that London clay has been extensively studied in its saturated states, whereby several researchers have found that specific geotechnical parameters (e.g., C_c and C_s) are very similar to each other regardless of the change in the sub-units of the clay. Several factors, e.g., soil structure, pre-consolidation, and consolidation stresses, have been conclusively found to influence the compressibility and creep index in saturated clays. In unsaturated testing of the London clay, there is a limited number of studies completed across a small suction range to draw definitive agreement. It appears that suction plays a vital role in the compressibility, pre-consolidation, and the swelling response of clays. During creep

tests of London clay, it appears that the volumetric creep deformations can be defined by a power law function, but this needs further analysis across greater vertical stresses and suction ranges. Due to the incomplete data set of unsaturated London clay in terms of stress dependencies, suction evolution, and validation needed for the creep law proposed, an extensive experimental program (in this thesis) will be conducted to understand the time-dependent behaviour of clays under greater stresses and more suction ranges.

Only a limited number of experimental studies have been undertaken involving 1D (oedometric) CRS testing on London Clay under saturated and unsaturated states. However, a conclusion can be drawn that the stress relaxation coefficient for clays in their saturated states is also valid for unsaturated clays. Moreover, the strain rate used on both saturated and unsaturated clays influences σ_p' along with suction that shifts the specimens' compression curve to the right. The pre-relaxation strain tests show that the relaxed stresses increase with pre-relaxation strains, and at each interval, the magnitude of relaxed stresses is affected by a factor of 2.2 – 3.6. With pre-relaxation strain rate influences the stress relaxation coefficient under constant suction. More tests are needed to draw a more significant conclusion with the relaxation coefficient in the pre-relaxation strain testing with greater relaxation periods.

Based on the information available in the literature regarding temperature changes, conflicting findings are reported on the geomechanical behaviour of saturated soils. Throughout thermal testing on the clays, it can be seen that the temperature testing range is relatively large, with small temperature changes analysed. Several studies have found that the clays' deformation depends more on the soil structure and stresses applied rather than temperature. Furthermore, it has been found that there are minimal studies completed on the thermo-mechanical behaviour of the London clay, which needs to be assessed.

Based on the insufficient data on the thermo-mechanical behaviour of soils during the pre-relaxation strain and stress relaxation stage, a complete experimental program needs to be designed and carried out. This will add vital information concerning the stress relaxation behaviour of stiff clays in a shallow subsurface and how potential geo-structures behave when subjected to temperature variations between 20 to 55°C.

Chapter 3 – Experimental Methodologies and Materials

This chapter presents the material used (London Clay) then will introduce the equipment used to study the time- and rate-dependency of stiff clays in saturated, unsaturated (partially saturated) and thermal conditions in one-dimensional (1D) compression.

3.1. Material: Bank Station, London Clay

3.1.1. Sample Location

The studied material (London Clay) was sourced from one site in central London. The bulk of the London Clay was recovered from the piling at the Bank Station capacity project upgrade. The British National Grid (BNG) coordinates for this site is E: 532806 N: 180785. This material was obtained at 30 meters depth along the Northern Line level, located in the London Clay unit B. The samples that were obtained from the site were distributed buckets. These were collected from the piles of waste material from the excavation process.

3.1.2. Characteristics of Bank Station Clay

This section presents the main characteristics of the studied material. It includes the mineralogical and chemical composition, particle size distribution (PSD), and the Atterberg limits. It also presents the soil water retention curve (SWRC) of the studied material and compares the SWRCs reported in the literature.

3.1.2.1. XRF Chemical Composition

Table 3.1 represents the chemical composition of the Bank Station London clay used in this study. This analysis was carried out by conducting a series of X-Ray

Fluorescence (XRF) tests using a Rigaku Primus IV Wavelength Dispersive X-Ray Fluorescence (WDXRF). Several pressed pellets were created to allow for sample homogenization and greater accuracy in the results obtained.

Table 3.1 - Main chemical composition of the Bank Station specimens.

Test	Na	Mg	Al	Si	K	Ca	Ti	Fe	Total
LC1	0.17	2	13	43	9.6	2.2	2.6	24	96.57
LC2	0.16	2	13	42	9.5	2.4	2.7	25	96.76
LC3	0.18	2	13	43	9.7	2.3	2.6	24	96.78
Mean	0.17	2	13	42.66	9.6	2.3	2.63	24.33	-
Std.	0.01	0	0	0.57	0.1	0.1	0.06	0.58	-
Max	0.18	2	13	43	9.7	2.4	2.7	25	-
Min	0.16	2	13	42	9.5	2.2	2.6	24	-
Note: LC = London Clay									

Unfortunately, there wasn't possibility at the time to conduct SEM or XRD testing to further analyse the mineralogical properties of the material used.

3.1.2.2. Index Property Classification Tests

Basic soil classification tests on Bank Station London clay were undertaken to assess the material's index properties.

Atterberg Limits

The plastic (w_P) and liquid (w_L) limit of the clay were measured using the thread rolling and the cone penetrometer method, respectively, as stated by BS 1377-2: 1990. The water contents at which Bank Station specimens' average plastic and liquid limits were obtained are 24% and 77%, respectively, with a corresponding plasticity index (I_P) of 53%. These values agree well with other tests performed on the same London clay units by Hight et al. (2011) (plastic limit 22-32% and liquid limit 61-77%) and Sorensen et al. (2010) (plastic limit 28% and liquid limit 65%).

Specific Gravity

The specific gravity of the solids (G_s) was measured following the BS 1377-2: 1990 classification, which used the small pyknometer method for oven-dried materials. The powdered material used for this method was obtained from the reconstituted process and filtered through a 0.063 mm sieve ready to be placed in the two standard 50 ml pyknometers. The average value of specific gravity is 2.69 for Bank Station specimens. The specific gravity value obtained in this study is consistent with that found in other studies and sites which tested unit B of the London clay formation. For example, Sorensen (2006) found the specific gravity of unit B London clay specimens at Heathrow T5 to range between 2.65 – 2.76.

Particle Size Distribution Curve and Sedimentation

The grading curve was obtained from dry sieving and sedimentation tests using the procedure stated in BS 1377-2: 1990. The PSD curve of Bank Station London clay contains 75.88% of particles smaller than 0.6 mm and 19.25% of particles smaller than 0.063 mm. For the sedimentation process, 30g of dry powder was added to a flask containing 100 ml of dispersing solution, stirring vigorously to bring the soil into suspension. The particles that passed through the 0.063 mm sieve were used for the sedimentation process following the hydrometer procedure described in BS 1377-2: 1990. The clay, silt and sand contents were obtained as 49%, 46% and 5%, respectively. The results from the sedimentation test show that the material is predominately clay-sized particles with nearly an equal amount of courser particles mixed within the reconstituted slurry used to create the specimens.

3.1.3. Sample Preparation

In preparation for testing, the disturbed specimens obtained from Bank Station were prepared by oven drying them for a minimum of 72 hours at 105°C, then crushed to have a particle diameter < 1.18 mm. The crushed reconstituted soil was then sieved

by following the BS 1377-5: 1990 for dry sieving to obtain the particle size distribution (PSD). Once sieved, the clay samples were prepared by mixing the soil powder obtained from the PSD with de-aired distilled water at 1.5 w_L until a homogeneous paste was obtained (Sorensen et al., 2010). The paste was then poured into a Perspex consolidometer (120 mm diameter for CRS and 100 mm diameter for oedometer samples) and then consolidated under vertical stress of 80 kPa for a minimum of five days (following the procedure stated by Bagheri (2018)). The consolidated paste was then quickly unloaded to minimise the swelling and water absorption. The samples were then cut into three equal pieces and allowed to room dry at ambient temperatures to pre-defined moisture contents. The moisture content of the unsaturated specimens (partially saturated) was derived from the SWRC and placed in an air-tight container to allow for moisture equilibrium. Oedometer specimens measure 75 mm in diameter and 20 mm in height, and CRS specimens measure 95 mm in diameter and 35 mm in height (ASTM D4186 (2006)). Preparation of the specimens was essential to the success of this project because of the mass reproducibility of the initial state of the specimen.

3.1.4. Soil Water Retention Curve

Soil water retention tests following the drying pathway were performed to determine the SWRC of reconstituted Bank Station London Clay specimens. The SWRC of Bank Station specimens was measured using continuous drying and filter paper methods. The continuous drying method using HCTs is a direct measurement of soil suction and has been widely discussed in the literature (Lourenço et al., 2008, Toll et al., 2011, Bagheri, 2018). The advantage of using this method is that it allows the monitoring of the soil suction to be made quickly and accurately. However, a drawback to the method is the long-term measurements of high suctions and the ability to analyse continuous measurements (Bagheri et al., 2018).

In contrast, the filter paper method indirectly measures soil suction. Although the accuracy is user-dependent, this method is the cheapest and simplest to use. This method uses two filter papers (Whatman No.42 and Schleicher & Schuell no.589-

WH), which range up to 30,000 kPa and have two calibration curves due to their unique properties (Ridley et al., 2003).

3.1.4.1. Continuous Drying Tests

To prepare the specimen for HCTs to measure the soil's suction, two holes were created on the specimen's surface using a mini auger, measuring 10 mm diameter and 6 mm depth, which accommodated the HCTs. These holes allow the HCTs lateral support to avoid movement throughout the tests. As stated by Bagheri (2018) , this method is believed to minimise the disturbance when the tensiometer is placed in the specimen and allows for suction to measure in the middle of the specimen, where evaporation is expected to be constant and uniform. The two HCTs were then placed into the holes created with a small amount of soil paste applied to the tip (as mentioned in section 3.1.3) to ensure full contact with the specimen. The specimen was then placed on a porous stone sitting on the digital balance with a 0.01 g resolution. The cables were suspended above the specimen to avoid any measurement issues with the HCTs cables and the digital balance. To minimise temperature and humidity fluctuations in the laboratory due to external work being conducted, these experiments were conducted during the weekend. The tests were performed on four identical reconstituted specimens (75 mm diameter and 20 mm height) cored from a single cylindrical sample consolidated from a slurry in a consolidometer following the procedure explained in section 3.1.3.

Figure 3.1 presents the SWRCs obtained from the continuous drying tests, which were developed as the specimens dried for 24-hours. As it can be seen, it illustrates that the onset of drying is slow until there is a sudden change during the saturated-unsaturated transition; this would imply that the evaporation rate impacts the HCTs measurements. After the saturated-unsaturated transition, the suction increase is gradual as the specimens continue to dry. Table 3.2 presents the initial and final conditions of the specimens, along with the maximum suction value and suction at air-entry value (s_{AEV}).

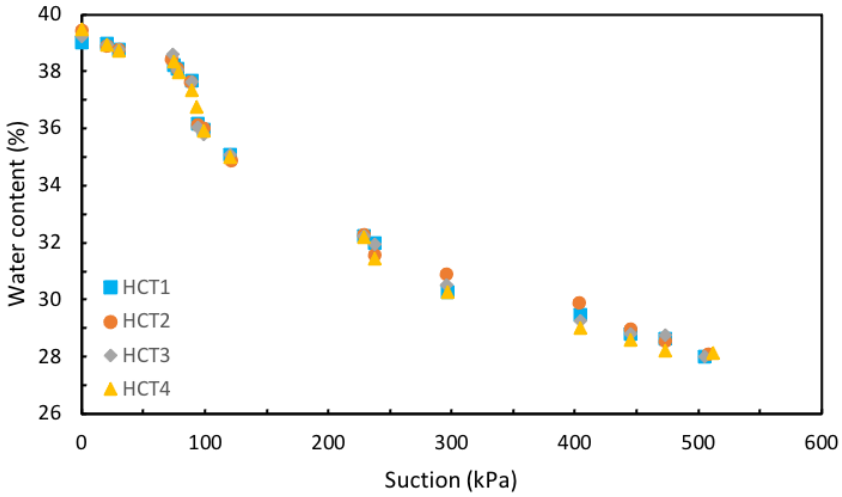

Figure 3.1 - SWRC obtained from the continuous drying method using HCTs.

Table 3.2 - Results of the continuous drying tests.

Test No.	HCT	Initial water content (%)	Final water content (%)	S_{AEV} (kPa)	Maximum suction value (kPa)
CDT1	HCT1	39.02	28.01	104	505
CDT2	HCT2	39.43	28.09	103	508
CDT3	HCT3	39.21	28.02	106	505
CDT4	HCT4	39.47	28.12	104	512
Note: CDT= Continuous drying tests. The average values are shown in this table. All tests were repeated to validate the reproducibility of the results.					

3.1.4.2. Filter Paper Tests

The filter paper test procedure follows various methods in the literature (Chandler and Gutierrez, 1986, Chandler et al., 1992, ASTM, 2003, Marinho and Oliveira, 2006, Bicalho et al., 2007, Bulut and Leong, 2008). The tests were performed on specimens of 50 mm diameter and 20 mm height. Three Whatman No.42 filter papers were cut to size and placed between the two specimens (as seen in figure 3.2); this allows for two filter papers to protect the test filter paper. Once the specimens were in contact, a small amount of electrical type was placed around the centre to avoid any measurement errors. The specimen was then placed in a glass jar for a minimum of one week to allow for equilibrium to be reached to evaluate the matric suction. Before starting each test, all the measurements of each specimen were recorded and allowed to air-dry to predefined water contents. All the filter paper values were

measured using an analytical balance with a resolution of 0.001g. The selection of the water content values was determined on the data available within the literature so that suction values could be correlated across the London clay formation. The filter paper tests were performed across 16 specimens due to the inaccuracy of this procedure.

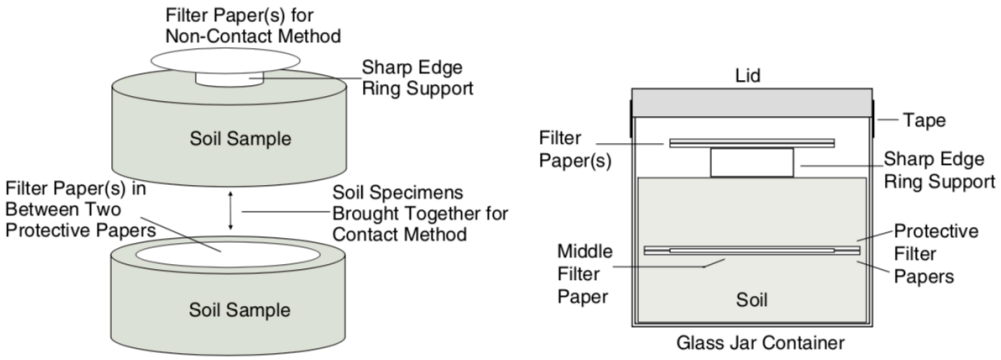

Figure 3.2 - Filter paper set up as described by (Bulut and Leong, 2008).

To evaluate the suction values of the reconstituted Bank Station specimens, a series of calibration curves were used to generate the values needed for the Whatman No.42 filter paper. The equations used in this study are listed below in table 3.3, allowing for a comparison between the different calibration curves.

Table 3.3 - Calibration curve equations for Whatman No.42 filter paper.

Reference	Suction	Water content (w_o) (%)	$\log 10$ (suction) (kPa)
ASTM (2003)	Total and Matric	w<45.3	5.327 – 0.0779w
	Total and Matric	w>45.3	2.412 – 0.0135w
Chandler et al. (1992)	Matric	w<47	4.842 – 0.0622w
	Matric	w>47	6.050 – 2.48$\log_{10}$w

The calibration equations used to generate the Whatman No.42 filter paper suction values for the tested water contents (37 to 28%) for Bank Station specimens are presented in figure 3.3 and table 3.4. It can be seen that the ASTM (2003) calibration curve equation displays slightly lower suction values for all water contents when compared with the Chandler et al. (1992) equation. Furthermore, calculating the specimens' matric suction shows that the ASTM (2003) values are between 23 – 61

kPa lower than that of Chandler et al. (1992). This illustrates that the suction values are subjective to the calibration equation used.

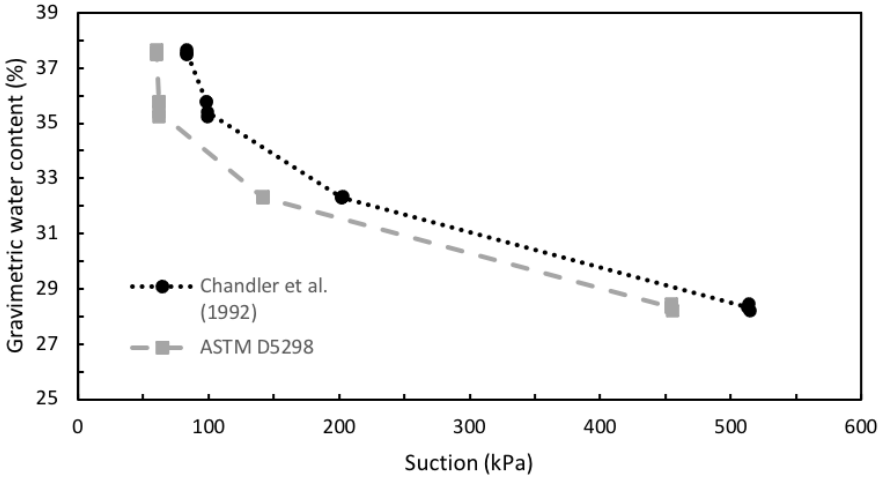

Figure 3.3 - Suction values derived from the two calibration equations for Bank Station specimens.

Table 3.4 - Results of the filter paper tests using two different calibration equations.

Test No.	Specimen water content (%)	Filter paper water content (w_o) (%)	Chandler et al. (1992) ($\log_{10}$) (suction)	ASTM D5298-03 (2003) ($\log_{10}$) (suction)	Chandler et al. (1992) (matric suction) (kPa)	ASTM D5298-03 (2003) (matric suction) (kPa)
A1	37.48	46.968	1.920590	1.777932	83.289528	59.969717
A2	37.48	46.962	1.920964	1.778013	83.361131	59.980903
A3	37.32	46.971	1.920404	1.777892	83.253749	59.964125
A4	37.28	46.969	1.920528	1.777919	83.277600	59.967853
B1	35.76	45.790	1.993862	1.793835	98.596614	62.206390
B2	35.72	45.791	1.993800	1.793822	98.582494	62.204457
B3	35.84	45.743	1.996785	1.794470	99.262544	62.297340
B4	35.76	45.774	1.994857	1.794051	98.822810	62.237337
C1	32.31	40.770	2.306106	2.151017	202.351301	141.584920
C2	32.35	40.771	2.306044	2.150939	202.322322	141.559526
C3	32.31	40.765	2.306417	2.151407	202.496257	141.711958
C4	32.31	40.770	2.306106	2.151017	202.351301	141.584920
D1	28.32	34.270	2.710406	2.657367	513.341056	454.325382
D2	28.30	34.272	2.710282	2.657211	513.194035	454.162425
D3	28.32	34.251	2.711588	2.658847	514.739860	455.876389
D4	28.32	34.264	2.710779	2.657834	513.782373	454.814603

3.1.4.3. Comparison of SWRC Results

Inspection of the SWRCs obtained from the continuous drying using HCTs, and the filter paper tests provide some interesting findings. Figure 3.4 presents the two techniques used to generate the SWRC for Bank Station London clay specimens. It is seen that the SWRCs for the filter paper tests shift left and sit below the SWRCs generated from the continuous drying tests. Moreover, the ASTM D5298-03 (2003) calibration equation displays a considerable difference in suction values compared to the values obtained from the HCTs, with the difference being more significant than 30% at specific water contents. In contrast, the Chandler et al. (1992) calibration equations allow suction values to be within a 10% error range when compared to the HCTs. Due to this finding, it can be confirmed that the Chandler et al. (1992) filter paper calibration equation provides reasonable acceptance with the continuous drying results. Furthermore, it must be noted here that the SWRCs differences presented in figure 3.4 may be caused by suction distribution at the mid-height of the tested specimens. Additionally, the errors associated with the filter paper tests, as stated in the literature (human user error), may cause the underestimation of the suction values for different calibration equations.

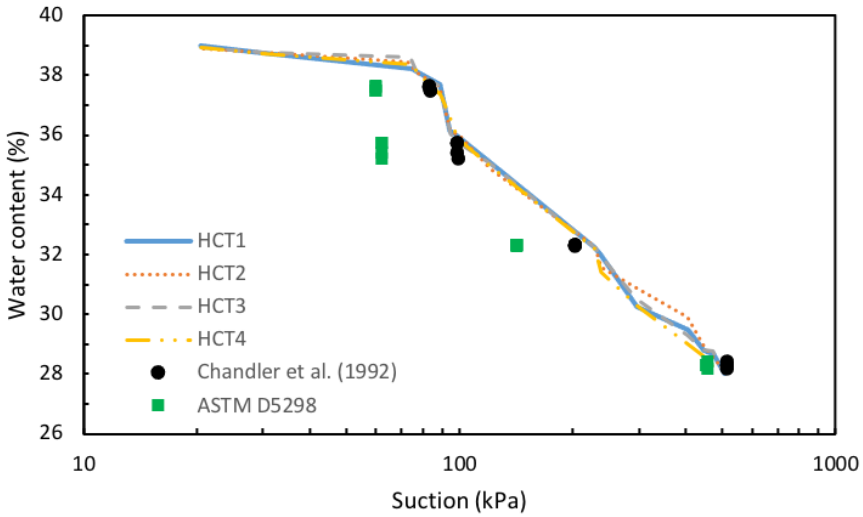

Figure 3.4 - Comparison of the SWRC methods.

Based on the findings within the literature, the unsaturated properties of Bank Station London clay have yet to be investigated. In general, only a small number of

unsaturated studies have been conducted on the London Clay formation, with the majority being towards the western part of the London basin (figure 3.5). Figure 3.5 shows the SWRCs of London clay specimens found in various studies. The study of Dineen (1997) presents a variation of moisture content for reconstituted London clay in a drying cycle. The samples obtained for the Dineen (1997) study were located at the Summerlease clay pit near Colnbrook, London. Other studies that have presented SWRCs are that of Monroy (2006), who obtained samples from an excavation Harlesden and used the HCT for suction measurements. In the excavation of Westminster Bridge, Mavroulidou et al. (2013) obtained the suction measurements using the filter paper technique. Located at New Hook Farm, the Isle of Sheppey, Bagheri (2018) obtained samples and analysed the suction measurements using HCTs by performing a series of continuous drying and controlled evaporation drying tests.

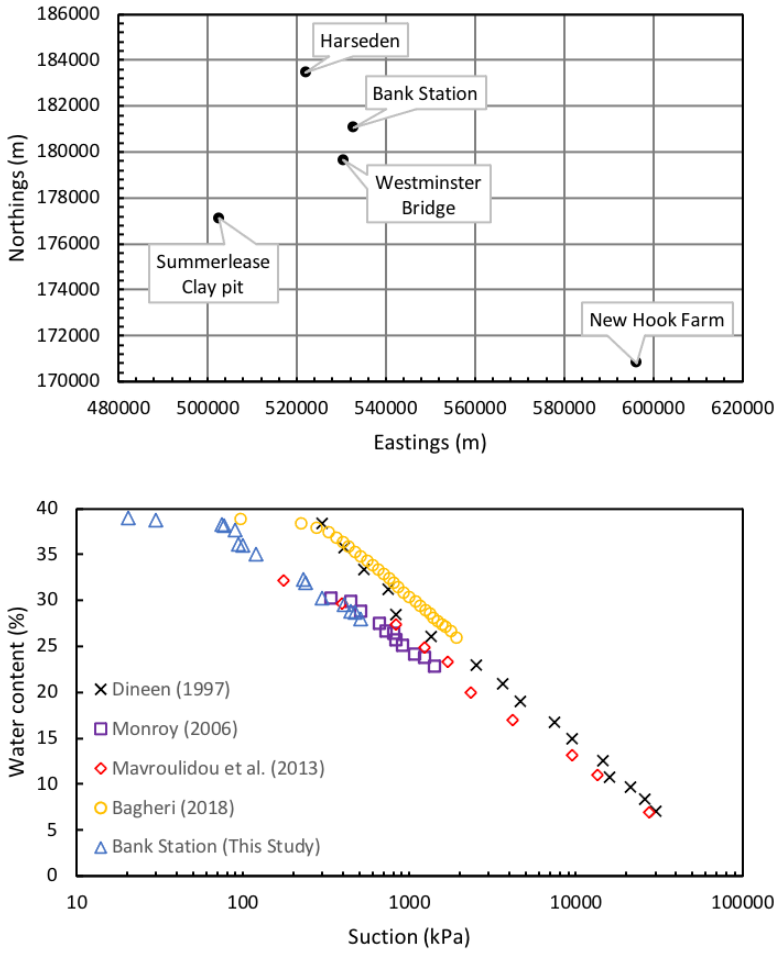

Figure 3.5 - Geographical location of the SWRC studies on London clay specimens and the SWRCs established for London Clay

3.2. Oedometer Test Set-up

This describes the three different oedometer devices used in this research to study the time- and rate-dependency of stiff clays under saturated, unsaturated, and thermal conditions. In addition to the experimental setup, the calibration and verification of the devices are presented.

3.2.1. Saturated Oedometer

Conventional oedometer tests were performed (using the BS1377: part 5) at different water contents (43 to 39%) and similar initial void ratios (1.35 to 1.23). These tests aimed to understand the compressibility behaviour of the selected material at different water contents and then use that data as a baseline for the thermo-mechanical tests.

The oedometer used to complete one-dimensional (1D) compressibility tests on Bank Station London clay was a back hanging oedometer which contained a loading ratio of 9:1 (Figure 3.6). The oedometer contained two saturated porous disks to allow for drainage, a linear vertical displacement transducer (LVDT) with a travel length of 10 mm and accuracy of 0.001 mm, and a cutting ring with the dimensions of 75 mm in diameter and 20 mm in height. The data acquisition of the displacement transducer is performed using a GEODATALOG 8 channel using DATACOM2 software. This system has a real resolution of 131,000 points. The water surrounding the oedometer during the saturated temperature is added at room temperature and ensures the specimens were always saturated and to avoid generations of suctions. The series of 1D tests were completed at room temperature (18°C ± 3°C) in the geotechnics lab at the University of Warwick.

Figure 3.6 - Setup of the standard oedometer tests completed at the University of Warwick.

3.2.1.1. Saturated Sample Test Set-up

Multi-staged loading (MSL) oedometer tests were performed with a 24-hour loading period on reconstituted Bank Station London clay specimens. The oedometer specimens have a dimension of 75 mm in diameter and 20 mm in height and were obtained by penetrating the cutting ring into the reconstituted soil cake (explained in section 3.1.3). Before cutting the specimens, the confining ring obtained a little grease lubrication to avoid friction and disturbing the specimens. Before the beginning of each test, the surfaces of the specimen were trimmed of any excess soil and flattened to ensure there were minimal errors when aligning the top cap of the oedometer and to prevent any errors within the displacement measurements. Furthermore, the properties of the soil are measured and recorded before each test, e.g., water content and specimen dimensions. Once measurements were recorded, the specimen was set up in the oedometer cell, and the loading cap and the hanger were placed. Drainage, as mentioned in section 3.2.1, is allowed through the

saturated porous disks placed at the top and bottom of the specimen. After preparing the oedometer specimen for testing and placing it in the oedometer cell, the specimen was allowed to reach equilibrium overnight under the weight of the loading cap and the hanger, and the LVDT recorded any swelling or compression. Once specimens reached equilibrium, a vertical load was applied stepwise (table 3.5) to the submerged specimens and sustained for 24-hours to ensure full dissipation of the excess pore-water pressure during each load step.

The vertical load was doubled for each load step, which is typical for conventional oedometer testing. After the desired load (stress state – 1280 kPa) was reached, the specimens were unloaded stepwise, and each unloading stage was kept for 24-hours to ensure complete swelling and evaluate the swelling response. The compression curves were finally obtained on the final settlement values recorded by the end of each load/unloading stage. Using this method ensures that the results can be compared with those already published in the literature regarding London clay specimens. The oedometer used at the University of Warwick was the imperial type with backloading hangers. Due to this setup, there was a limitation of maximum vertical stress (1280 kPa) applied to the specimens because of the limited amount of dead weights that could be simultaneously applied to the hangers of the oedometer apparatuses.

3.2.2. Unsaturated Oedometer

A series of unsaturated oedometer tests were performed in a specialised oedometer cell equipped with two high capacity tensiometers (HCTs). The unsaturated oedometer was used to analyse the compressibility behaviour of the selected material at various initial water contents corresponding to initial suction values of the specimens, based on information obtained from the soil water retention curve (SWRC) (see section 3.1.4).

The unsaturated oedometer cells used in this study were based on apparatus design developed by Bagheri (2018), which allowed for specimen dimensions of 75 mm in

diameter and 20 mm in height (Figure 3.7). The loading cap of the oedometer contained two high capacity tensiometers with an outer body dimension of 11 mm diameter. It contained two porous disks between the specimen and the loading cap. It contains a transparent membrane to seal the gap between the outer body and the loading cap that contains holes around the circumference of the membrane as well as the cell body, which secures the cover and fixes the cell by using screws to avoid any gaps. The oedometer apparatus contained a linear vertical displacement transducer (LVDT) with a travel length of 10 mm and accuracy of 0.001 mm, which allowed for data acquisition of the displacement transducer to be recorded using a GEODATALOG 8 channel using a DATACOM2 software. The tensiometer data is recorded using a LabVIEW code developed for the data acquisition of suction measurements. The series of 1D tests were completed at room temperature (18°C ± 3°C) in the geotechnics lab at the University of Warwick.

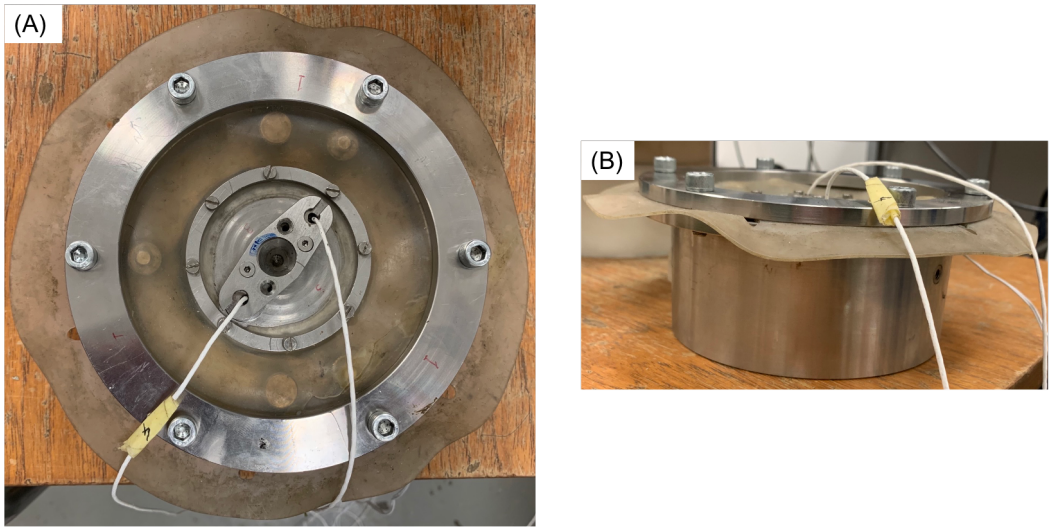

Figure 3.7 - The view of the unsaturated oedometer which tensiometers installed used in this study. (A) Top view, (B) Side view. (Details about the HCTs can be found in Bagheri 2018).

3.2.2.1. Unsaturated Sample Test Set-up

The test procedure of the unsaturated MSL oedometer tests is similar to that of the saturated oedometer MSL tests explained in section 3.2.1.1. Before starting each unsaturated experiment, the tensiometers were saturated and preconditioned following the procedures stated in Bagheri (2018) and discussed further in section

3.2.2.2. Once the specimen is placed in the unsaturated oedometer cell, the two HCTs are fitted in the designated holes within the loading cap. Prepare to connect the loading cap with the HCTs to the specimen, a small amount of soil paste was applied to the ceramic disks to prevent any desaturation (Toll et al., 2011, Bagheri, 2018) and small vertical stress (weight of the loading cap) was also applied to the specimen to ensure there was full contact with the tensiometers. Once full contact was ensured, the membrane and cell body were screwed together to avoid any air infiltration to the specimen, which could affect the HCTs measurements. After preparing the oedometer specimen for testing and placing it in the oedometer cell, the specimen was allowed to reach moisture equilibrium overnight under the weight of the loading cap and the hanger, and the LVDT recorded any swelling or compression. After the specimens reached moisture equilibrium, the values the HCTs recorded prior to the first loading stage were considered the initial suction value (s_o). To ensure the accuracy of the HCTs values, the values obtained by the HCTs did not exceed 5% of each other.

Before each test, the tensiometers were placed in a saturation chamber that clamps the HCTs so that the ceramic filter is prone to vacuum, water flooding and pressurisation. The saturation chamber contained a screw piston placed in the centre of the chamber, allowing the pressurisation of the water within the chamber. The procedure of saturating the HCTs was conducted by following the method stated by Tarantino and Mongiovì (2003) and Bagheri (2018). In brief, the following steps were conducted for the saturation:

- Saturation chamber had a vacuum pressure applied for a minimum of one hour to remove as much air as possible.
- The chamber was flooded with de-aired distilled water while under the vacuum pressure.
- 4 MPa pressure was applied to the chamber to remove any unwanted air dissolved into the solution.
- The screw piston increases the pressure within the chamber.

Once the saturation process was completed, an analysis of the saturation process was completed by conducting a series of load-unload cycles in increments of 100 kPa, and the response of the HCTs was monitored on the LabVIEW software. For the load and unload cycle, the duration of each stage was 20 minutes to ensure the sensors of the HCTs reached equilibrium with the pressure applied. Additionally, after the cycles were completed, the HCTs were removed from the saturation chamber and placed in free water for up to 2 hours to reach equilibrium before testing began (Tarantino and Mongiovì, 2003, Bagheri, 2018, Bagheri et al., 2018). After the HCTs reached equilibrium in the free water, each HCT was pre-conditioned in a series of -200 kPa up to -1000 kPa so that any possible changes in their performance could be accounted for.

The initial water contents (37 – 28%) of the specimens were selected based on the information obtained from the developed Soil Water Retention Curve (SWRC) for Bank Station London Clay (see figure 3.1). Furthermore, the water contents were selected so comparisons can be made regarding the unsaturated behaviour of London clay specimens in the literature and to see if the suction values alter across the London Clay formation.

3.2.2.2. Calibration of HCTs

In theory, tensiometers should be calibrated in negative pressure to measure the soil's suction values. However, the calibration in this negative range is difficult when applying high pressures; therefore, the most common method of calibration is carried out in a positive range, and linear extrapolation to the calibration equation is established for the negative range (Lourenço et al., 2008). The process for the calibration of the HCTs in a positive range was conducted by using a GDS pressure controller, which applies loading-unloading cycles to the HCTs within the saturation chamber in steps of 100 kPa and up to 900 kPa. A linear trend of the calibration data

is illustrated in figure 3.8 and an accurate calibration was conducted, which produced a small error in the range of 0.1 – 6.3%.

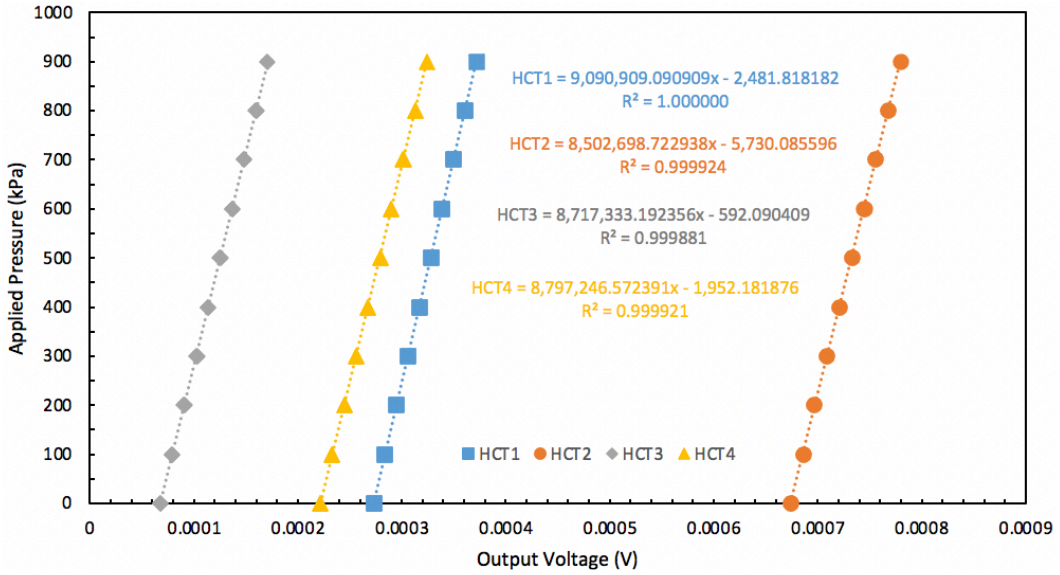

Figure 3.8 - Calibration of the HCTs used in the study.

3.2.3. Thermal oedometer

A series of temperature-controlled oedometer tests were performed using a conventional oedometer cell which was modified to investigate the influence of temperature (figure 3.9). The temperature-controlled oedometer cells were used to analyse the effect of four temperature intervals (20, 35, 45, and 55°C) which represent the typical temperatures surrounding energy geo-structures.

The temperature-controlled oedometer cells contained a conventional oedometer cell body with a confining ring of 75 mm diameter and 20 mm height; and two saturated porous disks placed below the specimen and below the loading cap, which allowed for drainage. To apply heat to the samples during oedometer tests, a 12Vdc RS PRO silicone heater mat (245-607) which was placed at the bottom of the cell using the adhesive backing measuring 100 mm in diameter. A 30V variable power supply controlled the heating of the cell. The temperature of the mat and the cell was controlled by two J-type thermocouples placed inside the cell close to the specimen and the second-placed close to the heating mat. The signal feedback from

the thermocouples allowed for constant temperature monitoring using a digital thermometer. The specimen's displacement was obtained using a linear vertical displacement transducer (LVDT) which contained a travel length of 10 mm and had an accuracy of 0.001 mm, which allowed for data acquisition to be recorded using a GEODATALOG 8 channel and a DATACOM2 software.

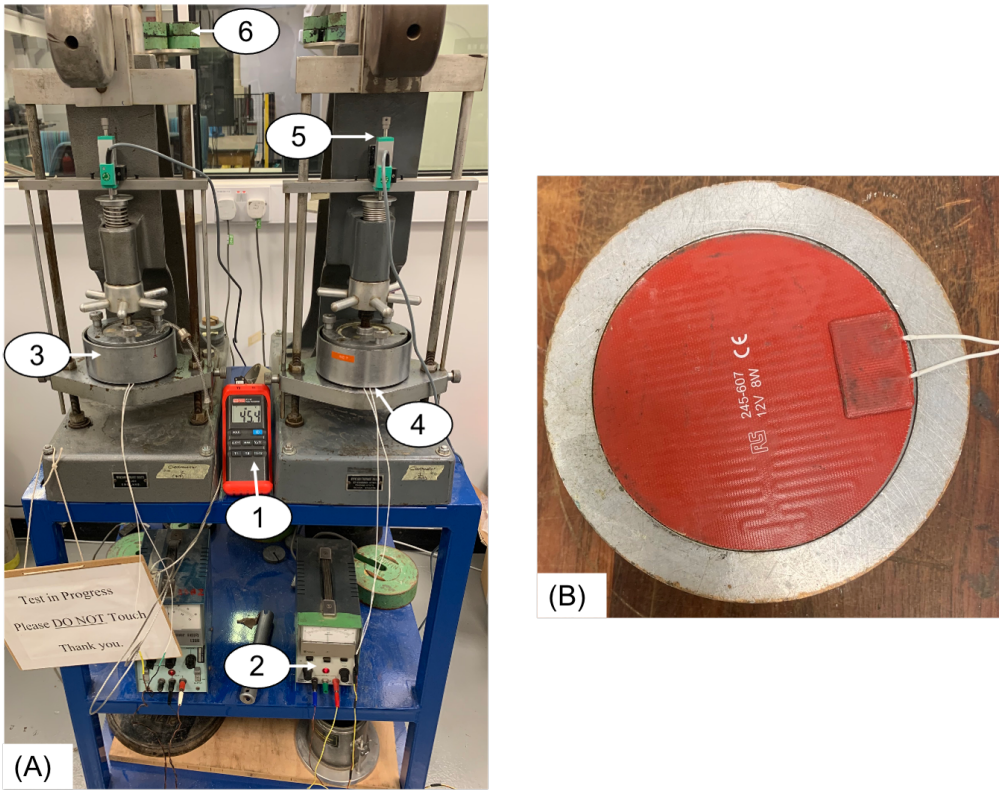

Figure 3.9 - Experimental set up of the temperature-controlled oedometer tests. (A) The setup of the equipment: 1) Digital thermometer with J-type thermocouple attached, 2) Power Supply, 3) Oedometer cell, 4) Heating mat stuck to the bottom of the oedometer, 5) LVDT, 6) Dead weights (load applied); (B) The top view of the adhesive heating mat stuck to the bottom of the oedometer.

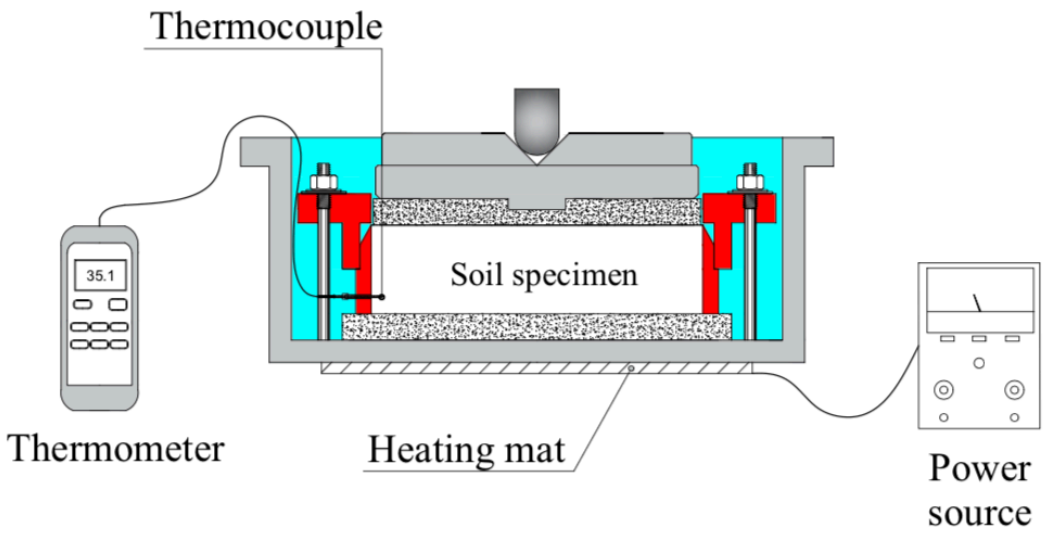

Figure 3.10 - Schematic diagram of the temperature-controlled oedometer cell.

3.2.3.1. Saturated Thermal Test Set-up

The test procedure of the unsaturated MSL oedometer tests is similar to that of the saturated oedometer MSL tests explained in section 3.2.1.1. Before starting each test, the target temperature of the heat mat is obtained by using an external power source to increase the temperature. Once the target temperature is reached, it is allowed to maintain that temperature overnight before each temperature-controlled oedometer test begins. Once the target temperature had reached equilibrium, the specimens were placed in the temperature-controlled cells with a porous disk placed above and below the specimen to allow for drainage. After preparing the oedometer specimens for testing and being placed in the oedometer cells, the specimens were allowed to reach equilibrium overnight under the weight of the loading cap and the hanger, and the LVDT recorded any swelling or compression. The heating was maintained constant throughout the experiments, and any water loss from the cell due to the evaporation was compensated by topping up the cell with water pre-heated to the test temperature.

3.2.3.2. Calibration of the Thermal Oedometer Cell

As the cell was influenced by temperature, and analysis of the thermal deformation of the cell had to be completed. The calibration process is completed by imposing the tested temperature intervals on the cell, and each interval is maintained for one hour to ensure the cell and specimen reach equilibrium. To ensure the correct temperature was being supplied from the power supply, a calibrated thermocouple probe was inserted close to the specimen. This constantly monitor the cell temperature throughout each test. From the calibration of the temperature-controlled cell, it can be seen that the oedometer did not undergo any thermal dilation or contraction when increasing or decreasing the temperature; therefore, the temperature effect on the cell was negligible (figure 3.11a). The accuracy of the temperature in the cell and the constant temperature monitoring using two thermocouples allowed the verification of the temperature imposed on the cell specimen (figure 3.11b).

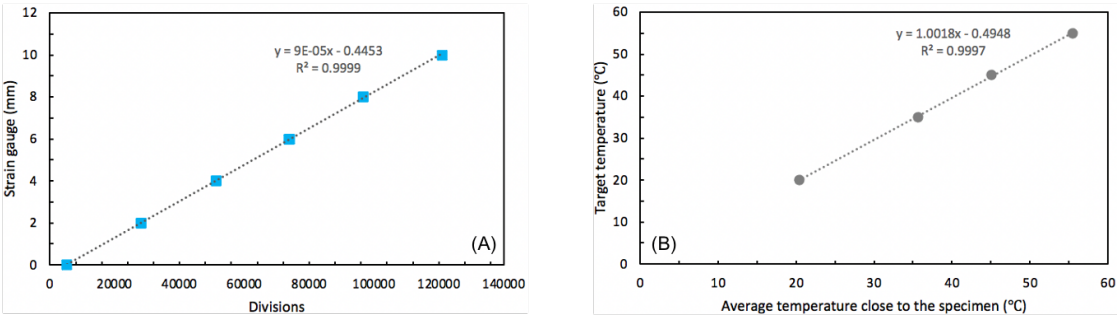

Figure 3.11 - (A) LVDT displacement during temperature calibration at 55°C and (B) the temperature recorded by the thermocouple close to the specimen.

During the testing of the thermal MSL experiments, the thermocouples monitored the temperature close to the specimen for the duration of the tests. The initial phase of the tests was measured on an hourly time scale, then increasing the timescale to twelve-hour intervals. From the monitoring of this data, it can be verified that the temperature stayed within the intended target temperature range and, therefore, validated the use of the power source and heat mat for thermal oedometer testing (figure 3.12).

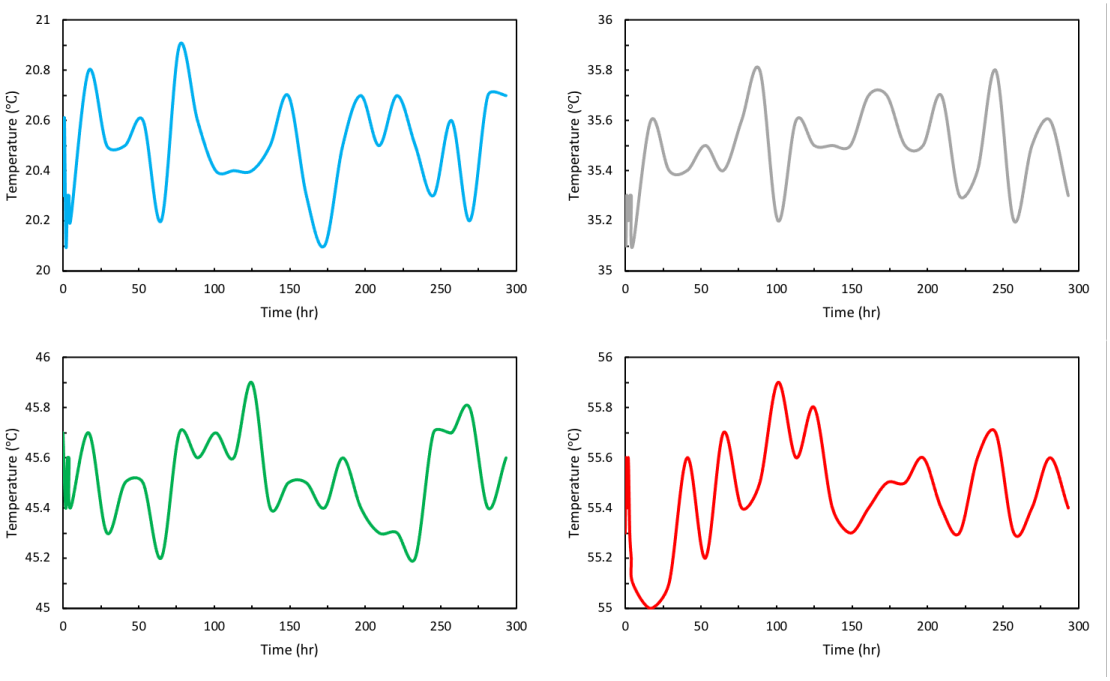

Figure 3.12 - Temperature fluctuations monitored from the thermocouples during the MSL tests.

3.3. CRS test set up

The CRS cell used in this study was designed by Bagheri et al. (2020) and was installed on a load frame-based system that contained a velocity-controlled loading piston. The loading frame from Wykeham Farrance had a maximum load capacity of 50 kN and a velocity range from 0.00001 to 50.8 mm/min. As stated by Bagheri et al. (2020), the cell was designed to satisfy the k_0 conditions and allowed for a specimen measuring 95 mm in diameter and 35 mm in height which is compatible with the dimensions stated by the ASTM standard for consolidation testing (ASTM D4186 (2006). The cell contained a 25 mm travel length linear potentiometric transducer (LPT) placed on the top platen of the cell for measuring axial strain. The axial force was measured by a 25 kN submersible load cell guided through a ball bearing shaft on the top platen of the cell. A loading cap was used to minimise the disturbance to the specimen. A 1 MPa pore-water pressure transducer (PWPT) was placed at the base of the specimen and was used to measure the pore-water generation. At the base of the cell, there is a 1.5 MPa porous disk at the bottom of the specimen with a porous stone placed at the top of the specimen to allow for a uniform disrupted load. A WATROD double-ended tubular heater element placed at the base of the cell and

two J-type thermocouples for measurement and monitoring of temperature variations on the cell's body and inside the specimen. One thermocouple was placed at a position close to the specimen inside the cell, and the second one was placed by the heater element. The signal feedback obtained from the thermocouple positioned by the heater element was used to keep the temperature constant by acting on the thermostat in the control unit. A GEODATALOG 8 channel was used to record the data obtained from the load cell, LPT, and PWPT (figure 3.13).

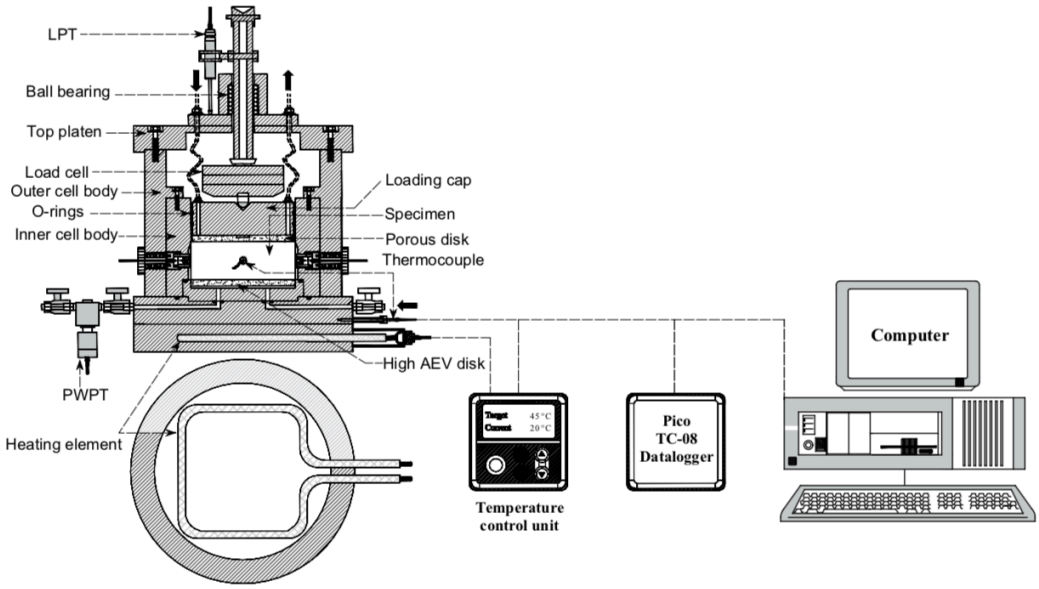

Figure 3.13 - Schematic diagram of the CRS cell structure and components (modified from Bagheri 2018).

3.3.1. Saturated Thermal CRS Test Set-up

Undrained CRS compression tests with continuous pore-water pressure monitoring were carried out on saturated reconstituted Bank Station London clay specimens prepared following the procedure explained in section 3.1.3. The CRS specimens had a dimension of 95 mm in diameter and 35 mm in height and were obtained by penetrating the cutting ring into the reconstituted soil cake. Before commencing each experiment, the preparation of the cell was carried out which involved the drainage lines and the PWPT were de-aired through vacuum and filled with de-aired water. Both upper and lower porous disks were also saturated by soaking them in

distilled water prior to testing. The thermostat was set to the target temperature and began to heat the cell. The prepared specimen in the cutting ring was then placed inside the cell chamber with a thin coat of hylosil instant gasket gel applied to the circumference of the cutting ring. The thin coat of gasket gel ensured there was full contact between the cutting ring and the lower porous disk and to avoid leakage of the pore-water pressure generation during the experiments. The loading cap, with its O-rings, was lubricated and positioned on top of the specimen, and the load cell, together with the top platen, was placed and fastened. The cell was set up on the load frame, and initial vertical stress of 10 kPa was applied to the specimen to eliminate any possible bedding effects. Axial load was applied to the specimen from the piston moving upwards at a constant rate of displacement, compressing the specimen. The selection of the strain rate (displacement rate) was determined by the ASTM D4186 (2006), which suggests the maximum value for strain rate to be used in CSR testing must be limited to a value such that the excess pore-water pressure/total stress ratio (PP_{ratio}) is less than 3 – 15% as this would allow for the strain rate to be reflective of what the soil experiences in the field and to allow for the generation of excess pore-water pressure to be controlled.

3.3.2. Calibration of the CRS Cell

Before any CRS tests began, a rigorous calibration process of the transducers was undertaken.

A simple calibration process was completed on the CRS cell to account for the effect of temperature on the axial strains. The cell was subjected to a heating cycle of 20 to 55°C in steps of 10°C, which correspond to the tested temperature intervals, and the corresponding axial deformation due to the thermal application was measured by the LPT. The values obtained from the LPT are negative with an increase in temperature, indicating the cell's thermal dilation during compression. The values of deformation obtained at each temperature interval were used to correct the measurements for the final values from the test programme (figure 3.14).

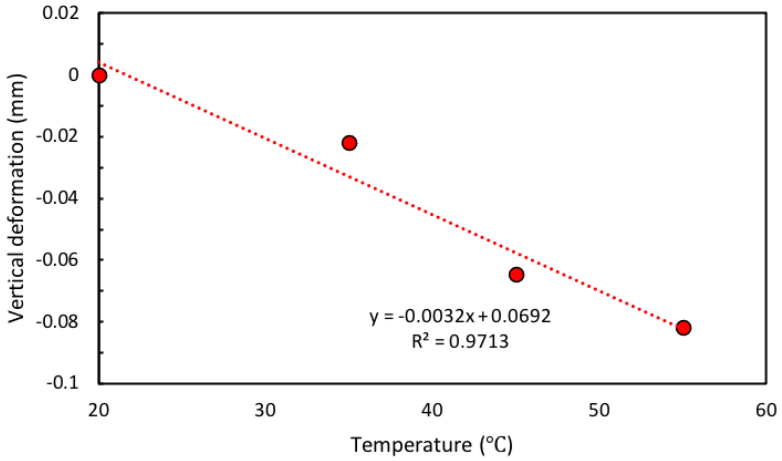

Figure 3.14 - Effect of temperature on the measured axial deformation of the CRS cell.

For monitor cell temperature during the CRS tests; two thermocouples were used to ensure the accuracy of the predefined target temperature. The first thermocouple was used to monitor the specimen's temperature and relay the data back to a Pico TC-08 Datalogger, and the second thermocouple monitored the heating system. Due to the difference in thermal conductivity of the cell and the soil specimen, a delay in the thermal equilibrium was displayed between the two. With the time lag, prior to each test, the temperature control unit applied the predefined temperature and was allowed to reach thermal equilibrium. This ensured no difference between the temperature being applied and the temperature of the soil specimen. Furthermore, the temperature of the tests was constantly monitored using a Pico TC-08 Datalogger to verify that the correct temperature was being applied (figure 3.15).

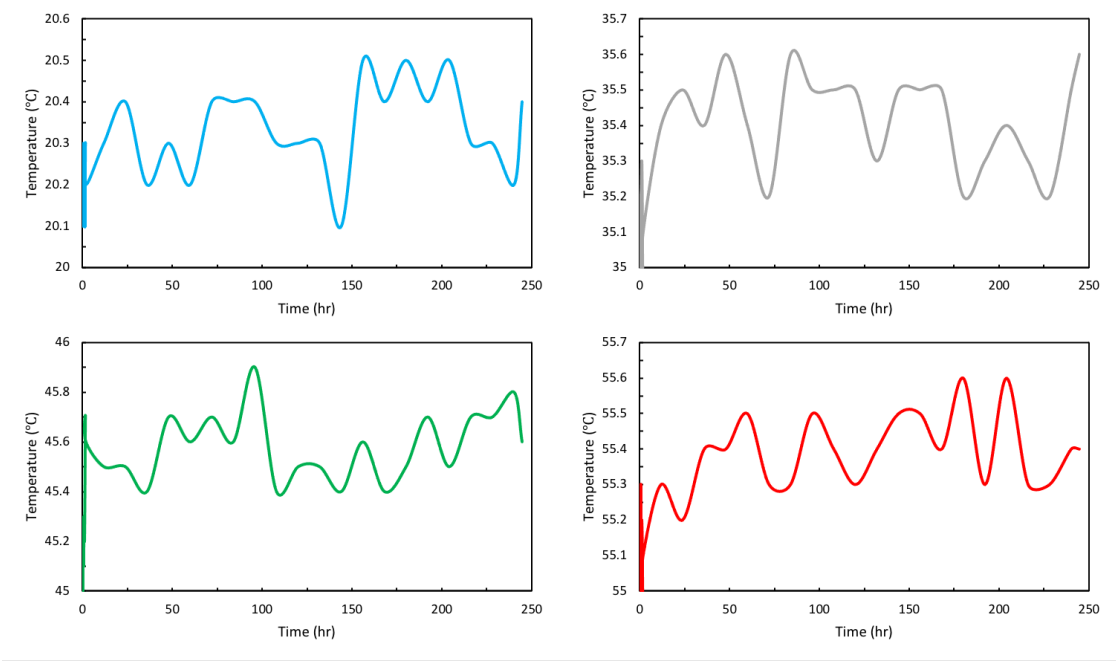

Figure 3.15 - The temperature monitored from the CRS tests obtained from the Pico TC-08 Datalogger.

3.4. Test Programme

An in-depth experiment program was performed by building on the research conducted by Bagheri (2018). The experimental program relied on conventional and advanced laboratory testing equipment. The influence of temperature on the viscous behaviour of saturated clays was investigated, along with the characterisation of the viscous behaviour in an unsaturated state (it must be noted that the 'unsaturated state' termed in this research study is reference to the soils 'partially saturated state'). The viscous behaviour analysed in this thesis includes creep, stress relaxation, and strain rate dependency during Thermo-Mechanical (TM) testing.

To achieve the objectives outlined in Section 1.2, three pieces of equipment were used to investigate the viscous behaviour: (i) an unsaturated oedometer cell comprising two high capacity tensiometers on the loading cap, which allowed for suction to be monitored on unsaturated specimens; (ii) an oedometer cell which contained a heating mat at the base to allow for THM analysis on saturated specimens; (iii) an advanced temperature-controlled CRS oedometer cell, which enabled the coupled effects of strain rate and temperature on the compression and

relaxation responses of the saturated specimens. The experimental program followed in this research is outlined as follows;

I. Conventional MSL oedometer tests on saturated and unsaturated specimens;
II. Thermal MSL oedometer tests at different temperatures on saturated specimens;
III. CRS oedometer tests at different strain rates and temperatures involving stages of stress relaxation.

All the thermal temperature tests were conducted over a range of 20 - 55°C corresponding to shallow burial geo-structures.

Due to COVID 19, the in-depth experimental program had to be modified to fit the new timescale. Therefore, the research study was unable to conduct all the tests as intended. Please refer back to the COVID19 Statement at the beginning of the thesis for more detail.

3.4.1. MSL oedometer tests

10 saturated and 12 unsaturated Multi-Stage Loading (MSL) oedometer tests were completed on reconstituted Bank Station London clay specimens at room temperature in this study. The specimens were tested across six different water contents (w_o), whereby the vertical stresses applied to samples ranged between 10 and 1280 kPa. The experimental programme consists of two series (table 3.5).

- *Series 1:* Tests MSLs43 to MSLs39 aim to determine, in the saturated state, the compressibility parameters (C_c, C_s, σ_p) and the creep behaviour ($C_{\alpha e}$). Each stage of loading and unloading was maintained for 24-hours to ensure primary and secondary consolidation parameters could be studied. The compressibility curves obtained from the tests are presented in an $e - \log \sigma'_v$ plot.

- *Series 2:* Tests MSLu37 to MSLu28 aim to determine, in an unsaturated state, the compressibility parameters (C_c, C_s, σ_p) and the creep behaviour ($C_{\alpha e}$). The same loading regime and timings were used as for Series 1 testing. The compressibility curves obtained from the tests are presented in a $e - \log \sigma'_v$ plot and the suction values obtained are presented in a $s - T_{hr}$ plot.

Table 3.5 - Experimental programme of MSL oedometer tests.

Series No.	Test No.	Load/unload sequence (kPa)	Duration (Days)	Suction (s) (kPa)
1	MSLs43-1	10-20-40-80-160-320-640-1280-640-320-160-80	12	-
	MSLs43-2			-
	MSLs43-4			-
	MSLs43-5			-
	MSLs43-6			-
	MSLs39-1			-
	MSLs39-2			-
	MSLs39-3			-
	MSLs39-4			-
2	MSLu37-1	10-20-40-80-160-320-640-1280-640-320-160-80	12	83
	MSLu37-2			
	MSLu37-3			
	MSLu35-1			120
	MSLu35-2			
	MSLu35-3			
	MSLu32-1			229
	MSLu32-2			
	MSLu32-3			
	MSLu28-1			507
	MSLu28-2			
	MSLu28-3			

The nomenclature chosen for MSL oedometer tests is described by the following letters. The letters “MSL” represent multi-staged loading, letters “s” and “u” represent saturated and unsaturated conditions, the initial water content values are represented by the number prior to the dash and the number after the dash represents the test number for tests with identical initial conditions.

3.4.2. Thermo-Mechanical Oedometer Tests

The thermo-mechanical oedometer experimental programme consists of 8 MSL tests completed using saturated reconstituted Bank Station London clay specimens. The tests were completed at four different temperatures ranging from 20°C to 55°C, and the vertical stress imposed was between 10 to 1280 kPa, and at one water content (39%). The stresses and temperature values are typical shallow depth waste repositories. This experimental programme will supplement the thermal CRS tests (section 3.4.3). The experimental programme consists of the following (Table 3.6):

- *Series 1:* Tests MSL20 to MSL55 aim to determine, the effect of temperature on the compressibility parameters (C_c, C_s, σ_p) and the creep behaviour ($C_{\alpha e}$). The specimens were loaded in stages from 10 to 1280 kPa (as stated in section 3.2.1.1).

Table 3.6 - Experimental programme of the thermal oedometer tests.

Test No.	Water content (w_o)(%)	Load/unload sequence (kPa)	Temperature (°C)	Duration (Days)
MSL20-1 MSL20-2	39	10-20-40-80-160-320-640-1280-640-320-160-80	20	12
MSL35-1 MSL35-2			35	
MSL45-1 MSL45-2			45	
MSL55-1 MSL55-2			55	
Note: Due to COVID19, there was no possibility to perform a third thermal MSL tests. Additionally, the reduced testing programme meant thermal unsaturated MSL tests could not be performed.				

The following letters describe the nomenclature chosen for MSL thermal oedometer tests. The letters “MSL” represent multi-staged loading, temperature intervals are represented by the number prior to the dash, and the number after the dash represents the test number for tests with identical initial conditions.

3.4.3. Thermal CRS tests

The thermal CRS tests completed in this study are split into two sections: (1) Single-staged compression relaxation tests and (2) Multi-staged compression relaxation tests. Both of the tests mentioned were completed using reconstituted saturated Bank Station London Clay specimens under an undrained condition, four different temperatures and three different strain rates (which have been previously used on London Clay specimens). The thermal CRS testing programme consists of 24 single-stage compression relaxation tests (SS-CRS) and 16 multi-staged compression relaxations tests (MSCRS), with both tests containing a 24- and 48-hour relaxation. The experimental programme consists of two series (table 3.7a-b).

- *Series 1:* A total of 24 single-staged compression relaxation tests (SS-CRS) were performed on the reconstituted Bank Station specimens across three different strain rates (ε_v = 0.01, 0.005 and 0.001 mm/min) and four different temperatures (20, 35, 45 and 55°C). Only 12 SS-CRS 48-hour relaxation tests were present in this study. The SS-CRS tests contained two stages: (1) specimen was loaded at a constant rate of displacement until reaching maximum load limit ≅ 3500 kPa, and (2) stress relaxation at zero rate of axial displacement for 48 hours immediately after the specimen reached the maximum load. The aim of the tests was to determine the effect of temperature and strain rate on the compression and relaxation responses of the Bank Station specimens.
- *Series 2:* A total of 16 multi-staged compression relaxation tests (MSCRS) were performed on the reconstituted Bank Station specimens across two strain rates (0.005 and 0.001 mm/min), and four different temperatures (20, 35, 45 and 55°C). The MSCRS tests comprised five stress relaxation intervals that were determined by the total deformation of the specimen from the SS-CRS tests and divided into five equal strain intervals. The specimen undergoing stress relaxation in this experimental series contains both the 24- and 48-hour relaxation periods. The aim of the tests was to determine the

effect of temperature, the pre-relaxation strain level, and strain rate on the stress relaxation responses of Bank Station specimens.

Table 3.7a - Experimental programme of the thermal single-staged compression relaxation tests.

Test No.	Water content (w_o)(%)	Temperature (°C)	Strain rate (mm/min) (ε_v)	Relaxation period (hr)	PP_{ratio}
SS-CRS20-a	39	20	0.01	48	14.61
SS-CRS35-a		35			13.06
SS-CRS45-a		45			12.48
SS-CRS55-a		55			12.50
SS-CRS20-b	39	20	0.005	48	10.22
SS-CRS35-b		35			10.04
SS-CRS45-b		45			8.63
SS-CRS55-b		55			6.43
SS-CRS20-c	39	20	0.001	48	5.12
SS-CRS35-c		35			5.78
SS-CRS45-c		45			4.74
SS-CRS55-c		55			4.86

Table 3.7b- Experimental programme of the thermal multi-staged compression relaxation tests.

Test No.	Water content (w_o)(%)	Temperature (°C)	Strain rate (mm/min) (ε_v)	Pre-relaxation strain level (ε_r)(%)	Relaxation period (hr)
MSCRS20b-i	39	20	0.005	6, 12, 18, 24, 30	24
MSCRS35b-i		35			
MSCRS45b-i		45			
MSCRS55b-i		55			
MSCRS20c-i	39	20	0.001		
MSCRS35c-i		35			
MSCRS45c-i		45			
MSCRS55c-i		55			
MSCRS20b-ii	39	20	0.005	6, 12, 18, 24, 30	48
MSCSR35b-ii		35			
MSCRS45b-ii		45			
MSCRS55b-ii		55			
MSCRS20c-ii	39	20	0.001		
MSCRS35c-ii		35			
MSCRS45c-ii		45			
MSCRS55c-ii		55			

The following letters describe the nomenclature chosen for SS-CRS and MSCRS thermal CRS tests. For the SS-CRS tests, the letters “SS” indicates single-stage compression relaxation, the “CRS” after the dash represents the constant rate of strain, and the number represents the temperature interval. The letter after the dash represents strain rate, with “a” being 0.01 mm/min, “b” being 0.005 mm/min and “c” being 0.001 mm/min. For the MSCRS tests, the letters “MSCRS” represent the multi-staged compression relaxation constant rate of strain, the temperature interval is represented by the number, and the letters after the number “b” and “c” represent the strain rate. The letters “i” and “ii” after the dash represent 24- and 48-hour relaxation periods, respectively.

3.4.4. Theoretical Framework

In MSL oedometer tests the compression index (C_c), swelling index (C_s), and reloading index (C_r) were calculated as the slope of respectively normal consolidation line (NCL), swelling (unloading) line, and reloading line in e – log σ'_v space where e is void ratio and σ'_v is vertical effective stress. Apparent preconsolidation stress (σ_p) was obtained based on the Casagrande method, and the creep index ($C_{\alpha e}$) was calculated as the slope of the linear part of the void ratio versus logarithm of time (e – log t) graph from 6 – 24 hours during each load increment since the primary consolidation was found to be completed within the first 5 – 6 hours. The generation of the apparent preconsolidation stress (σ_p) was determined using the Casagrande (1936) method.

The C_c value is calculated as the slope of the NCL, and the yield vertical net stress (σ_p) is determined as the intersection of the best-fitted lines to the pseudoelastic and plastic sections of the compression curve. Bagheri et al. (2019) evaluated the stress relaxation process using three main parameters: the coefficient of relaxation (R_α), relaxed stress ($\Delta\sigma$), and the residual stress ratio (ξ). In stress relaxation stage of the CRS compression tests, the value of R_α can be determined as the slope of the plot of σ_{vnet} versus time (t) in log σ_v – log t space

$$R_\alpha = -\frac{\Delta log\ (\sigma_{vnet})}{\Delta log\ (t)} \tag{17}$$

The relaxed stress ($\Delta\sigma$) is defined as

$$\Delta\sigma = \sigma_0 - \sigma_s \tag{18}$$

The stress value at the end of the relaxation stage is known as the residual total vertical stress (σ_s). The ratio of σ_s to pre-relaxation total vertical stress (σ_0) is defined as the stress ratio

$$\xi = \frac{\sigma_s}{\sigma_0} \tag{29}$$

Chapter Four – Oedometer Tests

4.1. Time-Dependency in Saturated and Unsaturated Conditions

4.1.1. Saturated MSL Oedometer Tests

This section presents details of an investigation into the behaviour of saturated reconstituted Bank Station London clay specimens through conventional MSL oedometer tests using the information in table 3.5 in section 3.4.1. The tests aimed to understand the effect of water content on the compressibility parameters and the creep rate. The findings found within this section will provide a basis for which the experimental programme of this study is conducted upon.

4.1.1.1. Compressibility of Saturated Specimens

Figure 4.1 presents the normalised compression curves for saturated reconstituted Bank Station London clay specimens. As can be seen, a decrease in the water content results in a reduction in the compressibility of the specimens by 9.51%. Figure 4.1 illustrates that a decrease in the water content causes a reduction in void ratio, which causes an increase in the apparent preconsolidation stress by 17.20%. The change from 43 to 39% w_o (MSLs43 to MSLs39) results in the average apparent preconsolidation stress increase from 93 to 109 kPa. MSLs39 tests were characterised by average C_c and C_s values of 0.387 and 0.095, respectively, which were obtained from the compression tests on reconstituted specimens having an initial void ratio of 1.19 and initial water content of 39%. For MSLs43 tests, which had an initial water content of 43%, average C_c and C_s values of 0.412 and 0.098, respectively, were measured. Similar C_c and C_s values were reported in the literature; for example, Gasparre (2005) reported C_c and C_s values to be 0.386 and 0.148, respectively, for the Heathrow Terminal 5 site, and Sorensen (2006) also reported C_c values to be in the range of 0.41 – 0.51 for reconstituted Heathrow

Terminal 5 specimens. In the Eastern part of the London Basin, Rezania et al. (2020) reported C_c and C_s values to be 0.383 and 0.125 for reconstituted Sheppey London clay with a moisture content of 39%.

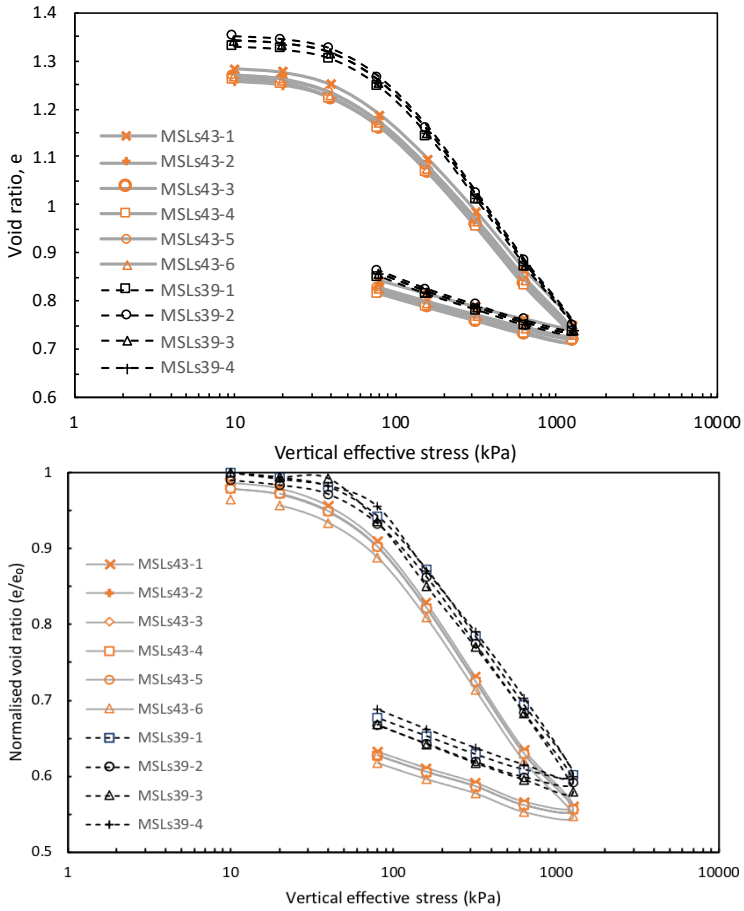

Figure 4.1 - Compression curves of saturated MSL oedometer tests for reconstituted Bank Station London clay specimens.

4.1.1.2. Stress-Dependency of the Compression Index

Further analysis of the compressibility of saturated specimens can be evaluated by the variation of the compression index with vertical effective stress. The compression index can be calculated at each load increment (C_c^*) using as $\Delta e/\Delta \log \sigma_v'$, with Δe being the change of void ratio over one load increment and $\Delta \log \sigma_v'$ being the change in effective stress over the same load increment. Figure 4.2 shows the saturated incremental compression index (C_c^*) against normalised stress σ_v'/σ_p. For values < 1 on the σ_v'/σ_p axis represent C_r and values > 1 on the σ_v'/σ_p axis represent C_c. As can be seen, the C_r values are gradually increasing before the apparent preconsolidation stress. Following σ_p, the values of C_c appear to be affected by the water content of

the specimen. As it can be seen, the MSLs39 test specimens show a slight decrease before a sharp increase prior to the end of loading, whereas MSLs43 test specimens appear to increase slightly before a constant value of C_c. One anomaly is shown in figure 4.2, which is MSLs43-1, which shows a decrease in C_c as the end of loading is completed. It can be seen that the peak value for MSLs43 tests is at stress levels between (8-10) σ_p, apart from MSLs43-1, which is (2-4) σ_p, and the MSLs39 tests show peak values at stress levels between (10-13) σ_p. These results are consistent and similar to those seen by others (e.g., Bagheri (2018); Rezania et al. (2020)). The reason behind high values of C_c^* in the post apparent preconsolidation zone can be related to the degradation of inter-particle bonds occurring at higher vertical stress.

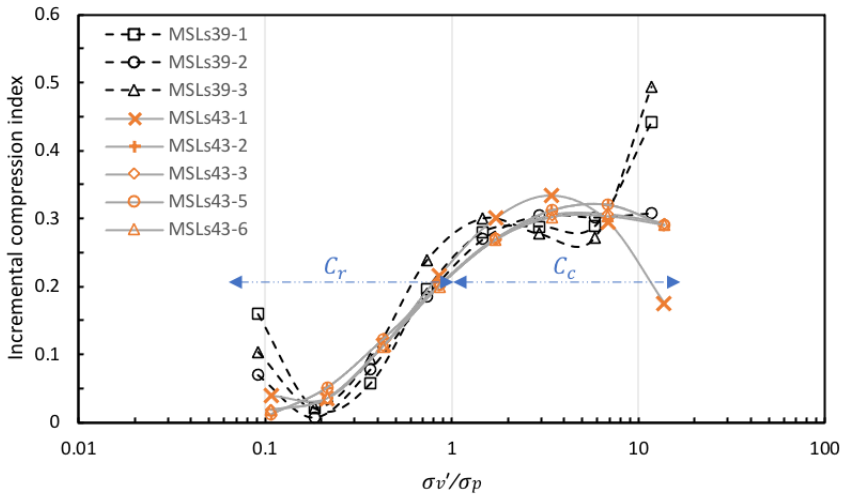

Figure 4.2 - Stress-dependency of the slope of compression (C_c^*) for saturated reconstituted Bank Station London clay specimens.

4.1.1.3. Stress-Dependency of the Secondary Consolidation Index

Figure 4.3 presents the variation of the secondary consolidation ($C_{\alpha e}$) with normalised stress σ_v'/σ_p for reconstituted specimens. The values of $C_{\alpha e}$ were determined between the 6 – 24-hour stage of the MSL oedometer tests after primary consolidation was reached. The variation in secondary consolidation was calculated as $\Delta e/\Delta \log t$, with Δe being the change of void ratio over one load increment and $\Delta \log t$ being the change in time over one load increment after the end of primary consolidation. For vertical stresses lower than apparent preconsolidation stress, $C_{\alpha e}$

increases slowly for specimens with w_o = 43%. For stresses in the normal consolidation zone (C_c), it can be seen that the MSLs43 test specimens reach the peak value at stress levels in a range of (2-13) σ_p. However, in the specimens with a lower water content (w_o = 39%), the variation of $C_{\alpha e}$ with normalised stress is slightly different, with $C_{\alpha e}$ increasing dramatically until reaching the peak value at stresses between (1-2) σ_p, then in the normal consolidation zone, $C_{\alpha e}$ values decrease sharply. The maximum value of $C_{\alpha e}$ falls approximately in the range of 0.018 – 0.019 for w_o = 39% and 0.009 – 0.010 for w_o = 43%. These values are similar to the average values reported by Sorensen (2006), who found $C_{\alpha e}$ to be 0.016 for reconstituted London clay specimens from the Heathrow T5 project and by Bagheri (2018), who found $C_{\alpha e}$ to be in the range of 0.012 – 0.013 for reconstituted Sheppey London clay.

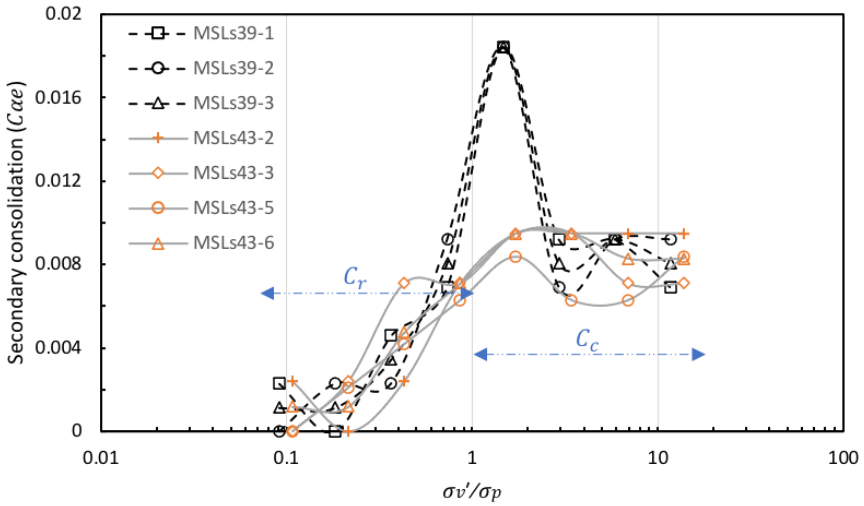

Figure 4.3 - Stress-dependency of the secondary consolidation parameter ($C_{\alpha e}$) for reconstituted Bank Station London clay specimens.

4.1.1.4. $C_{\alpha e}/C_c$ Ratio

Figure 4.4 presents the variation of the $C_{\alpha e}/C_c$ ratio with normalised stress σ'_v/σ_p for reconstituted specimens. As can be seen, the $C_{\alpha e}/C_c$ ratio is noticeably scattered at lower stresses (stresses lower than the apparent preconsolidation stress), which could be noted as experimental measurement errors. However, at higher stresses, the $C_{\alpha e}/C_c$ ratio values are less scattered and decrease gradually, with the α value ranging from 0.015 to 0.030 at the end of loading, apart from MSLs43-2, which contains an α value of 0.054 at the end of loading. It is noticeable that the specimens

with a lower water content (w_o = 39%) peak at a higher α value and define a less scattered trend compared with specimens with higher water content (w_o = 43%). Figure 4.4 illustrates that the $C_{\alpha e}/C_c$ ratio is stress-dependent and varies with effective stress and water content. The α values in this study are 1.69 to 2.13 times greater than the values reported by Bagheri (2018) for reconstituted Sheppey London clay specimens. The α values produced in this study provide sufficient evidence to disprove the hypothesis that the $C_{\alpha e}/C_c$ ratio is constant for clays. Furthermore, for the $C_{\alpha e}/C_c$ ratio to converge at a constant value, it would require larger stresses to cause degradation of the inter-particle bonds, and in this study, it was not possible to apply the stresses required due to the equipment used.

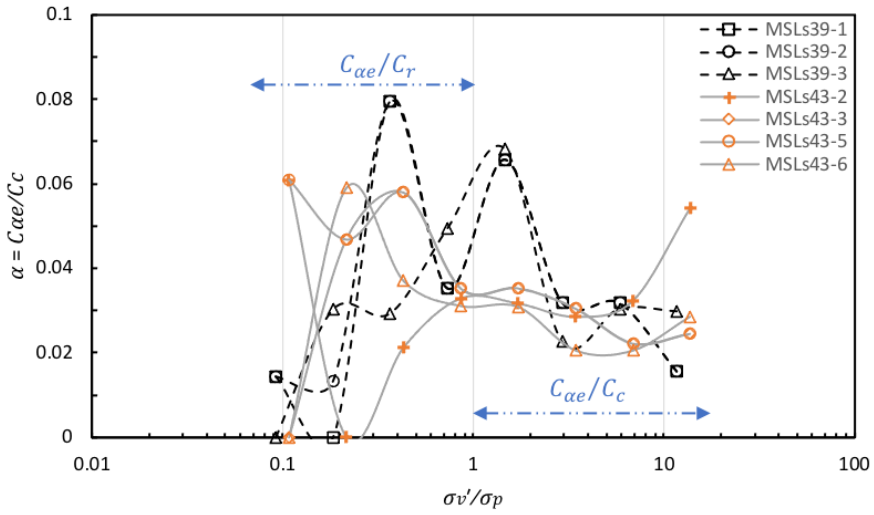

Figure 4.4 - Stress-dependency of the $C_{\alpha e}/C_c$ ratio for reconstituted Bank Station London clay specimens.

4.1.2. Unsaturated MSL Oedometer Tests

This section presents details of an investigation into the behaviour of unsaturated reconstituted Bank Station London clay specimens through advanced MSL oedometer tests using the information from table 3.5 in section 3.4.1. The tests aimed to understand the effect of suction on the compressibility parameters and creep rate. The findings presented in this section would allow for spatial comparison of the effect of suction on stiff clay specimens in the London Basin and further increase the limited knowledge of the mechanics of unsaturated clays.

4.1.2.1. Compressibility of Unsaturated Specimens

Figure 4.5 presents the normalised compression curves for unsaturated reconstituted Bank Station specimens. As can be seen, the influence of suction alters the location of the compression curves; an increase in suction and a decrease in water content results in the compression curves shifting upwards. An increase in suction results in a decrease in the overall compressibility of the specimen; for example, the increase of suction by 424 kPa from MSLu37 to MSLu28 causes the compressibility of the specimen to decrease by 31.19%. Furthermore, an increase in suction results in an increase in the apparent preconsolidation stress (figure 4.6) and this finding is supported by various authors in the literature (Wheeler and Sivakumar, 1995, Colmenares Montanez, 2002, Monroy, 2006, Haghighi, 2011, Rezania et al., 2020).

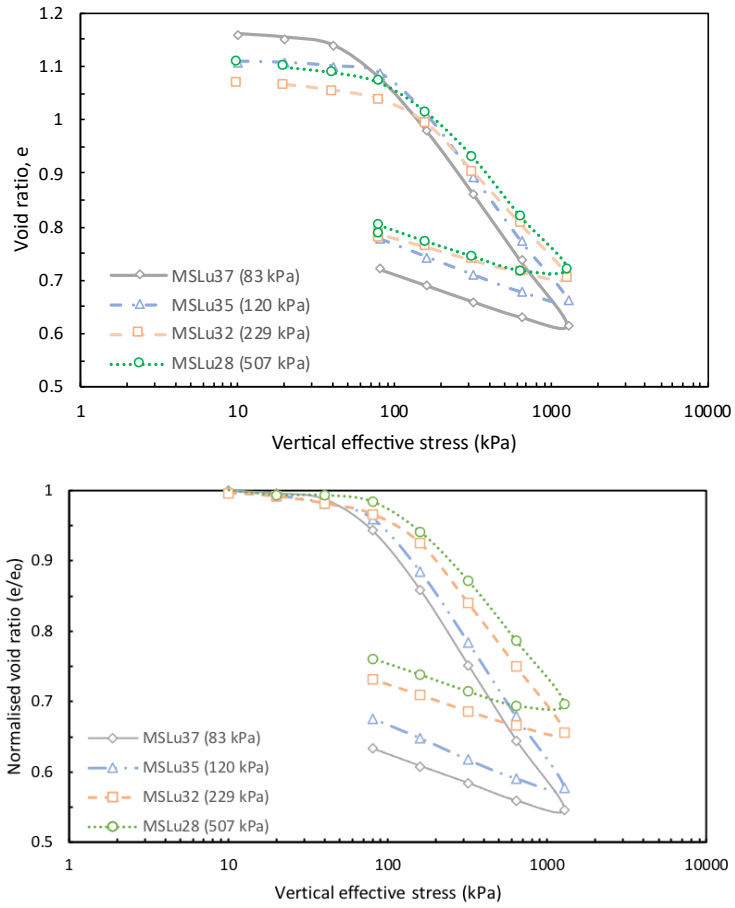

Figure 4.5 - Compression curves for unsaturated reconstituted Bank Station London clay specimens. (Note: only one compression curve of each unsaturated test is shown to allow the graph to be easily interpreted)

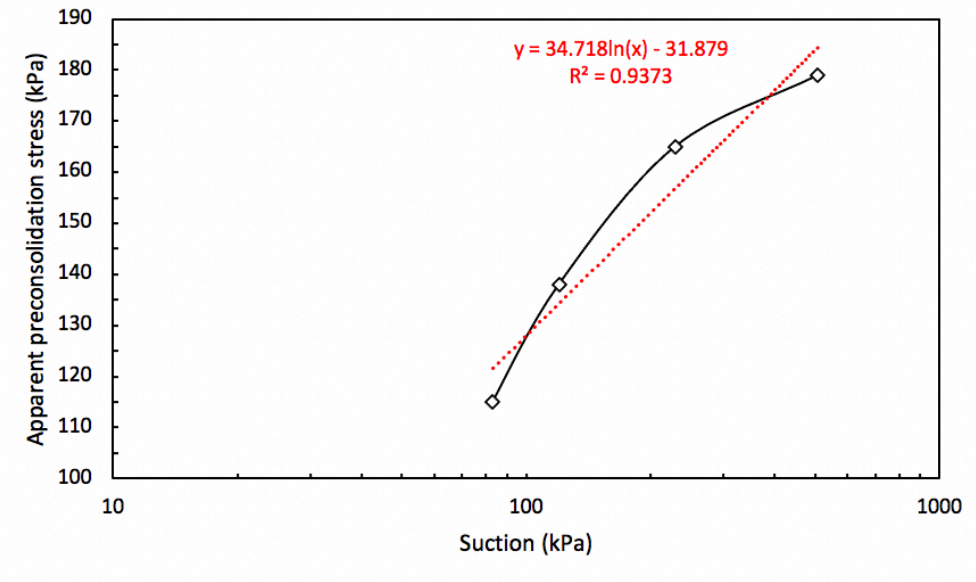

Figure 4.6 - Variation of apparent preconsolidation stress with suction.

To further investigate the effect of suction on the compressibility parameters, the values of C_c and C_s were calculated. It is evident in table 4.1 that a decrease in water content and an increase in suction results in the values of C_c decreasing. Overall, it can be stated that the values of C_s also decrease with an increase in suction. However, it is noted that between the MSLu37 and MSLu35 tests, there is a slight increase in C_s. Therefore, it can be found that C_c and C_s are dependent on suction.

Table 4.1 - Effect of suction on the C_c, C_s, and σ_p values (Note: the average values are reported here).

Test No.	Water content (w_o)(%)	Suction (kPa)	C_c	C_s	σ_p
MSLu37	37	83	0.3540	0.0869	115
MSLu35	35	120	0.3363	0.0888	138
MSLu32	32	229	0.2951	0.0834	165
MSLu28	28	507	0.2832	0.0727	179

Figure 4.7 presents the variation of pore-water pressure (u_w) during the loading and unloading stages of the MSLu37, MSLu35, MSLu32 and MSLu28 unsaturated oedometer tests. As can be seen in Figure 4.7, during the loading stages, the tensiometers recorded a sudden increase in u_w which resulted in a decrease in suction, followed by a gradual pressure equalisation after peak u_w was reached at

each loading stage. Furthermore, it can be seen that during all the loading stages, the suction state is preserved. Hence, it can be confirmed that the condition of constant water content was accepted throughout the experiment due to no water being expelled from the specimen. Equally, during the unloading stages, the tensiometers recorded a sudden decrease in u_w, which increased suction, followed by a gradual pressure equalisation after peak suction was reached at each unloading stage. The findings found in Figure 4.7 illustrate that the pore-fluid is compressible during consolidation. As in the unsaturated tests, there is a decrease in air volume and a reduction in void ratio due to an increase in the degree of saturation, which is consistent with the findings in the literature (Colmenares Montanez, 2002; Cuisinier and Laloui, 2004; Ileme, 2017; Bagheri, 2018; Rezania et al., 2020).

Moreover, it is evident that the greater increase in the load, the increase in the amount of pore-water pressure generated (decrease in suction). As can be seen in Figure 4.7, the variation in the pore-water pressure with vertical stress is low during the early stages of the MSL tests (load-interval < 160 kPa) but increases in higher stress states, as it is shown that at the 1280 kPa load-interval (168 hr), it contains the most significant spike in pore-water pressure generation. However, there is no clear trend between the initial suction and vertical stress during the 1280 kPa load-interval as the MSLu37, MSLu35, MSLu32, and MSLu28 tests record a variation of pore-water pressure of 491, 477, 151, and 509 kPa respectively. Similarly, during the unloading of the specimen, it is seen that the first unload stage provides the largest increase in suction in all tests apart from MSLu37, where the greatest increase in suction is at 240 hr.

During the recording of the pore-water pressure changes during the loading and unloading of the unsaturated oedometer tests, it was expected that the development of suction would be equal to the incremental unloading of the specimen (i.e., suction would be equal to the known effective stress value) (Ridley and Burland, 1993). It was expected during the unloading of the Bank Station specimens that similar outcomes would be seen. However, it was found that only one unload stage (the last unload stage - 80 kPa) would produce similar outcomes,

and this was found in the MSLu37 and MSLu28 tests. These findings were similar to Bagheri (2018), as it was seen that the tensiometer data would record suctions lower than the imposed effective stresses. The potential reasons for the behaviour observed could be linked to the confinement of the oedometer ring as only vertical swelling is permitted, which would allow the HCTs to record an instant response, or could be linked to the swelling of the specimen caused by air bubbles in the soil pores during unloading of the specimen (Ridley and Burland, 1993).

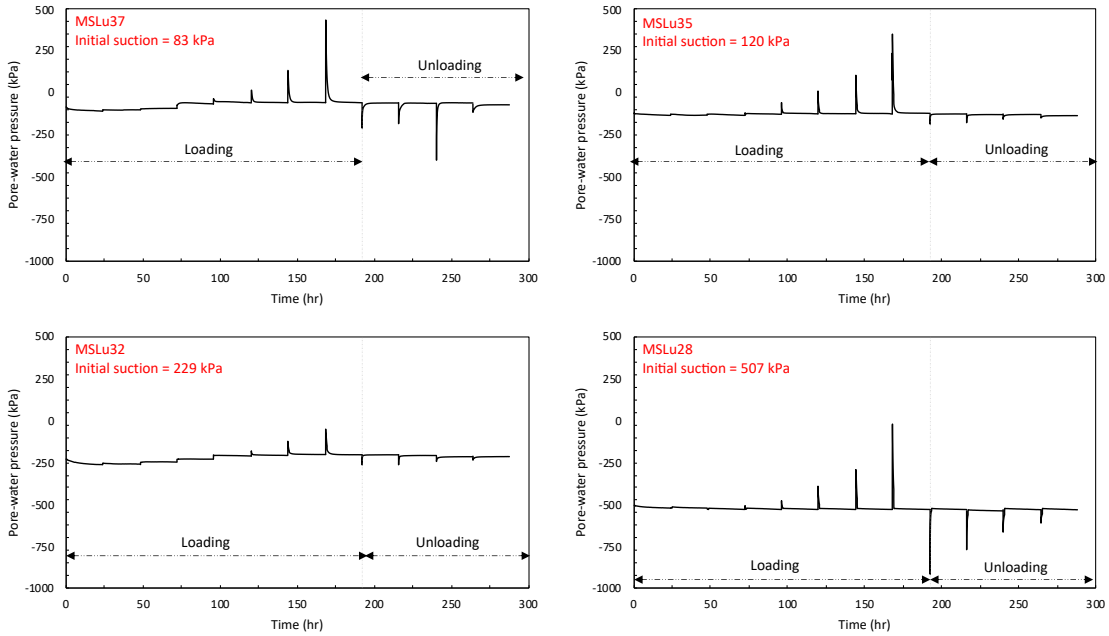

Figure 4.7 - Monitoring suction changes during the loading and unloading stages of unsaturated MSL oedometer tests.

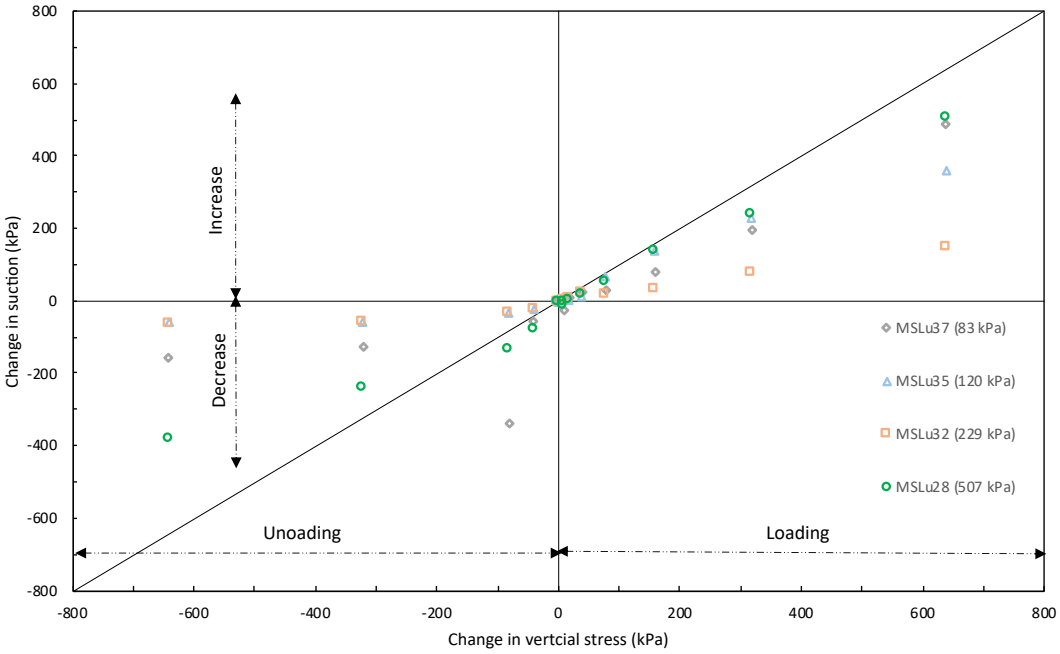

Figure 4.8 - Change in pore-water pressure at each load increment.

4.1.2.2. Suction-Dependency of the Compression Index

Figure 4.9 presents the relationship between the unsaturated compression index and applied vertical stress for unsaturated reconstituted Bank Station London clay specimens. Similar to the saturated reconstituted MSL tests, the compression index at each load increment (C_c^*) exhibited stress-dependency and increased with increased applied vertical stress. Similarly, like the saturated MSL tests, a peak value was observed, after which the C_c^* decreases. The findings found in figure 4.9 contradicts the results found by Rezania et al. (2020), who reported that there was no apparent peak value for the unsaturated reconstituted Sheppey London clay specimens. It can be observed that with an increase in suction, the decrease in C_c^* becomes more apparent at higher initial suction, as seen in MSLu35, MSLu32, and MSLu28 tests. Furthermore, the higher the initial suction, the higher the peak value of C_c^*, as the MSLu35, MSLu32, and MSLu28 tests reach a peak value at 640 kPa, whereas MSLu37 reaches peak value at 320 kPa. The findings reveal the suction- and stress-dependency of C_c^*.

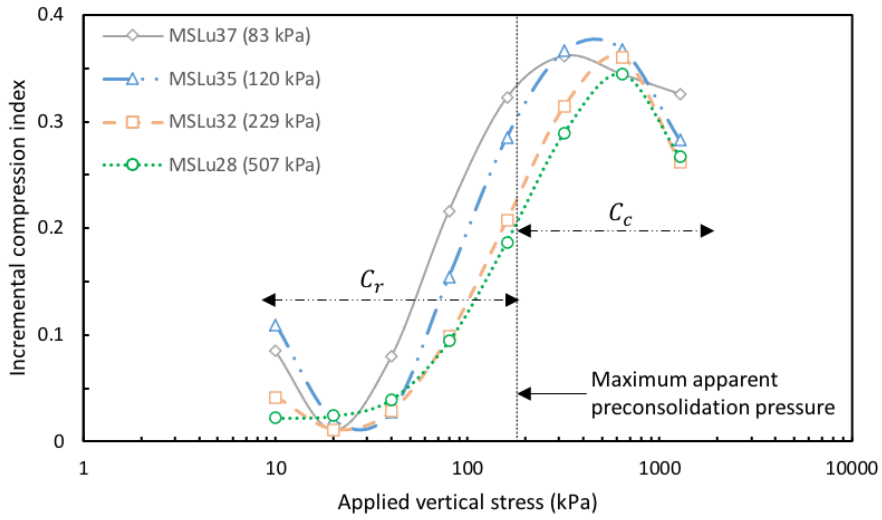

Figure 4.9 - Suction- and stress-dependency of the slope of compression for reconstituted Bank Station London clay specimens.

4.1.2.3. Suction-Dependency of the Secondary Consolidation Index

Figure 4.10 presents the relationship between the unsaturated secondary consolidation ($C_{\alpha e}$) and applied vertical stress for unsaturated reconstituted Bank Station London clay specimens. Similar to the saturated reconstituted MSL tests, the secondary consolidation ($C_{\alpha e}$) at each load increment exhibited stress-dependency and increased applied vertical stress. Unlike the study of Rezania et al. (2020), in figure 4.10, it is evident that a peak value can be observed, after which the $C_{\alpha e}$ value decreases. For tests MSLu37, MSLu35, MSLu32 and MSLu28, the peak value of $C_{\alpha e}$ appears at 160, 320, 80, and 640 kPa vertical total vertical stress, respectively. It can be seen that the change in initial suction (decrease in water content) causes the peak value of $C_{\alpha e}$ to be reached at higher stress when suction increases. However, in the MSLu32 tests, it is shown that the peak value of $C_{\alpha e}$ was reached at low stresses and is an anomaly to the trend.

Furthermore, it is observed that increase in suction results in a decrease of the $C_{\alpha e}$ values (apart from the anomaly MSLu32). At the end of loading, the values of $C_{\alpha e}$ appear to converge between 0.0066 – 0.0091. The findings of the $C_{\alpha e}$ results can be acknowledged by the development of tensile stress in the soil grains, which is generated by the water menisci at the inter-particle contacts developed due to the

negative pore-water pressure. Moreover, the extra forces being applied cause a reduction of particle rearrangement under constant vertical effective stress, which results in reduced soil creep with an increase in suction. The results illustrate the suction- and stress-dependency of $C_{\alpha e}$.

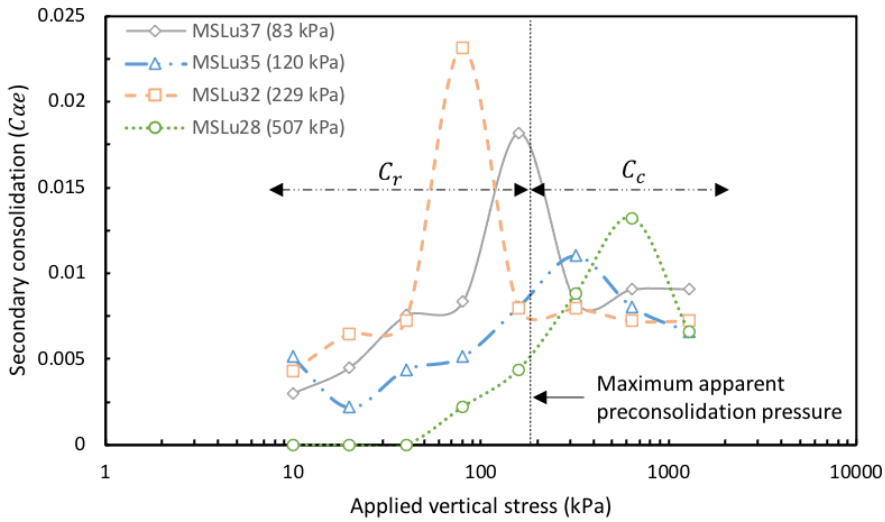

Figure 4.10 - Suction- and stress-dependency of $C_{\alpha e}$ for reconstituted Bank Station London clay specimens.

4.1.2.4. $C_{\alpha e}/C_c$ Ratio

Figure 4.11 presents the variation of the $C_{\alpha e}/C_c$ ratio with applied vertical stress for unsaturated reconstituted Bank Station London clay specimens. At low-stress levels (< 179 kPa), the values of $C_{\alpha e}/C_c$ decrease with an increase in applied total stresses, as supported in the literature (Rezania et al., 2020). At stresses exceeding the maximum apparent preconsolidation stress (> 179 kPa), it can be seen that the values of $C_{\alpha e}/C_c$ are slightly scattered but fall within a range of 0.019 – 0.038 with MSLu35 displaying values of α outside the range found. It is observed that the findings of the unsaturated α values appear to fall in a range similar to the one observed in saturated conditions (0.015 – 0.030) (figure 4.4). Furthermore, it can be observed that the unsaturated conditions illustrate a convergence and that the $C_{\alpha e}/C_c$ ratio is constant with an increase in stress level, whereas saturated conditions differ as there is no convergence or trend represented in the $C_{\alpha e}/C_c$ ratio. The values of the $C_{\alpha e}/C_c$ ratio appear to be similar to those reported for unsaturated reconstituted Sheppey

London clay by Rezania et al. (2020), who reported α to be within a range of 0.023 – 0.030. However, the findings also contradict the results of Rezania et al. (2020), who reported no convergence in the α value, but in figure 4.11, it is seen that there is a convergence in the α value.

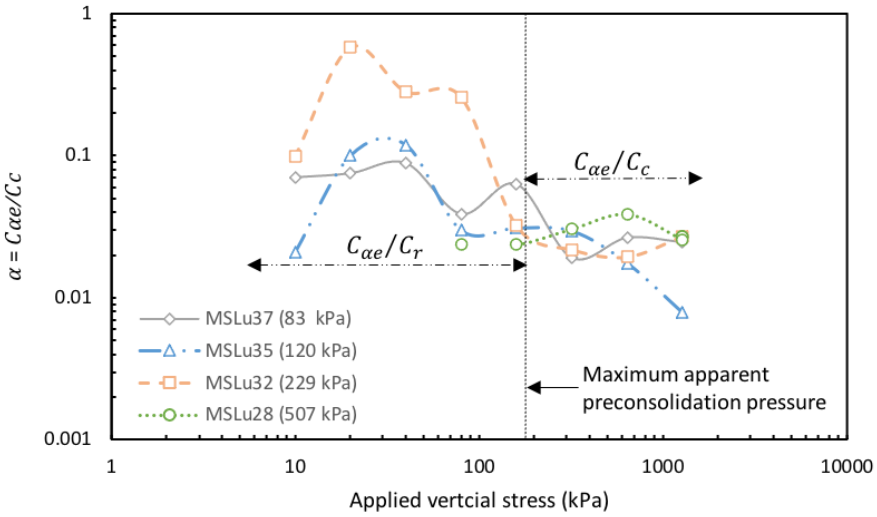

Figure 4.11 - Stress-dependency of the $C_{\alpha e}/C_c$ ratio for reconstituted Bank Station London clay specimens.

4.2. Thermal MSL Oedometer Tests

This section presents details of an investigation into the thermal-mechanical behaviour of reconstituted Bank Station London clay specimens through MSL oedometer tests using the information from table 3.6 in section 3.4.2.

4.2.1. Effect of Temperature on the Compressibility Behaviour

Figure 4.12 presents the normalised compression curves for saturated reconstituted Bank station London clay specimens under thermal conditions, using the details in table 3.6. It presents four compression curves plotted in an $e - \log \sigma'_v$ space. As can be seen, as temperature increases, the compression curves shift downwards. The overall compressibility of the specimens is seen to increase as temperature increases. The observation from figure 4.12 shows that the clays consolidation behaviour is temperature-dependent and promotes the hypothesis of thermal softening at higher temperatures, whereby the change in viscosity of pore-water alters the inter-particle

contact forces leading to higher deformability characteristics (Kaddouri et al., 2019, Lahoori et al., 2021).

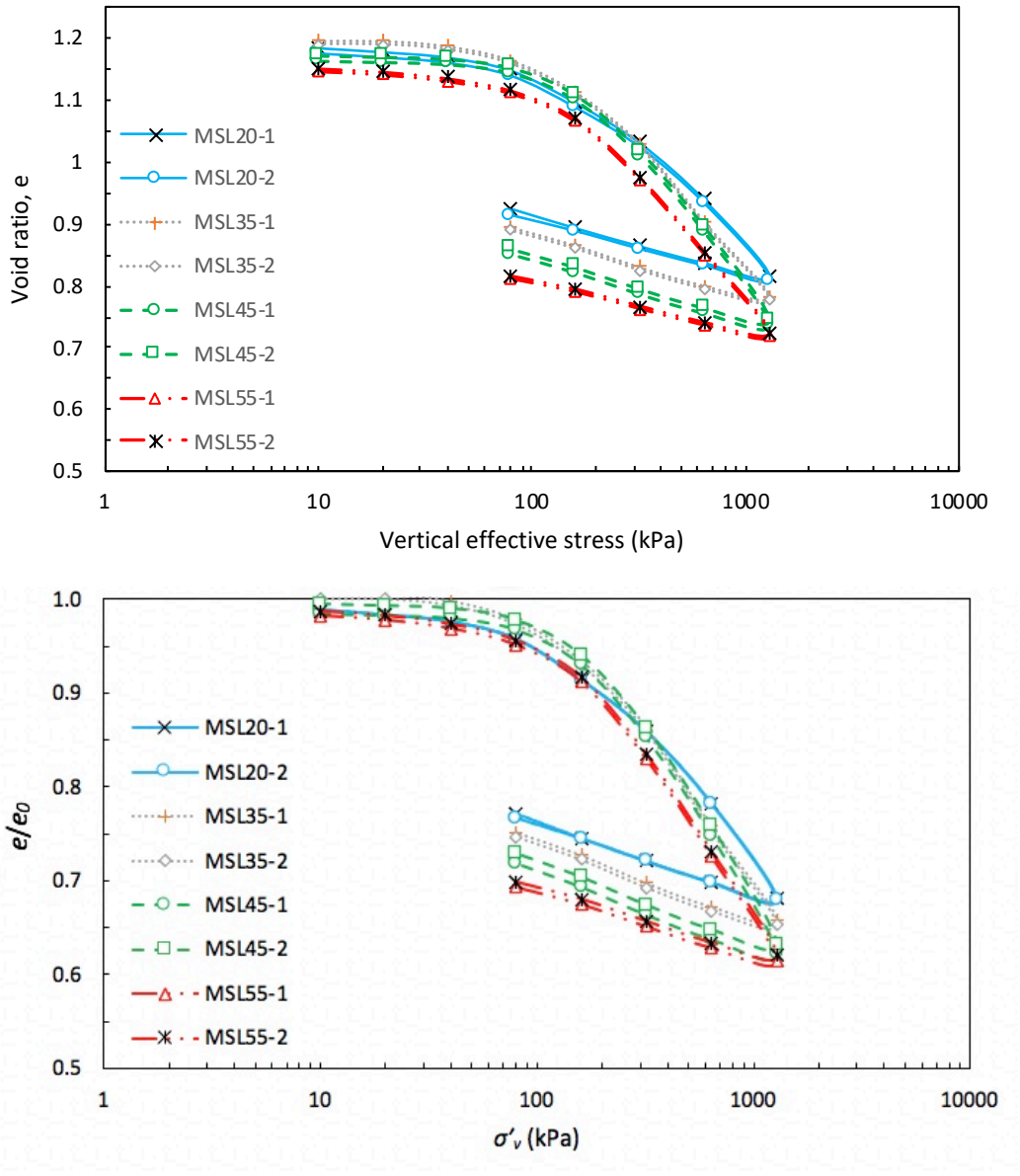

Figure 4.12 – Compression curves for reconstituted Bank Station London clay during thermal MSL oedometer tests.

Based on the compression curves in figure 4.12, the variation of the compression ($C_c = \Delta e/\Delta \log \sigma'_v$) and swelling index ($C_s = \Delta e/\Delta \log \sigma'_v$) were calculated (Table 4.2). Figure 4.13 presents the variation of the compression and swelling index with a temperature change. It can be seen that the range of C_c is between 0.338 to 0.347 and C_s between 0.077 to 0.089. Furthermore, increasing the temperature from 20 to 55°C appears to have a minimal impact on the C_c and C_s parameters. However,

increasing the temperature from 35 to 45°C shows a slight increase in the C_c and C_s values. Therefore, it can be stated that the compressibility parameters can be temperature-independent between 20 and 55°C. The slight variation of C_c and C_s values with an increase in temperature is consistent with literature data (explained in section 2.2.2). As it appears, the changes in C_c and C_s values with an increase in temperature may weaken the inter-particle and intra-particle bonds within the clay clusters resulting in a decrease in stiffness and hence, increased overall compression and swelling.

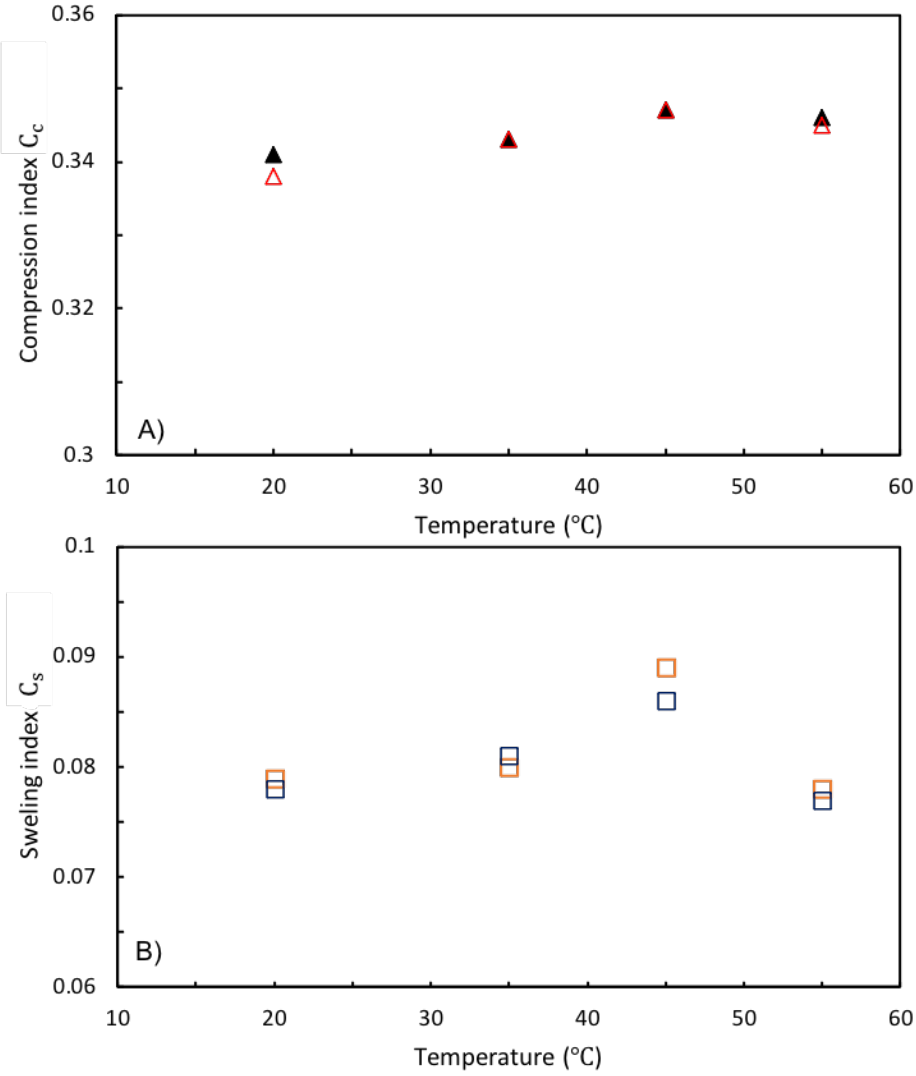

Figure 4.13 - Effect of temperature on the compressibility parameters: A) C_c and B) C_s for reconstituted Bank Station London clay specimens.

Figure 4.14 presents the relationship between temperature and the apparent preconsolidation (σ_p). The eight thermal MSL oedometer tests observed that the

higher the temperature, the lower the σ_p. It can be seen that the decrease in σ_p as the temperature is increased displays a linearly decreasing trend (R^2 = 0.95). Figure 4.14 shows that the increase in temperature from 20 to 55°C causes a reduction in σ_p by 24.02%. The results illustrated in figure 4.14 and table 4.2 show that σ_p is temperature-dependent, which corresponds to the hypothesis of thermal softening, and similar results are found within the SS-CRS tests (Chapter 5, section 5.2.2).

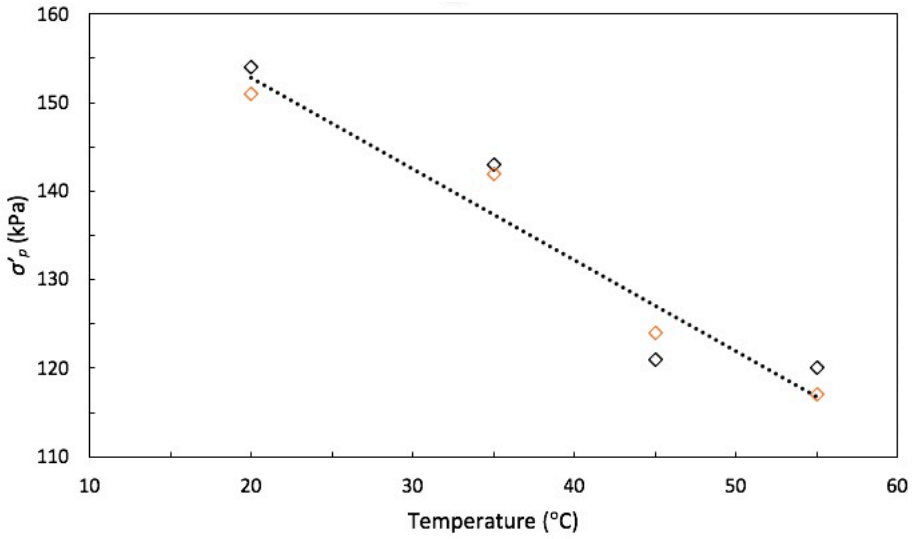

Figure 4.14 - Effect of temperature on the σ_p values in thermal MSL oedometer tests for reconstituted Bank Station London clay specimens.

Table 4.2 - Effect of temperature on C_c, C_s and σ_p values.

Test No.	Temperature (°C)	C_c	C_s	σ_p
MSL20-1	20	0.341	0.079	151
MSL20-2		0.338	0.078	154
MSL35-1	35	0.343	0.081	142
MSL35-2		0.343	0.080	143
MSL45-1	45	0.347	0.089	124
MSL45-2		0.347	0.086	121
MSL55-1	55	0.345	0.077	117
MSL55-2		0.346	0.078	120

4.2.2. Effect of Temperature on the Stress-Dependency of the Compression Index

The use of incremental compression analysis from the thermal MSL oedometer tests makes it possible to study the combined effect of temperature and vertical stress on the compressibility of the clay. The compression index at each incremental load (C_c^*) is calculated as $\Delta e / \Delta \log \sigma_v'$, with Δe being the change of void ratio over one load increment and $\Delta \log \sigma_v'$ being the change in effective stress over the same load increment. Figure 4.15 presents the incremental compression index against the vertical stress for Bank Station specimens. It can be seen that the C_c^* values during the first 80 kPa increase slightly as stress increases, and there is no significant variation in C_c^* as temperature increases. Once the values of stress exceed 100 kPa, it is seen that the C_c^* values start to increase more gradually until they reach a peak of 640 kPa, where it is seen that the higher temperatures seem to display lower C_c^* values, apart from the MSL35 tests. After the peak was observed, the MSL20 to MSL45 tests decreased slightly, apart from the MSL55 tests, which show a sharp decrease at the 1280 kPa load interval. The decrease in C_c^* after the peak was reached was 15.08%, 18.47%, 16.20%, and 44.48% for MSL20, MSL35, MSL45 and MSL55 respectively.

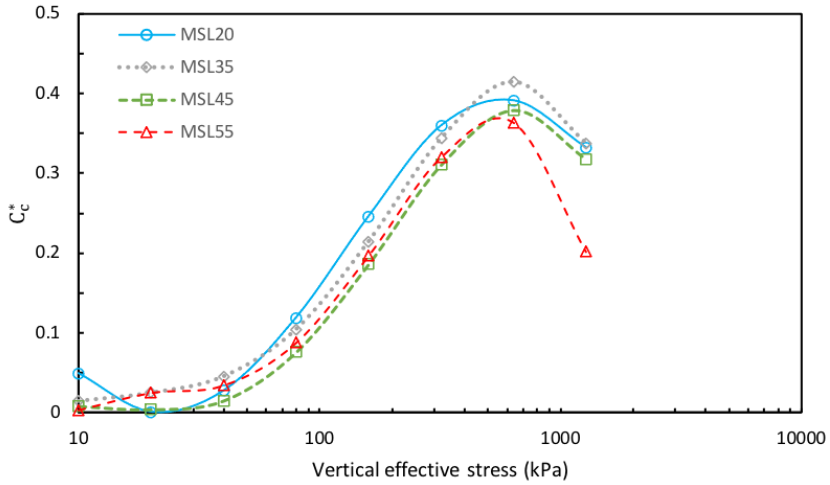

Figure 4.15 - Effect of temperature and vertical stress on the incremental compression index (C_c^*) of reconstituted Bank Station London clay specimens (Note: only one line is shown for each temperature due to very close nature of each test).

Figure 4.16 shows the incremental compression index (C_c^*) against the normalised stress σ_v'/σ_p. This shows the variation of temperature and stress during the C_r (over consolidated zone) and C_c (normal consolidated zone) stages. For σ_v'/σ_p < 1 represent C_r and σ_v'/σ_p > 1 represent C_c values. During the initial loading stages, the values present a scattered trend, with no apparent influence of temperature or vertical stress (figure 4.16). However, as the values start to reach the end of the over consolidation zone and reach the apparent preconsolidation stress, it is seen that the lower temperature contains a sharper increase in C_c^*, whereas the higher temperatures show a gradual increase. Following the σ_p, the values continue to increase until reaching a peak value around (4 - 6) σ_p, after which a decrease in compressibility is observed. Based on the findings in figure 4.15 and figure 4.16, it can be observed that C_c^* values illustrate temperature-dependency at higher effective stresses or once the σ_p values have been exceeded.

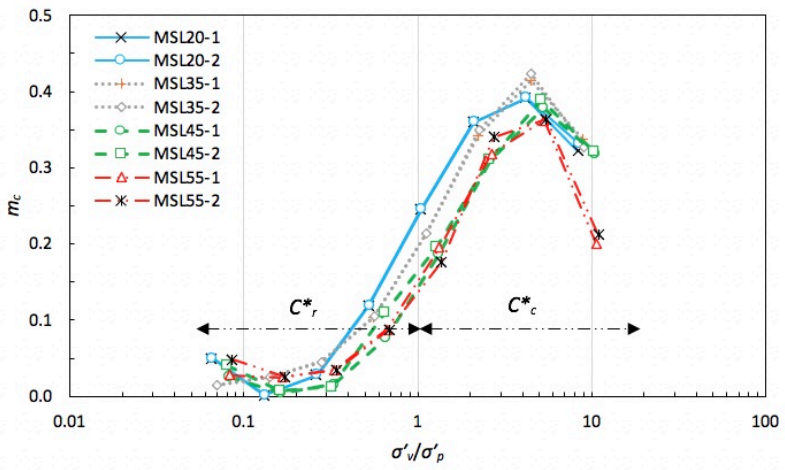

Figure 4.16 - Stress-dependency curve of the slope of compression in a σ_v'/σ_p space for reconstituted Bank Station London clay specimens.

4.2.3. Effect of Temperature on the Secondary Consolidation

To study the combined effect of temperature and vertical stress on the secondary consolidation parameter ($C_{\alpha e}$), the values of $C_{\alpha e}$ were determined between the 6 to the 24-hour stage of the thermal MSL oedometer tests after primary consolidation was completed at each load interval. The variation in secondary consolidation was calculated as $\Delta e/\Delta \log t$, with Δe being the change of void ratio over one load increment and $\Delta \log t$ being the change in time over one load increment after the end of primary consolidation. Figure 4.17 presents the variation of $C_{\alpha e}$ with temperature and vertical stress in a linear plot. As can be seen, during the early stages of loading at lower vertical stress (< 160 kPa), the values of $C_{\alpha e}$ display a large scatter regardless of temperature. However, as temperature and vertical stress increase, the values of $C_{\alpha e}$ increase. It is seen that the higher temperatures (35, 45, and 55°C) reach a peak at 320 kPa before $C_{\alpha e}$ values begin to decrease or plateau, but the MSL20 tests reach a maximum peak of 640 kPa before decreasing. At the end of the loading stages, figure 4.17 shows that the values begin to converge with the higher temperatures containing the higher values of $C_{\alpha e}$. The maximum value of $C_{\alpha e}$ falls in the range of 0.008 to 0.015 with an average value of 0.0062. The findings from these tests are in agreement with those of Green (1969) and Moritz (1995), who found $C_{\alpha e}$ to reach peak values at high temperatures and lower effective stresses.

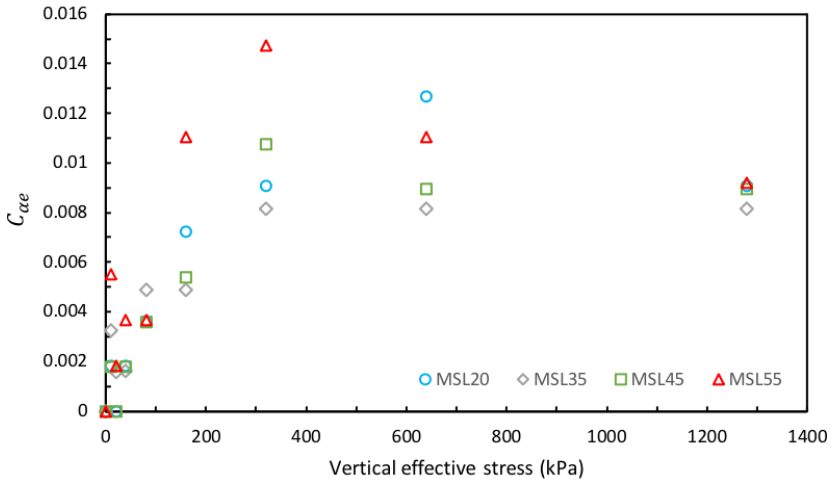

Figure 4.17 - Effect of temperature on the stress-dependency of the secondary consolidation ($C_{\alpha e}$) behaviour for reconstituted Bank Station London clay specimens (Note: only one data set is shown for each temperature due to very close nature of each test).

Further analysis of the effect of temperature on the $C_{\alpha e}$ behaviour on a semi-log plot is displayed in figure 4.18. It is shown that for stress levels prior to the apparent preconsolidation stress, $C_{\alpha e}$ values of MSL20, MSL35, and MSL45 can be seen to be increasing gradually, but the MSL55 test values appear to plateau. For stresses above the apparent preconsolidation stress, it is seen that the MSL20, MSL35, and MSL45 continue to increase gradually until reaching a peak value at stress levels in a range of (2-3) σ_p for MSL 35 and MSL45, whereas MSL20 reach a peak value of stress in a range of (4-5) σ_p. However, for stresses above σ_p for the MSL55 tests, it can be seen that there is a sharp dramatic increase in $C_{\alpha e}$ until reaching the peak range of stress in a range of (2-3) σ_p. Once the peak value of stress had been reached, the values of $C_{\alpha e}$ began to decrease, with MSL55 producing the largest decrease of $C_{\alpha e}$ by 37.5%.

Based on Figure 4.18, it can be seen that $C_{\alpha e}$ shows stress- and temperature dependencies. The general trend suggests an overall increase in $C_{\alpha e}$ with temperature; however, it is difficult to conclude whether $C_{\alpha e}$ increases or decreases with an increase in temperature due to the scattered data. As it can be seen, the higher temperatures reach peak $C_{\alpha e}$ at lower stresses, and vice versa. The large scatter found within the stress levels below the apparent preconsolidation stress (< 160 kPa) could be a consequence of the mechanical loading rate and the initial void ratio of the specimens.

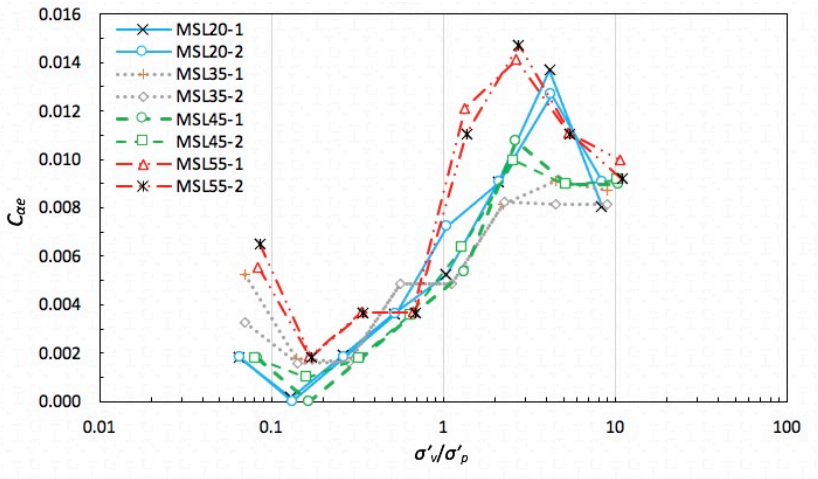

Figure 4.18 - Stress-dependency curve of the secondary consolidation parameter ($C_{\alpha e}$) in a σ'_v/σ_p space for reconstituted Bank Station London clay specimens.

4.2.4. Effect of Temperature on the $C_{\alpha e}/C_c$ Ratio

Figure 4.19 presents the variation of the $C_{\alpha e}/C_c$ ratio with stress on a linear plot for the thermal MSL oedometer tests. It is evident for lower stresses (< 100 kPa), the values of the $C_{\alpha e}/C_c$ ratio are relatively consistent and experience a slow increase as stresses increase for MSL20 to MSL45 tests but for the MSL55 tests, the $C_{\alpha e}/C_c$ ratio decreases before increasing. Once stresses exceed 100 kPa, the $C_{\alpha e}/C_c$ ratio begins to increase gradually for all tests apart from MSL55, where it is seen to have a sharp increase between 80 to 160 kPa, then a gradual increase until the peak α value is reached at 320 kPa. After the peak values were reached, it can be seen that the $C_{\alpha e}/C_c$ ratio decreased gradually with an increase in stress until they converged between an α value of 0.0229 to 0.0307. At the highest stress level (1280 kPa), the increase in temperature from 20 to 55°C results in α to increase by 16.44%, which illustrates the temperature influence on the $C_{\alpha e}/C_c$ ratio.

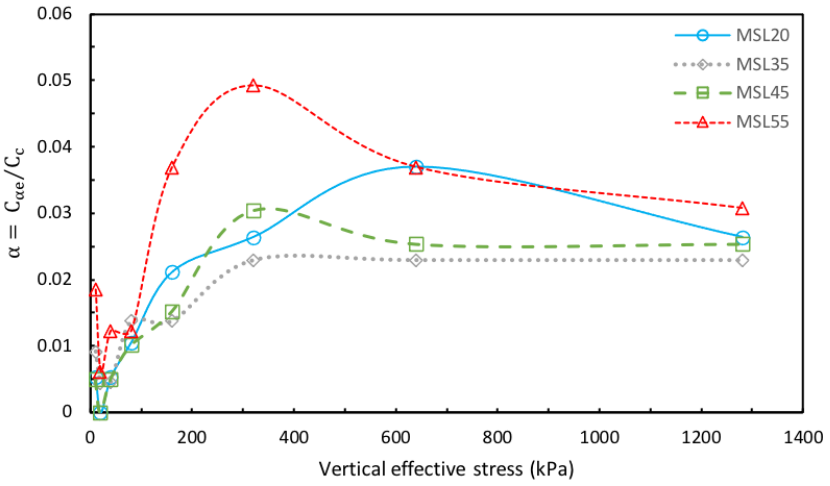

Figure 4.19 - Effect of temperature and stress on the $C_{\alpha e}/C_c$ ratio for reconstituted Bank Station London clay specimens (Note: only one line is shown for each temperature due to very close nature of each test).

Figure 4.20 presents the variation of the $C_{\alpha e}/C_c$ ratio with normalised stress σ'_v/σ_p for the reconstituted Bank Station London clay specimens under varying temperature conditions. The values of the $C_{\alpha e}/C_c$ ratio appear to be considerably scattered at lower stresses (i.e., overconsolidation region), and this scattered trend continues at higher stresses (i.e., normal consolidation region) ($C_{\alpha e}/C_c$). The values of α fall

approximately in a range of 0.0050 - 0.0492. Similar to $C_{\alpha e}$ data in figure 4.18, it can be seen that the effect of temperature is more pronounced at stresses higher than σ_p. Based on the findings in Figure 4.20, It is clear that the $C_{\alpha e}/C_c$ ratio shows stress- and temperature dependencies, as it varies with effective vertical stress and temperature. Moreover, the increase in the $C_{\alpha e}/C_c$ ratio at higher temperatures can be linked to the weakening of the particle bonds or resistance between the particles due to a reduction in the viscosity.

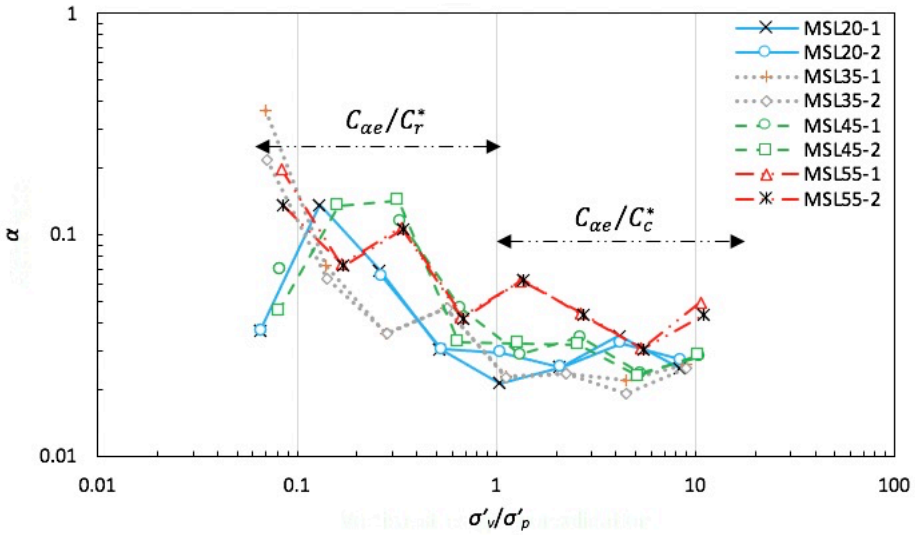

Figure 4.20 - Stress-dependency curve of the α ratio in a σ'_v/σ_p space for reconstituted Bank Station London clay specimens.

4.3. Summary

In this chapter, 1D consolidation tests were performed on reconstituted Bank Station London clay specimens under saturated, unsaturated and thermal conditions. The following conclusions from the MSL oedometer tests can be drawn;

- In the saturated tests, the values of C_c and C_s are in good agreement with previous values published within the literature. The compressibility of the Bank Station specimens decreases as water content decreases, resulting in values of C_c to decrease and σ_p to increase.
- The process of destructuration of Bank Station specimens appears continuous post σ_p and reaches a peak value at stress levels in a range of

(8–13) σ_p. The findings are consistent with previous studies on London clay, which found destructuration to be linear until peak values at stress levels in a range of (8-10) σ_p.

- It was seen that the change in water content affects the values of creep, as the lower water content is seen to display a dramatic increase in $C_{\alpha e}$ at stress levels in a range of (1-2) σ_p, where the higher water content displays a gradual increasing $C_{\alpha e}$ until reaching a peak value at stress levels in a range of (2-13) σ_p. Furthermore, it can be seen that values of $C_{\alpha e}$ are similar to findings in the literature.
- The increase in suction causes the compressibility of Bank Station specimens to decrease, which results in the σ_p increasing. Furthermore, the increase in suction results in values of C_c and C_s decreasing within the tested range of stresses.
- Generally, an increase in suction causes a decrease in the slope of the compression curve and secondary consolidation. However, the results contradict the findings in the literature, as the Bank Station London clay specimens in this study observed a peak value of $C_{\alpha e}$ and C_c^* before decreasing, unlike previous research.
- During the thermal MSL oedometer tests, an increase in temperature caused the compression curves to shift downward and increased the compressibility of the specimens.
- The hypothesis of increased temperature causing softening of London Clay and reduction in preconsolidation stress was proven to be correct, as an increase in temperature causes a reduction in σ_p. However, it can be seen that the C_c and C_s values contain a slight change as temperature increased between 20 - 55°C.
- Subjecting the samples to higher temperatures resulted in C_c to peak value at stress levels in a range of (4-6) σ_p. Similarly, the increase in temperature results in $C_{\alpha e}$ reaching peak values at lower stress ranges.

- Overall, the Bank Station London clay specimens in a reconstituted state can be found to be suction- and temperature-dependent for the range of stresses (10 – 1280 kPa) tested in this study.
- According to the classification proposed by Mesri et al. (1994), Bank Station London clay lies in the zone of shale or mudstone whose α values range from 0.02 to 0.04. Similar to the findings of Bagheri (2018), the $C_{\alpha e}/C_c$ ratio was stress-, temperature- and suction-dependent and, therefore, cannot be considered a constant value.

Chapter Five – Constant Rate of Strain (CRS) Tests

5.1. Introduction

In this chapter, details of an investigation into the thermal-mechanical behaviour of reconstituted Bank Station London clay specimens, through single-stage and multi-staged compression-relaxation tests, are presented using the information from table 3.7 in section 3.4.3. The single-staged thermal compression-relaxation (SS-CRS) tests aimed to understand the effect of temperature and strain rate on the compression and stress relaxation processes. Whereas the multi-staged thermal compression-relaxation (MSCRS) tests were to determine the effect of temperature, the pre-relaxation strain level, and strain rate on the stress relaxation processes across two relaxation periods (24- and 48-hour).

5.2. Single-Staged Thermal Compression-Relaxation Tests

5.2.1. Effect of Temperature on the Stress-Strain Relationship

Figure 5.1 (a-c) illustrate the results of the CRS tests. The compression curves in this study are shown in terms of axial strain (ε_α) against total vertical stress (σ_o). The changes in pore-water pressures within the CRS tests are also displayed in figure 5.1 (a-c) with pore-water pressure obtained from the PWPT against the total vertical stress.

Inspection of the results in figure 5.1 (a-c) reveals a temperature-dependency of the stress-strain behaviour during 1D compression. As can be seen, the compressibility of the specimens does not alter significantly with the change in temperature as all the tests contain roughly a 10.5 mm deformation. It is seen that the influence of temperature on the compression of the specimens during the SS-CRS-b tests does not provide a clear trend, whereas, in the SS-CRS-a tests, the compressibility of the specimen appears to decrease by 16.67% as temperature increases. However, as

shown in figure 5.1c, an increase in temperature during the SS-CRS-c tests causes an increase in compressibility. Hence the SS-CRS-c tests would agree with the thermal MSL oedometer results in section 4.2.1, whereas the SS-CRS-a test results would disagree.

Moreover, an increase in temperature causes the overall trend of the compression curves to shift towards the left (reducing yield stress) in the SS-CRS-a and SS-CRS-b tests. The shift to the left was more pronounced within the SS-CRS-b tests (0.005 mm/min) (figure 5.1b). However, the SS-CRS-c tests (0.001 mm/min) show that an increase in temperature from 35 to 55°C causes the compression curves to shift to the right slightly (and increases the yield stress slight). The shifting of the compression curves causes a decrease in σ_p as temperature increases (discussed in section 4.2.1). Similar behaviour is seen by Tsutsumi and Tanaka (2012) and Jarad et al. (2019), who reported that higher temperatures and slower strain rates result in the compression curves shifting to the right.

Figure 5.1 (a-c) illustrates the pore-water pressure generated during the stress-strain tests (represented by the dotted lines). Inspection of the results reveals a temperature-dependency of the pore-water pressure generation during 1D compression. The SS-CRS-a and SS-CRS-b tests display a similar trend: the pore-water pressure generation is slow during the first 700 kPa of stress applied to the specimens before a sharp exponential increase. The SS-CRS-c tests begin to generate pore-water pressure within the first 100 kPa of stress applied to the specimen. Furthermore, figure 5.1 (a-c) show that when temperature increases from 20 to 55°C in all tests, there is a delay in the generation of pore-water pressure. The decrease in pore-water pressure generation during high- temperature SS-CRS tests is evident (Figure 5.1). The behaviour in reducing pore-water pressure during high-temperature tests could be related to the decrease of water viscosity, which accommodates expulsion or dissipation of the water.

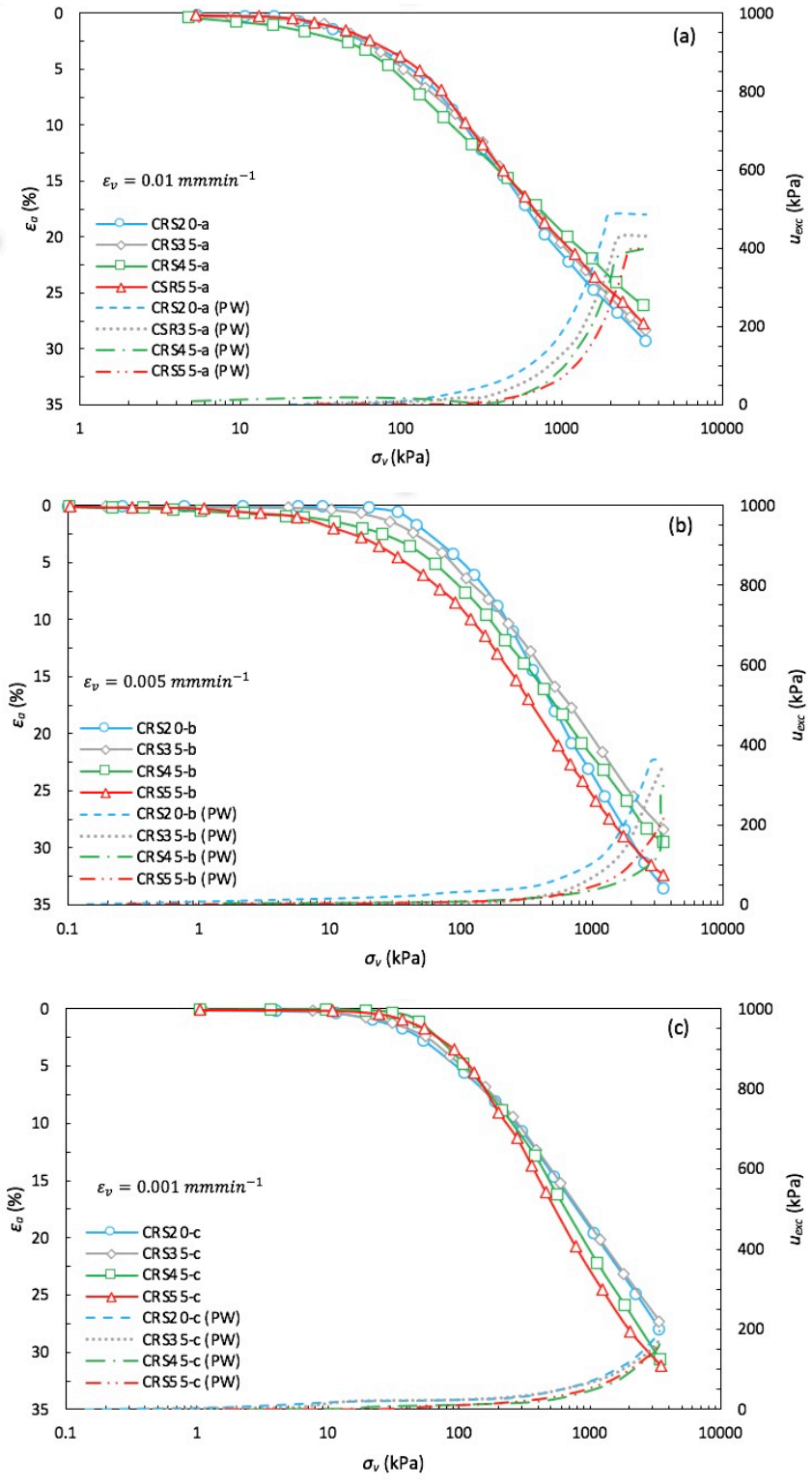

Figure 5.1 - CRS compression curves for the different strain rates tested at the four selected temperatures.

5.2.2. Effect of Temperature on the Compressibility Parameters

Figure 5.2 illustrates the variation of C_c with the change in temperature and strain rate during the SS-CRS tests. The values of C_c range between 0.2614 to 0.3481 for all tests at strain rates of 0.01 to 0.001 mm/min and a temperature range of 20 to 55°C (table 5.1). As can be seen, an increase in temperature causes the values of C_c to decrease linearly. However, the change in C_c is minimal, as the maximum difference in C_c is 8.82% when the temperature was increased from 20 to 55°C, which is illustrated by the SS-CRS-c tests. Furthermore, it can be seen that the values of C_c decreased when increasing the strain rate by a factor of 5 or 10. Based on the findings found in figure 5.2, C_c is temperature-independent but strain rate-dependent. This finding agrees well with the results from the thermal MSL oedometer tests presented in section 4.2.1. The variation in C_c with a change in strain rate and temperature is due to the viscous behaviour of the specimens as they become more resistant to deformation (Tsutsumi and Tanaka, 2012).

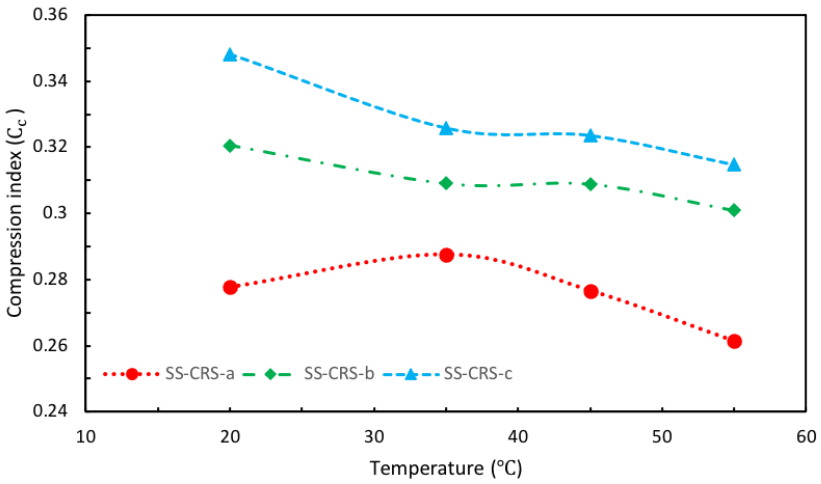

Figure 5.2 - Effect of temperature on the compression index at different temperatures and strain rates. (SS-CRS-a = 0.01mm/min, SS-CRS-b = 0.05mm/min, SS-CRS-c = 0.001mm/min)

Figure 5.3 presents the variation σ_p with temperature and strain rate for all SS-CRS tests. At a constant temperature, the higher the strain rate, the higher the σ_p. Similarly, at a constant strain rate, the higher the temperature, the higher the σ_p. Moreover, a decrease in σ_p with temperature appears to follow an approximately

linear trend for all strain rates. This finding illustrates the temperature- and strain rate-dependency of σ_p, as it can be seen that a decrease in strain rate by a factor of 10 (0.01 to 0.001 mm/min) results in a reduction of σ_p by 11.36% at the 20°C. Contrastingly, by increasing the temperature and decreasing the strain rate, it can be seen that the values of σ_p converge at 55°C between the SS-CRS-b and SS-CRS-c tests which results in a slight increase of σ_p by 1.47% as the strain rate decreases from 0.005 to 0.001 mm/min. The dependency of σ_p on the strain rate and temperature is further highlighted by the fact that the values of σ_p decrease by 17.04%, 15.68% and 12.82% for SS-CRS-a, SS-CRS-b, and SS-CRS-c tests respectively, as temperature increases from 20 to 55°C. The dependency of the strain rate-σ_p relationship with temperature would contradict the findings of Leroueil (1994), who found the strain rate-σ_p relationship to be independent of temperature. However, the results would support the findings of Marques et al. (2004), who found the strain rate-σ_p relationship to be dependent on temperature (figure 2.6) as it would produce similar results as seen in figure 5.3. Additionally, the variation in strain rate can alter the σ_p values due to the rate sensitivity of the cementation bonds (Vaid et al., 1979). The reduction of σ_p with an increase in temperature is consistent with the findings in the MSL oedometer tests and thermal softening hypothesis (section 4.2.1).

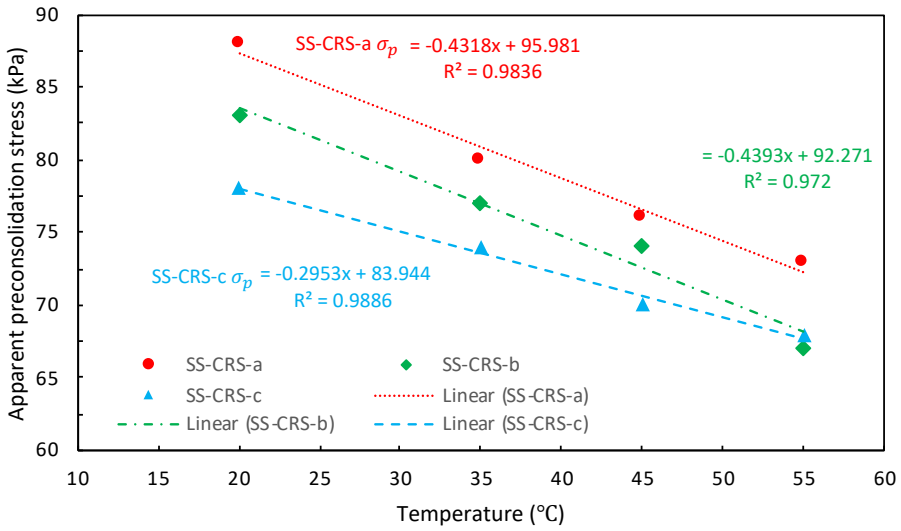

Figure 5.3 - Effect of strain rate and temperature on the apparent preconsolidation stress (σ_p).

Table 5.1 - Effect of temperature on the compressibility parameters of the SS-CRS tests.

Test No.	Strain rate (mm/min)	Temperature (°C)	σ_p (kPa)	C_c	$\sigma_{pCRS}/\sigma_{pMSL}$
SS-CRS20-a	0.01	20	88	0.2776	0.57
SS-CRS35-a		35	80	0.2875	0.56
SS-CRS45-a		45	76	0.2766	0.62
SS-CRS55-a		55	73	0.2614	0.61
SS-CRS20-b	0.005	20	83	0.3204	0.54
SS-CRS35-b		35	77	0.3090	0.54
SS-CRS45-b		45	74	0.3088	0.60
SS-CRS55-b		55	67	0.3009	0.56
SS-CRS20-c	0.001	20	78	0.3481	0.51
SS-CRS35-c		35	74	0.3258	0.52
SS-CRS45-c		45	70	0.3235	0.57
SS-CRS55-c		55	68	0.3146	0.57

As illustrated in table 5.1, the $\sigma_{pCRS}/\sigma_{pMSL}$ ratio lies between 0.51 to 0.62 for all strain rates and temperatures tested. The findings contradict results by Marques et al. (2004), who found σ_{pCRS} to be 20 – 25% higher than σ_{pMSL}, whereas the σ_{pCRS} values in this study were 37 – 48% smaller than σ_{pMSL} values. Furthermore, the results would disagree with the findings of Bagheri et al. (2019), who found the $\sigma_{pCRS}/\sigma_{pMSL}$ ratio to be 1.29 for saturated London clay specimens with w_o = 39%. It was observed that for a constant strain rate, the higher the temperature, the higher the $\sigma_{pCRS}/\sigma_{pMSL}$ ratio. Similarly, the lower the strain rate at a constant temperature, the lower the $\sigma_{pCRS}/\sigma_{pMSL}$ ratio (figure 5.4). However, it is seen that the green line (SS-CRS-b) at 55°C does not follow the trend as the other tests. This could be potentially down to interpretation or testing errors (such as difference in pre-testing conditions during sample preparation). The values obtained in this study are below the average value reported in the literature for stiff saturated clays, as Bagheri (2018) reported values to be 50 - 60% higher for Isle of Sheppey London Clay specimens. Therefore, the $\sigma_{pCRS}/\sigma_{pMSL}$ ratio can be considered as a function of loading and affected by temperature and strain rate.

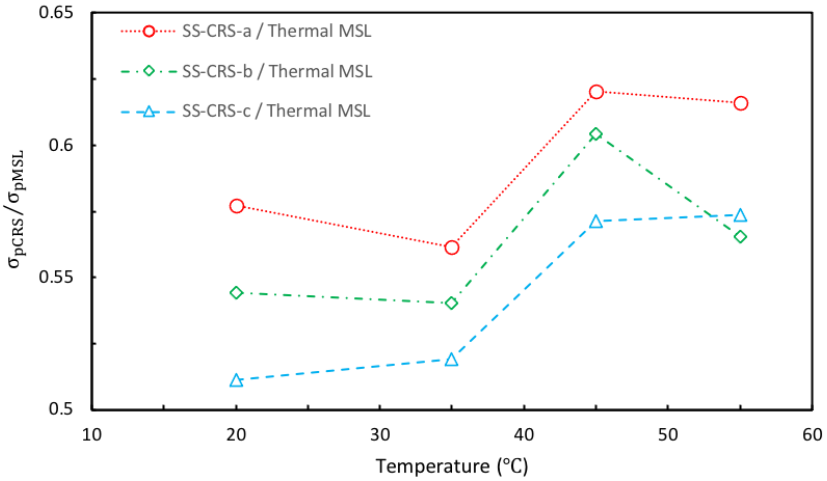

Figure 5.4 - Showing the variation in the $\sigma_{pCRS}/\sigma_{pMSL}$ ratio with a change in temperature and strain rate.

5.2.3. Effect of Temperature and Strain Rate on the Stress Relaxation Process

As previously mentioned (section 3.4.3), the stress relaxation process was initiated once the specimen reached the maximum load. The gradual decrease of stresses with time was recorded and used to evaluate the effects of pre-effects of pre-relaxation strain rate, temperature and relaxation time on the stress relaxation process. Table 5.2 summaries the characterisation parameters.

Table 5.2 - Characterisation of the stress relaxation parameters for the SS-CRS tests.

Test No.	Total stress (σ_o) (kPa)	Residual stress (σ_s) (kPa)	Relaxed stress ($\Delta\sigma$) (kPa)	$\Delta\sigma/\sigma_o$ (%)	Residual stress ratio (ξ)	Coefficient of stress relaxation (R_a)
SS-CRS20-a	3329	1776	1553	46	0.53	0.04628
SS-CRS35-a	3300	2231	1069	32	0.67	0.04232
SS-CRS45-a	3197	2734	463	14	0.85	0.04047
SS-CRS55-a	3196	2753	443	13	0.86	0.03441
SS-CRS20-b	3498	2465	1033	29	0.70	0.03816
SS-CRS35-b	3466	2611	855	24	0.75	0.03691
SS-CRS45-b	3493	2700	793	22	0.77	0.03427
SS-CRS55-b	3495	2810	685	19	0.80	0.03354
SS-CRS20-c	3376	3086	290	8	0.91	0.02069
SS-CRS35-c	3350	3084	266	7	0.92	0.02187
SS-CRS45-c	3401	3132	269	7	0.92	0.02525
SS-CRS55-c	3450	3135	315	9	0.90	0.03038

The values presented in Table 5.2 illustrates that an increase in temperature would cause a decrease in the relaxed stresses ($\Delta\sigma$) and consequently an increase in the residual stress ratio (ξ) during the SS-CRS-a and SS-CRS-b tests, which caused a reduction of 33% and 10% in the $\Delta\sigma/\sigma_o$ ratio respectively. Similar observations were reported by Murayama (1969), who found that a temperature increase would decrease relaxed stresses when performing tests on Osaka clay specimens. However, it is seen that the values for the SS-CRS-c tests display a different trend from that of the previous strain rates. As it can be seen, an increase in temperature results in a decrease in $\Delta\sigma$ when changing the temperature from 20 to 35°C, but $\Delta\sigma$ increases as the temperature is increased from 35 to 55°C. The values obtained for ξ and $\Delta\sigma/\sigma_o$ would be relatively close as the temperature increases, as they are between 2% and 0.02, respectively, during the slowest strain rate studied (0.001 mm/min). Furthermore, the stress relaxation parameters obtained illustrate that the coefficient of stress relaxation (R_a) is dependent on temperature and strain rate. As can be seen, an increase from 0.001 to 0.01 mm/min and an increase in temperature from 20 to 55°C caused the R_a values to increase by a factor of 1.13 to 2.23. Moreover, an increase in the pre-relaxation strain rate by a factor of 10 was found to significantly affect the magnitude of relaxed stresses, resulting in an increase of the $\Delta\sigma$ values by 16.04 to 71.87%.

Figure 5.5 (a-c) present the stress-relaxation curves with time on a semi-log plot. These have been presented by using the normalised relaxed stress with respect to pre-relaxation stress. At a constant strain rate, temperature appears to influence the stress relaxation process, as an increase in temperature causes the stress relaxation curves to be situated above the previous temperature interval. Moreover, the higher the temperature, the lower the rate of relaxation as temperature increases during SS-CRS-a and SS-CRS-b tests. In the SS-CRS-c tests, the higher the temperature, the higher the rate of relaxation. Similarly, at a constant temperature, the higher the pre-relaxation strain rate, the lower the magnitude of residual stress. Furthermore, it is illustrated in figure 5.5 (a-c) that a change in pre-relaxation strain rate coupled with a temperature change alters the stress relaxation curves.

As the SS-CRS-b and SS-CRS-c stress relaxation curves observe a linearly decreasing trend, it is seen in the lower temperature test of the higher pre-relaxation strain rate (SS-CRS-a), the stress relaxation curve appears in three distinct parts during the SS-CRS20-a test but begins to decrease linearly as the temperature is increased during the SS-CRS-a tests. As suggested by Bagheri et al. (2019), the stress relaxation process can be split into three phases (as mentioned in Chapter 2, section 2.3.2 – figure 2.15); (1) fast relaxation, which is associated with the quick release of energy accumulated inside the specimen, (2) decelerating relaxation, and (3) residual relaxation which are associated to the time-dependent particles re-arrangement and dissipation of energy. At a constant temperature, strain rate appears to influence the stress relaxation process during decelerating and residual relaxation phases. From the results, it can be stated that the strain rate and temperature affect the stress relaxation process.

During relaxation of the specimen, the pore-water pressure built up from the loading stage begins to dissipate. Figures 5.5 (a-c) present the pore-water pressure with time on a semi-log plot. As can be seen, pore-water pressure dissipation over time follows similar trends regardless of temperature. During the SS-CRS-a tests, pore-water pressure dissipation reduced rapidly over the first 10 hours, beyond which the dissipation rate started to retard. In the SS-CRS-b tests, it can be seen that the dissipation rate is dependent upon temperature; the SS-CRS20-b, SS-CRS35-b, and SS-CRS45-b tests have a quicker rate of dissipation over the first 10 hours than the SS-CRS55-b test which has a slow, gradual dissipation curve. However, specimens during the SS-CRS-c tests show that the dissipation of pore-water pressure during the first 10 hours is minimal; after 10 hours mark, it is seen that there is a sharp increase in the rate of dissipation for all tests until the end of relaxation. The dissipation rate is further illustrated for each strain rate tested, and the specimens see a reduction of 91 – 99%, 84- 89%, and 40 – 56% of pore-water pressure within the specimen for SS-CRS-a, SS-CRS-b, and SS-CRS-c, respectively. This shows that the pore-water pressure during stress relaxation is dependent on strain rate and temperature.

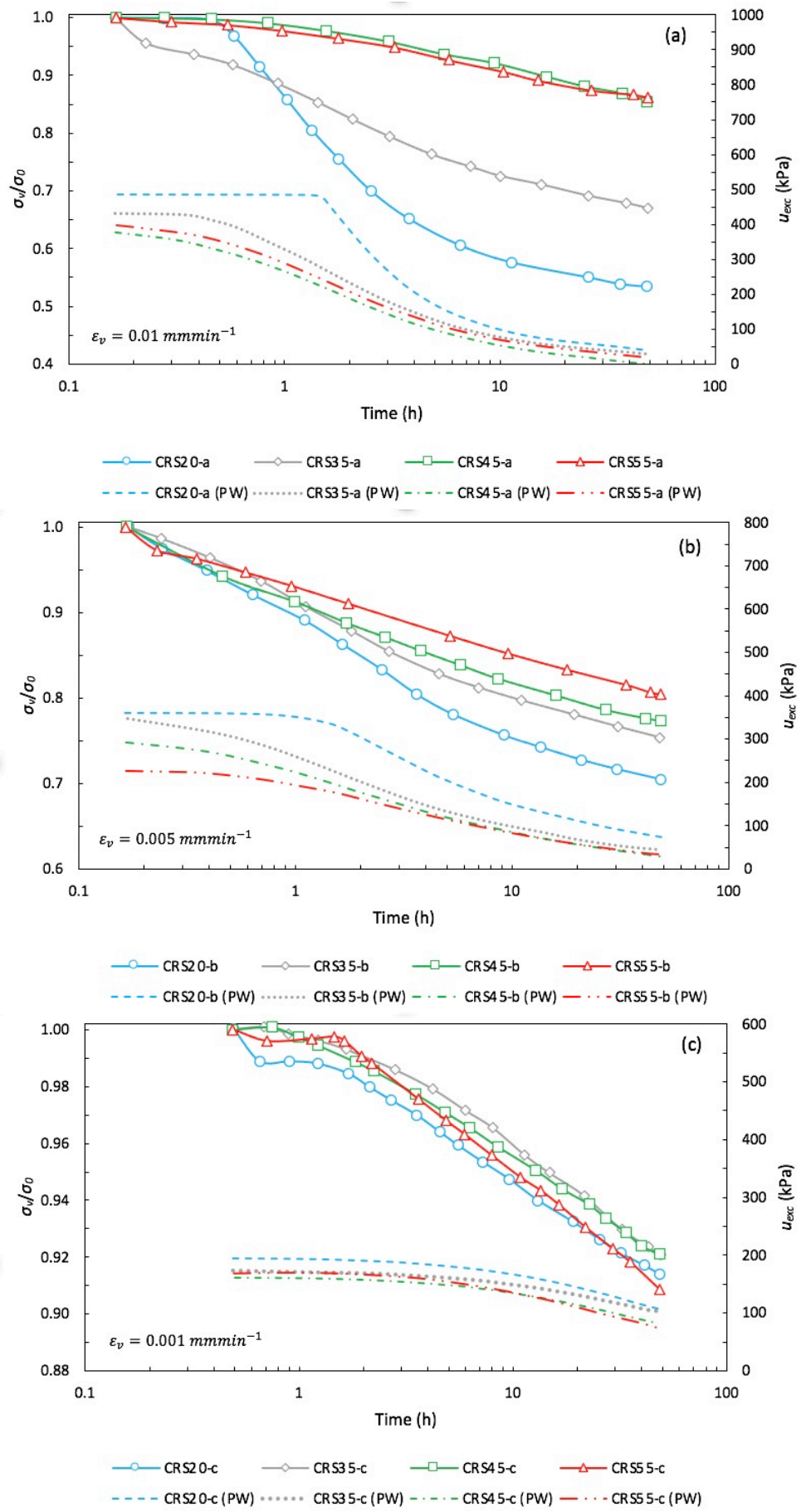

Figure 5.5 - The change of stresses and pore-water pressure through stress relaxation.

Figure 5.6 presents the variation of the coefficient of stress relaxation (R_a) with temperature for the SS-CRS-a, SS-CRS-b and SS-CRS-c tests. It can be observed that R_a displays a clear difference between temperature and strain rate. As can be seen, the SS-CRS-a and SS-CRS-b tests produce a linearly decreasing R_a value as temperature increases, whereas SS-CRS-c tests produce a linearly increasing R_a value as temperature increases. It is noted that the higher the pre-relaxation strain rate, the higher the temperature, and the lower the R_a. Similarly, the lower the pre-relaxation strain rate, the higher the temperature, and the higher the R_a. Furthermore, it can be seen that as temperature increases during the stress relaxation process of the SS-CRS tests, the value starts to converge around the 55°C intervals, as the difference between the three tested strain rates is 0.004.

Additionally, it can be seen that a change in strain rate (SS-CRS-a to SS-CRS-c) by a factor of 10 results in the R_a values to reduce by 55% at 20°C and 11% at 55°C between SS-CRS-a and SS-CRS-c. Moreover, the increase in the stress relaxation behaviour during the SS-CRS-c tests can be linked to the increase in thermal energy, which results in a significant breakdown of particles that promotes stress relaxation. Whereas, in the quicker CRS tests (0.01 and 0.005 mm/min), it is seen that the decrease of stress relaxation can be associated with the lack of strain energy stored within the specimens as relaxation stages were initiated, as it would allow the specimens to reach an equilibrium state due to the quicker release of strain energy (Wang et al., 2011). From the results observed, it can be stated that R_a is dependent on temperature and strain rate.

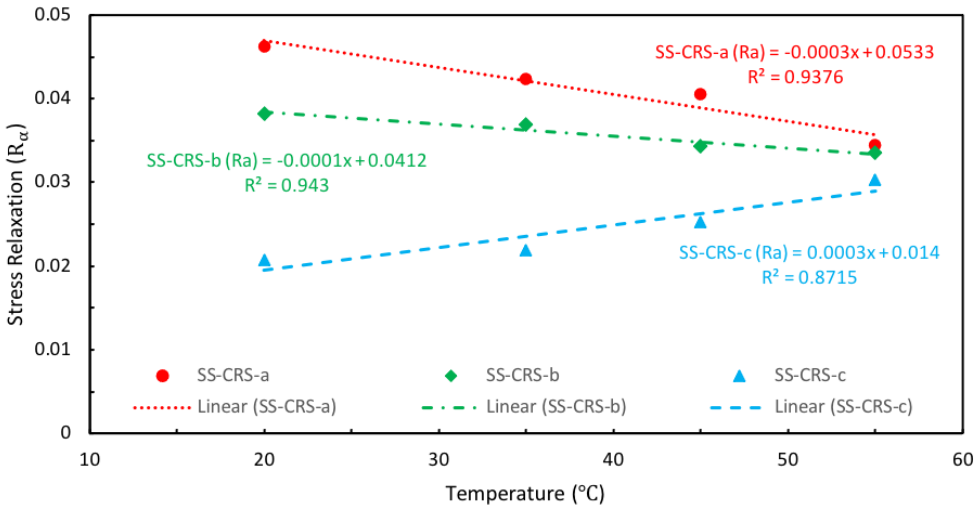

Figure 5.6 - Variation of the coefficient of stress relaxation (R_a) at different temperatures and strain rates.

Table 5.3 presents the relationship between the coefficient of stress relaxation (R_a) and the $C_{\alpha e}/C_c$ ratio. It was previously mentioned in Chapter 2, section 2.3.2.1 and stated by Bagheri et al. (2019) that $R_a = \alpha$ is acceptable for stiff clays such as London clay. As seen in table 5.3, it is evident that the stress relaxation behaviour obtained from the thermal MSL oedometer tests using $R_a = C_{\alpha e}/C_c$ complies well with the SS-CRS-c stress relaxation values. Furthermore, an increase in temperature shows more thermal MSL $C_{\alpha e}/C_c$ ratio values to correlate with all SS-CRS tests. Moreover, calculating the secondary consolidation behaviour ($C_{\alpha e}$) from the SS-CRS tests using $C_{\alpha e} = R_a C_c$, it is found that the values obtained comply with the thermal MSL oedometer results. However, as can be seen, only the SS-CRS35-c test result falls within the $C_{\alpha e}$ range found from the thermal MSL oedometer tests, as the SS-CRS-a and SS-CRS-b tests at 35°C sit above the range.

The ranges provided in table 5.3, illustrate that the applicability of $R_a = \alpha$ and $C_{\alpha e} = R_a C_c$ can be valid for thermal saturated reconstituted London clay specimens. However, it was determined that $C_{\alpha e} = R_a C_c$ provides a better correlation when understanding the relationship between stress relaxation and creep, and therefore, proposes $R_a = \alpha$. Furthermore, it can be suggested that CRS stress relaxation tests can replace the conventional MSL oedometer tests due to deriving acceptable creep values which can be obtained within shorter timescales.

Table 5.3 - Relationship between R_a and $C_{\alpha e}$

Test No.	CRS R_a	$R_a = C_{\alpha e}/C_c$	MSL $C_{\alpha e}$	$C_{\alpha e} = R_a C_c$
MSL20	-	0.0052 – 0.0369	0.0018 – 0.0121	-
MSL35	-	0.0044 – 0.0229	0.0016 – 0.0082	-
MSL45	-	0.0050 – 0.0304	0.0018 – 0.0107	-
MSL55	-	0.0061 – 0.0492	0.0018 – 0.0147	-
SS-CRS20-a	0.04628	-	-	0.0128
SS-CRS35-a	0.04232	-	-	0.0121
SS-CRS45-a	0.04047	-	-	0.0111
SS-CRS55-a	0.03441	-	-	0.0089
SS-CRS20-b	0.03816	-	-	0.0122
SS-CRS35-b	0.03691	-	-	0.0114
SS-CRS45-b	0.03427	-	-	0.0105
SS-CRS55-b	0.03354	-	-	0.0100
SS-CRS20-c	0.02069	-	-	0.0072
SS-CRS35-c	0.02187	-	-	0.0071
SS-CRS45-c	0.02525	-	-	0.0081
SS-CRS55-c	0.03038	-		0.0095

5.3. Multi-Staged Thermal Compression-Relaxation Tests

5.3.1. Effect of Temperature on the Pre-Relaxation Stress Level

The multi-staged compression-relaxation tests with a 24-hour relaxation period are shown in figure 5.7 (a-d), which illustrates the variation of stress (σ_v) with time (hr). The monitoring of the pore-water pressure with time during the testing phase is also shown in figure 5.7 (e-h). It can be seen in figure 5.7 (e-h) that an increase in temperature results in a decrease in pore-water pressure throughout the testing phase. However, the MSCRS45c-i test contained measurement problems. The characterisation of the stress relaxation parameters during the MSCRS-i tests for the 24-hour stress relaxation stages is summarised in table 5.4.

Table 5.4 - Characterisation of the stress relaxation parameters for the MSCRS tests during 24-hour relaxation periods.

Test ID.	ε_r	σ_o (kPa)	σ_s (kPa)	$\Delta\sigma$ (kPa)	$\Delta\sigma/\sigma_o$ (%)	ξ	R_a
MSCRS20b-i	6	138	85	53	38	0.62	0.0870
	12	301	206	95	31	0.68	0.0796
	18	633	470	163	26	0.74	0.0561
	24	1332	1031	301	23	0.77	0.0458
	30	3459	2679	780	22	0.78	0.0418
MSCRS35b-i	6	101	57	44	44	0.56	0.1003
	12	235	164	71	30	0.69	0.0496
	18	537	407	130	24	0.75	0.0534
	24	1032	816	216	21	0.79	0.0400
	30	3398	2730	668	19	0.80	0.0390
MSCRS45b-i	6	92	56	36	39	0.61	0.0851
	12	261	187	74	28	0.72	0.0611
	18	548	427	121	22	0.78	0.0509
	24	1079	868	211	19	0.79	0.0410
	30	3435	2746	689	20	0.80	0.0369
MSCRS55b-i	6	124	82	42	33	0.66	0.0866
	12	335	255	80	24	0.76	0.0661
	18	671	537	134	19	0.80	0.0469
	24	1469	1199	270	18	0.81	0.0383
	30	3424	2608	816	24	0.76	0.0261
MSCRS20c-i	6	98	76	22	22	0.77	0.0578
	12	294	250	44	15	0.85	0.0354
	18	480	406	74	15	0.84	0.0398
	24	882	761	121	13	0.86	0.0386
	30	3133	2821	312	10	0.90	0.0303
MSCRS35c-i	6	215	142	73	34	0.66	0.0912
	12	620	501	119	19	0.80	0.0662
	18	1514	1312	202	13	0.86	0.0403
	24	3105	2769	336	11	0.89	0.0377
	30	3221	2881	340	10	0.89	0.0377
MSCRS45c-i	6	130	102	28	21	0.78	0.0435
	12	319	262	57	17	0.82	0.0386
	18	685	584	101	14	0.85	0.0331
	24	1364	1178	186	13	0.86	0.0328
	30	3372	3094	278	8	0.91	0.0267
MSCRS55c-i	6	143	96	47	33	0.67	0.0953
	12	410	338	72	18	0.82	0.0486
	18	914	787	127	14	0.86	0.0414
	24	2014	1787	227	11	0.89	0.0325
	30	3233	3196	37	1	0.99	0
Note: During the MSCRS55c-i tests at 30% pre-relaxation strain level, there was an error system error with the equipment. Hence no true stress relaxation values can be calculated.							

The values presented in table 5.4 show findings which were consistent with the SS-CRS results, as an increase in temperature would cause the relaxed stresses ($\Delta\sigma$) to decrease and the residual stress ratio (ξ) to increase, which would result in the $\Delta\sigma/\sigma_o$ ratio to decrease as temperature increased with an increase in the pre-relaxation

strain level (ε_r). However, the values of the $\Delta\sigma/\sigma_o$ ratio during the MSC35b-i and MSC35c-i tests were above the previous temperature tested (MSCRS20) and did not appear to follow the general trend during the pre-relaxation strain level (ε_r) of 6%. It was seen in the MSCRS55b-i test that the $\Delta\sigma/\sigma_o$ ratio decreased from 33 to 18% for an increase in ε_r from 6 to 24%, then increased from 18 to 24% for an increase in ε_r from 18 to 30%, respectively. It is evident from table 5.4 that the larger relaxed stresses were observed with an increase in pre-relaxation strains (and pre-relaxation stresses). Similar observations were observed by Bagheri et al. (2019) during the testing of unsaturated Sheppey London clay specimens.

However, during the testing of the 0.005 mm/min strain rate (MSCRSb-i), an increase in temperature did not cause an increase in pre-relaxation stresses as pre-relaxation strains increase when comparing it with the MSCRS20b-i test until reaching ε_r = 30%, where it is clear that an increase in temperature from 20 to 55°C causes the pre-relaxation stresses to increase. In comparison, the MSCRSc tests show that an increase in temperature causes an increase in pre-relaxation stresses as the pre-relaxation strain increases. Though it appears during MSCRS35b-i, MSCRS45b-i, and MSCRS45c-i test, the pre-relaxation stresses at the largest pre-relaxation strain level (ε_r = 30%) would decrease as the temperature is increased from 20°C by 14.35, 11.66, and 10.89% respectively. Furthermore, increasing the pre-relaxation strain rate by a factor of 5 at each temperature interval considerably affected the magnitude of relaxed stresses at each pre-relaxation strain level, resulting in an increase of $\Delta\sigma$ values by a factor of 1.29 – 2.5. Moreover, an increase in the pre-relaxation strain rate was found to significantly affect the residual stress ratio (ξ) at each pre-relaxation strain level, resulting in ξ to decrease from 8.13 to 21.79%.

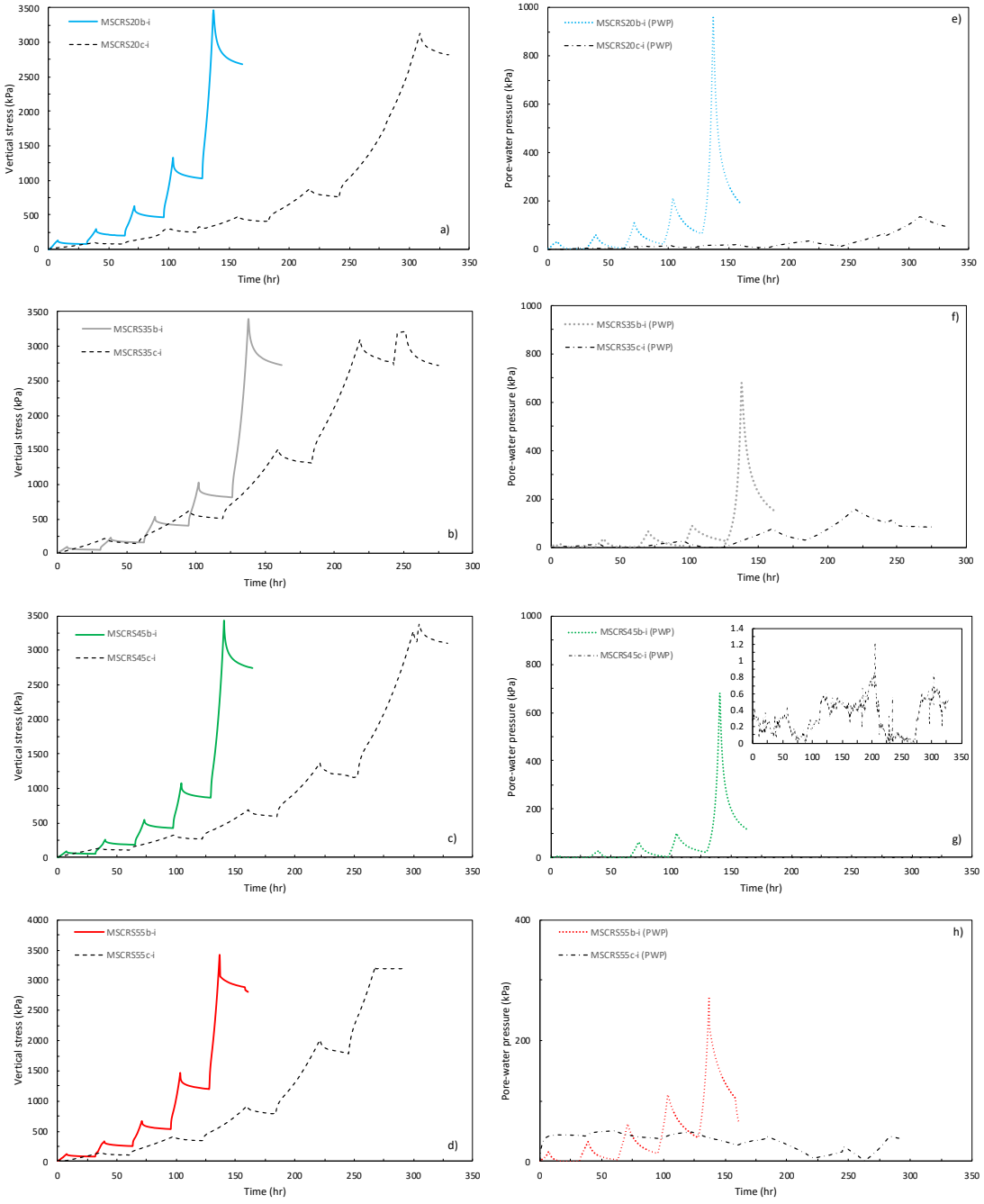

Figure 5.7 – 24hr-MSCRS compression-relaxation stages (a-d) and pore-water pressure during the MSCRS tests (e-h).

To further investigate the influence of temperature on time- and rate-dependent behaviour of Bank Station London clay specimens during multi-staged compression-relaxation tests, a total of eight MSCRS tests were completed with a 48-hour relaxation period. The MSCRS-ii tests with the increased relaxation period are presented in figure 5.8 (a-h), with the variation of stress (σ_v) against time (hr), along with the pore-water pressure change. Similar to the results obtained during the

MSCRS-i tests, an increase in temperature decreased pore-water pressure generation. The characterisation of the stress relaxation parameters during MSCRS-ii tests for 48-hour stress relaxation stages is summarised in table 5.5.

Table 5.5 - Characterisation of the stress relaxation parameters for the MSCRS tests during 48-hour relaxation periods.

Test ID.	ε_r	σ_o (kPa)	σ_s (kPa)	$\Delta\sigma$ (kPa)	$\Delta\sigma/\sigma_o$ (%)	ξ	R_a
MSCRS20b-ii	6	110	58	52	47	0.52	0.1009
	12	329	234	95	28	0.71	0.0483
	18	662	498	164	24	0.75	0.0412
	24	1284	986	298	23	0.76	0.0312
	30	3430	2702	728	21	0.78	0.0304
MSCRS35b-ii	6	101	54	47	46	0.53	0.1007
	12	235	157	78	33	0.66	0.0614
	18	536	391	145	27	0.72	0.0546
	24	1032	729	303	29	0.70	0.0422
	30	3398	2264	1134	33	0.66	0.0313
MSCRS45b-ii	6	129	76	53	41	0.58	0.1335
	12	285	204	81	28	0.71	0.0415
	18	642	485	157	24	0.75	0.0406
	24	1239	971	267	21	0.78	0.0338
	30	3433	2725	708	20	0.79	0.0156
MSCRS55b-ii	6	266	182	84	31	0.68	0.0774
	12	424	314	110	25	0.74	0.0619
	18	786	599	186	23	0.76	0.0443
	24	1541	1221	319	20	0.79	0.0332
	30	3393	2884	508	14	0.85	0.0210
MSCRS20c-ii	6	99	73	26	26	0.73	0.0597
	12	294	239	55	19	0.81	0.0630
	18	480	392	88	18	0.82	0.0524
	24	882	738	144	16	0.83	0.0451
	30	3133	2757	376	12	0.87	0.0329
MSCRS35c-ii	6	216	128	88	41	0.59	0.0699
	12	620	480	140	22	0.77	0.0632
	18	1514	1277	237	15	0.84	0.0444
	24	3106	2711	395	13	0.87	0.0330
	30	3222	2705	517	16	0.84	0.0318
MSCRS45c-ii	6	130	100	30	23	0.76	0.0485
	12	319	252	67	21	0.78	0.0441
	18	685	575	110	16	0.83	0.0371
	24	1364	1158	206	15	0.84	0.0367
	30	3372	3064	308	9	0.90	0.0225
MSCRS55c-ii	6	143	85	58	41	0.59	0.1206
	12	410	319	91	22	0.78	0.0612
	18	915	756	159	17	0.83	0.0505
	24	2018	1764	254	13	0.87	0.0241
	30	3233	3196	37	1	0.99	0
Note: Again, it is seen during MSCRS55c-ii tests at 30% pre-relaxation strain level, equipment error (power cut) allows no stress relaxation values to be recorded.							

The values presented in Table 5.5 show the findings of the multi-staged compression-relaxation tests when doubling the relaxation period from 24- to 48-hours. Overall, the values of relaxed stresses ($\Delta\sigma$) were found to decrease with an increase in the pre-relaxation strain (ε_r) and cause the residual stress (ξ) to increase for both MSCRSb-ii and MSCRSc-ii tests. Furthermore, an increase in the relaxation period increases relaxed stresses; as seen, an increase to 48-hours relaxation during the 0.005 mm/min (MSCRSb) tests caused the relaxed stresses to increase by a factor of 1.02 – 2 as temperature and pre-relaxation strain level increased. The increase in the relaxed stresses during a 48-hour relaxation period was also evident in the 0.001 mm/min (MSCRSc) tests, as they increased by a factor of 1.07 – 1.52. However, during the MSCRS20b-ii, $\Delta\sigma$ values decreased slightly as the relaxation period increased. Additionally, the decrease in $\Delta\sigma$ during the MSCRS55b-ii test at ε_r = 30% can result in a measurement error in the MSCRS55b-i test at the end of relaxation.

Moreover, the increase in the pre-relaxation period caused the $\Delta\sigma/\sigma_o$ ratio to be more pronounced during the 48-hour relaxation period than during the 24-hour. The results are consistent with the SS-CRS test results, as an increase in temperature with an increase in pre-relaxation strain level would decrease the $\Delta\sigma/\sigma_o$ ratio. However, during the MSCRS35b-ii test, the $\Delta\sigma/\sigma_o$ ratio decreased from 46 to 27% for an increase in ε_r from 6 to 18%, then increased from 27 to 33%, respectively for pre-relaxation strains of 18 to 30%. Generally, in the MSCRSb-ii tests, it was seen that the increase in the relaxation period resulted in an increase in the deviatoric stress (σ_o) during the pre-relaxation strain levels of 6 to 24%, resulting in the visco-plastic hardening effect. The increase in the deviatoric stress as the relaxation period increases support the findings of Cui et al. (2021), who found similar results when increasing the relaxation period from 24- to 72-hours during the testing of shear zone soils (which are defined as gravelly soil with inhomogeneously embedded coarse particles).

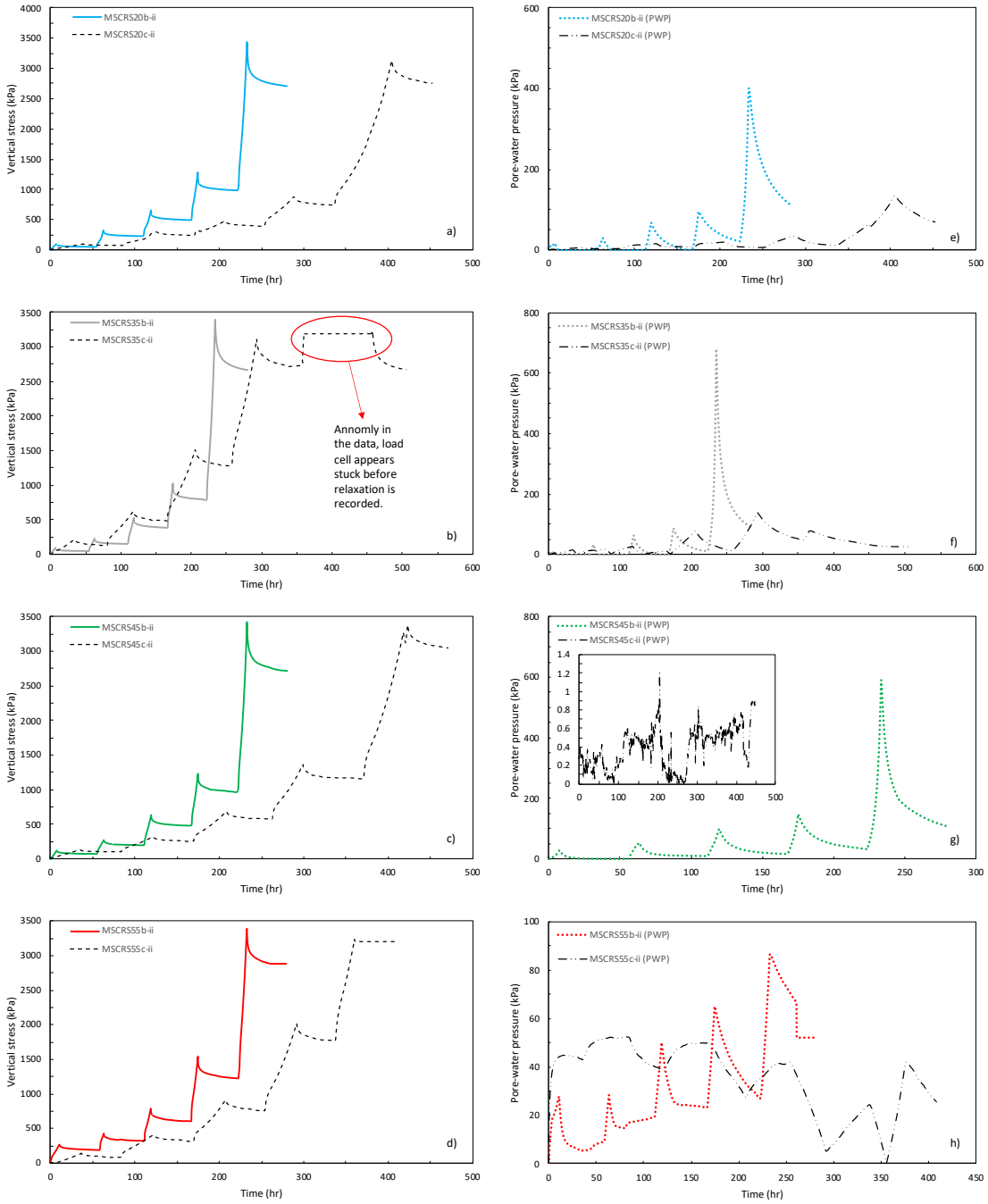

Figure 5.8 - 48hr-MSCRS compression-relaxation stages (a-d) and pore-water pressure during the MSCRS tests (e-h).

5.3.2. Effect of Temperature and Pre-Relaxation Strain Level on the Stress Relaxation Process

This section presents the five stress-stress relaxation stages to show the effect of temperature and pre-relaxation strain levels. To be consistent with the SS-CRS test results and allow for comparisons, only the MSCRSb-ii and MSCRSc-ii test results are shown here, illustrating the 48-hour relaxation. The data obtained in table 5.5 shows the variation of relaxed stresses at each pre-relaxation strain level in Figure 5.9. Figure 5.9 illustrate the relaxed stresses with time on a semi-log scale. As evident in table 5.5 and figure 5.9, it can be seen that higher stress-relaxation rates were observed for higher pre-relaxation strains, which supports the findings of Bagheri et al. (2019). The relationship between vertical total stress and time in figure 5.9 illustrates a linear trend during the relaxation of stresses. Furthermore, it would appear that there is no conclusive trend between temperature and stress relaxation curves at temperatures 20 to 55°C. This finding would differ from the results during the SS-CRS-b and SS-CRS-c tests, as an increase in temperature causes the stress relaxation curves to shift upwards. It can be observed from table 5.5 that the MSCRS55c-ii contains very minimal relaxation of stresses and this is related due to measurement problems (lab power cuts) experienced within the testing phase. Similar results regarding the linear relationship between total vertical stress and time have been reported in the literature for clays (e.g., Lacerda (1973); Yin and Graham (1989); Sheahan et al. (1994); Kim and Leroueil (2001); Yin et al. (2014); Bagheri et al. (2019)).

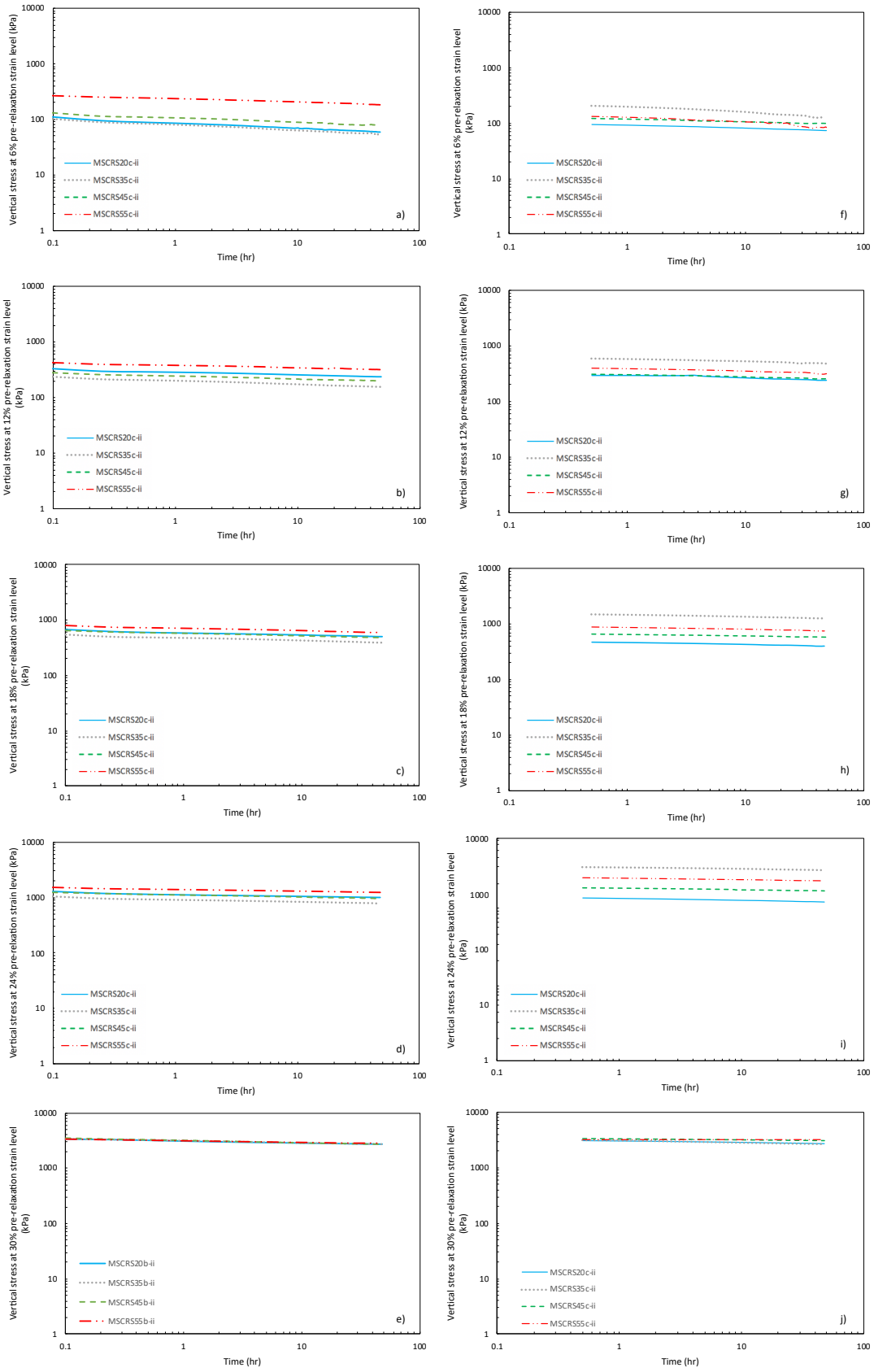

Figure 5.9 - MSCRS-ii stress relaxation curves at different stages of pre-relaxation strain levels and temperatures. MSCRSb-ii stress relaxation curves are illustrated in a-e, and MSCRSc-ii stress relaxation curves are illustrated by f-j.

As seen in table 5.5, with a change in pre-relaxation strain level (ε_r) and an increase in temperature, the coefficient of stress relaxation (R_a) decreases. It was seen that the 24-hour R_a values vary within the ranges of 0.0261 – 0.1003 and 0.0267 – 0.0912, respectively, for MSCRSb-i and MSCRSc-i tests. With an increase in the relaxation period, the values of R_a vary within the ranges of 0.0156 – 0.1335 and 0.0225 – 0.0699, respectively, for MSCRSb-ii and MSCRSc-ii tests. The addition of five stress relaxation stages is seen to affect the R_a values, where R_a begins to decrease as temperature increases during MSCRSc-i and MSCRSc-ii tests. The MSCRSc results would illustrate a contradicting trend between 20 to 45°C when comparing it to the SS-CRS-c R_a values, whereas at 55°C, it would be seen that the higher temperature would correlate well with SS-CRS-c R_a values, as an increase in temperature causes an increase in R_a. Moreover, the increase in relaxation is generally seen to decrease R_a; however, it is not the case for all temperatures and strain rates. The observed values of R_a for the 48-hours relaxation stages of the MSCRS tests were, however, higher than ranges obtained from the SS-CRS tests with the same relaxation period. Furthermore, the average value of R_a from each MSCRS test is seen to increase by a factor of 1.32 – 1.57 and 1.49 – 2.44, respectively, for MSCRSb-ii and MSCRSc-ii tests (figure 5.10).

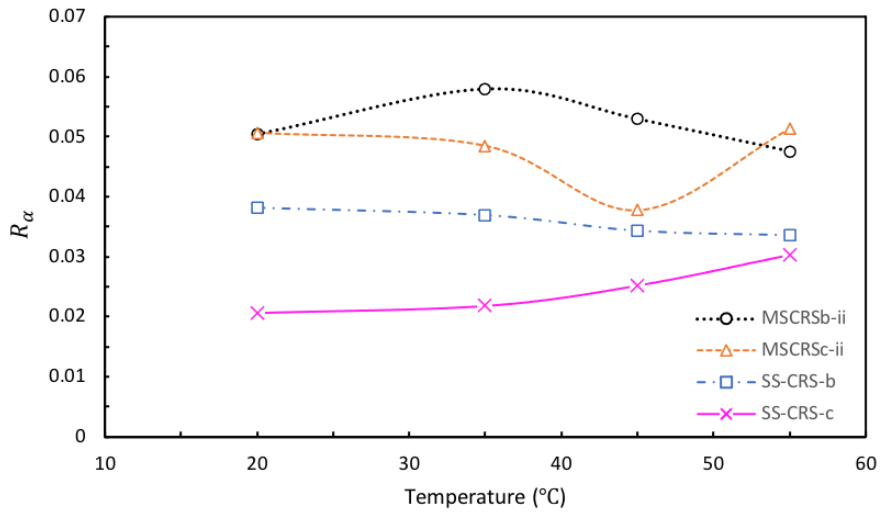

Figure 5.10 - Variation in R_a with the change in strain rate and temperature. The MSCRS values are obtained from calculating the average R_a from the five stress relaxation stages.

Figure 5.11 presents the variation of the coefficient of stress relaxation (R_a) with temperature and pre-relaxation strain levels (ε_r). As can be seen, the MSCRSb-ii tests show a significant decrease in R_a as the pre-relaxation strain level increases, whereas the MSCRSc-ii tests have gradually decreasing R_a values. Figure 5.11 indicates the dependency of R_a on the pre-relaxation strain and strain rate. The general trend suggests an overall decrease in R_a with temperature; however, it is difficult to conclude whether R_a increases or decreases with an increase in temperature due to the scattered data in MSCRSb-ii tests (figure 5.11a). Whereas in the MSCRSc-ii tests, it is clear that an increase in temperature causes the values of R_a to decrease (figure 5.11b). It would appear from figure 5.11 that the higher R_a values are associated with the decelerating relaxation phase, characterised by higher relaxation rates, while SS-CRS R_a values are associated with the residual relaxation phase, characterised with lower relaxation rates. It is seen that the results generated from the MSCRS tests contradict the findings of Bagheri et al. (2019), who found R_a to increase as pre-relaxation strain level increases in unsaturated Sheppey London clay specimens. However, due to the limited results in the literature, it is difficult to determine a correct relationship between pre-relaxation strain level, temperature, and stress relaxation.

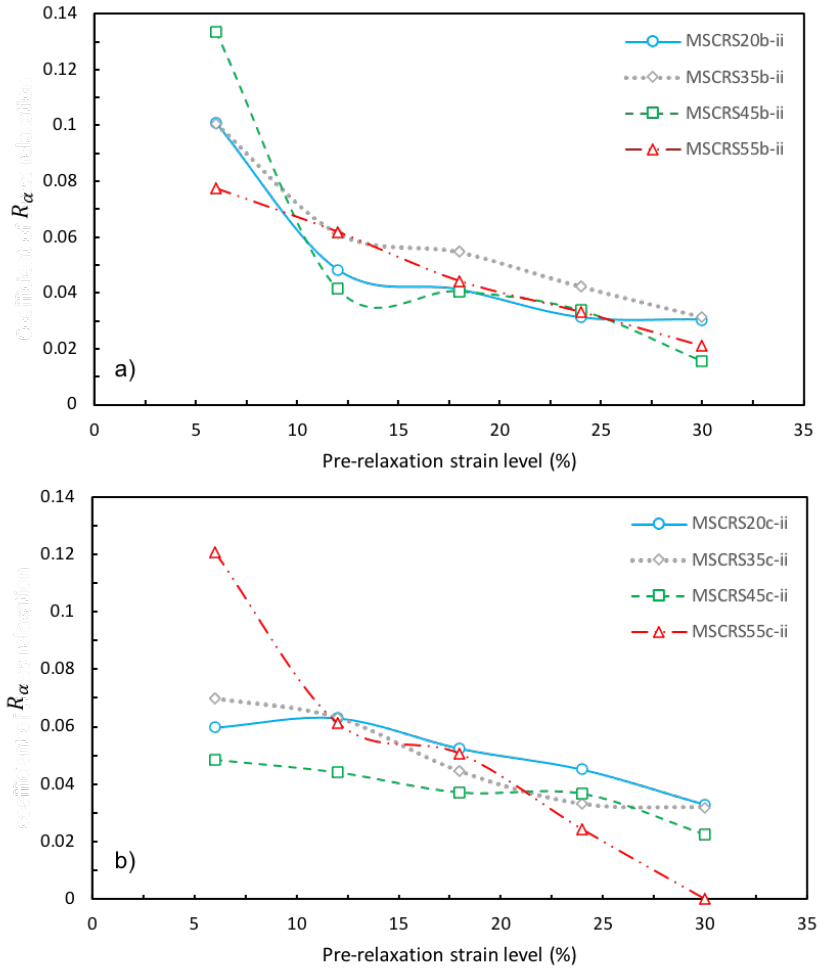

Figure 5.11 - Variation of R_a with pre-relaxation strain level, temperature, and pre-relaxation strain rate: a) MSCRSb-ii and b) MSCRSc-ii.

5.4. Summary

This chapter performed a series of CRS tests on reconstituted Bank Station London clay specimens under saturated conditions, varied temperatures and strain rates. The results of the SS-CRS and MSCRS tests were presented, and the following conclusions can be drawn;

- Increase in strain rate results in an increase of σ_p and a decrease in C_c values. Coupled with the effect of temperature, C_c were seen to slightly change as temperature increased. Moreover, at a constant temperature, the higher the strain rate, the higher the σ_p. Similarly, at a constant strain rate, the higher the temperature, the lower the σ_p.

- Compression curves from CRS tests exhibit a lower σ_p than the MSL tests. Moreover, the compression curves shift to the left as temperature increases during CRS tests.
- A decrease in σ_p with temperature appears to follow an approximately linear trend for all strain rates.
- At constant pre-relaxation stress, an increase in temperature results in a decrease in stress relaxation rate during decelerating and residual relaxation phases, as well as in the magnitude of the overall relaxed stresses. However, the increase in temperature resulted in the relaxed stresses during SS-CRS-c tests to increase.
- R_a is seen to decrease as temperature increases during SS-CRS-a and SS-CRS-b tests. However, as temperature increases during SS-CRS-c tests, R_a increased. Furthermore, it is seen that the relationship between temperature, strain rate and coefficient of relaxation follows an approximately linear trend.
- The $R_a = \alpha$ suggested by Yin et al. (2014) for saturated soft clays appears, with an approximation, to be valid for saturated reconstituted London clay in the range of applied vertical stresses and temperatures considered in this study.
- A higher rate and magnitude of relaxed stresses were observed with an increase in pre-relaxation strains.
- An increase in the pre-relaxation strain rate by a factor of 5 at each temperature interval was found to considerably affect the magnitude of relaxed stresses at each pre-relaxation strain level, resulting in an increase of $\Delta\sigma$ values by a factor of 1.29 – 2.5.
- At a constant temperature, an increase in the pre-relaxation strain level decreased R_a. Furthermore, it was seen that an increase in the relaxation period caused the values of R_a to decrease further.
- Overall, it was seen that R_a was dependent upon temperature and strain rate.

Chapter Six – Discussion of Results

6.1. Compressibility Behaviour Oedometer Tests

The results of the MSL and CRS oedometer tests present some differences, but also some similarities with previous published results concerning saturated and unsaturated London Clay specimens, and thermo-mechanical behaviour of saturated soils reviewed in Chapter 2.

As in the existing studies on London Clay specimens (e.g., Gasparre 2005; Nishimura 2006; Sorensen 2006; Bagheri 2018), a reduction in the water content of the specimens resulted in a decrease in compressibility. It can be seen that during 1D MSL saturated oedometer tests (see section 4.1.1.1), the compressibility curves shift upwards as the water content is reduced. This is similar to findings made by Bagheri (2018) who found saturated Isle of Sheppey London Clay to reduce in compressibility as water content values decreased. Though, Bagheri (2018) found the changes in the compressibility of the specimens to be affected by the soil structure rather than the changes in water content. This would agree with the findings of Gasparre et al., (2011) who found the open structure of the clay being displayed would affect the compressibility of the London Clay specimens. However, these statements by Gasparre et al., (2011) and Bagheri (2018) along with the findings in this research study would disagree with Ma et al., (2018) who stated that the changes in water content would influence the clays compressibility behaviour.

A general observation regarding the compressibility of saturated London Clay specimens is that the C_c and C_s values across the London Basin and London Clay Formation are similar (Gasparre 2005; Nishimura 2006; Sorensen 2006; Bagheri 2018). However, the compressibility behaviour of London Clay specimens varies across the London Clay Formation and London Basin due to different sub-units being tested by the various studies. Gasparre (2005) found that shallower specimens would be more susceptible to compressibility. Although this statement is in agreement with the findings of Bagheri (2018), in section 4.1.1.1 it would show that the Bank Station

London Clay specimens, which are retrieved from a shallower sub-unit would disagree with this statement due to the reduction in the compressibility of the specimens (shown in figure 4.1). Therefore, the behaviour of this may be attributed to the modified PSD of the reconstituted Bank Station specimens and presence of coarser material that results in an increased resistance against compressibility.

In section 4.1.1.3, results of $C_{\alpha e}$ at constant water content and increasing effective stresses were presented. The results showed that the reconstituted Bank Station London Clay specimens exhibited significantly lower the $C_{\alpha e}$ values in comparison to their intact states when comparing to intact Isle of Sheppey London Clay specimens from Bagheri (2018). This behaviour is associated with the compact nature of stiff clays that results in reduced particle rearrangement under sustained vertical effective stress. However, the intact specimens contain low initial water contents and have localised unsaturated pockets with sustainable water menisci developed at inter-particle contacts preventing orientation and rearrangement of particles into a more packed state (Bagheri, 2018).

The unsaturated compressibility behaviour of London Clay (and stiff clays) is limited within the literature with only a handful of studies being completed. Thus, the decrease in compressibility with increasing suction seen in section 4.1.2.1 is in agreement with the limited stiff clay data available (e.g., Monroy et al. 2008; Bagheri 2018; Rezania et al. 2020) and various other studies concerning unsaturated clays (e.g., Benatti et al. 2010; Haghighi 2011; Ileme 2017). This can be explained by considering the structural changes associated with increasing suction. At higher suction values (507 kPa in this study), the water meniscus at the inter-particle contacts allows the stability of the soils to increase (Wheeler et al. 2003). The water meniscus identified between the inter-particle contact produces additional forces that prevent sliding and rearrangement of the macrostructure (Romero, 1999). This explains the observations identified in this study. As the increase in suction, the inter-particle contacts are influenced by the water meniscus, thus providing the specimens additional rigidity against sliding, which reduces the compressibility as suction

increase. The restriction in particle rearrangement and sliding also causes a reduction in the $C_{\alpha e}$ with an increase in suction.

Additionally, it was identified that σ_p increases with increasing suction (seen in section 4.1.2.1). This response agrees with those reported in the literature (Wheeler and Sivakumar, 1995, Colmenares Montanez, 2002, Monroy, 2006, Haghighi, 2011, Rezania et al., 2020) and the decrease in plastic strain and an increase in σ_p, is also known as suction hardening.

In section 4.1.2.1, it was also observed that a decrease of C_c with an increase in suction support the findings of Rezania et al. (2020), who performed a series of unsaturated oedometer tests on London clay specimens and Esfandiari et al. (2021), who studied the effect of suction on unsaturated bentonite soils subjected to drying-wetting cycles using a modified osmotic oedometer. However, it must be stated that the reduction in C_c as suction increases; although agrees with authors within the literature, this finding appears to be a misconception and considering a wider range of stresses, C_c is not influenced by suction (Khalili et al., 2022). Conversely, the findings of C_c contradict the observations of Monroy et al. (2008), who performed a series of suction-controlled oedometer tests on London clay specimens that reported C_c to increase as suction increased (as discussed in Chapter 2).

The contradictory findings of C_c can be related to the sample preparation and initial specimen conditions. By using a similar technique (stated in Chapter 3) to the one reported by Rezania et al. (2020), it provides values in agreement with each other. Whereas, Monroy et al. (2008) prepared the specimens by static compaction to an initial suction, and then decrease the suction by hydrating the specimens to different suction levels. Therefore, the compressibility responses can be explained by the differences in sample preparation and initial specimen conditions. The observations found regarding the C_s values agrees with Rezania et al. (2020) but contradicts the findings of Sivakumar (1993), who reported that the swelling lines are almost independent of suction.

During the thermal MSL oedometer test and CRS oedometer tests, it can be seen that the influence of temperature can alter the compressibility behaviour of the reconstituted Bank Station London Clay specimens. It was identified in section 4.2 that an increase in temperature to 55°C increased the compressibility of the Bank Station specimens and shifted the compression curve downwards. These findings are in line with other findings in the literature (e.g., Abuel-Naga et al. 2007; Di Donna and Laloui 2015; Kaddouri et al. 2019). The increase in temperature during MSL and CRS oedometer causes the compression curve to shift to the left during loading, and this outcome is known as thermal softening which has been found by various other studies such as Baldi et al. 1988, Abuel-Naga et al. 2007, Kaddouri et al. 2019, Lahoori et al. 2021. The structure of the London Clay specimens is made of inter- and intra-aggregate pores that contain absorbed water located in the intra-aggregate pores which is considered as part of the soil skeleton (Hueckel, 2002). Temperature is seen to affect the soil through the water situated within the void space. The thermal softening seen in this study can be explained based on changes in the absorbed water and inter-particle contacts.

However, in this study it is found that thermal softening is not always the case when considering a change in strain-rate during thermal CRS tests as demonstrated in Chapter 5. It can be seen that an increase in temperature and increase in strain-rate as seen in section 5.2.1 would agree with the general consensus of thermal softening and findings within the literature (e.g., Eriksson 1989; Tsutsumi and Tanaka 2012; Jarad 2016; Jarad et al. 2019). It was identified that an increase in temperature and decrease in strain-rate (SS-CRS-c in this study) would disprove the thermal softening effect. Tsutsumi and Tanaka (2012) and Jarad et al. (2019) also reported that higher temperatures and slower strain rates result in the compression curves shifting to the right, which is believed to be due to the creation of some structure types during CRS compression tests which is accelerated at higher temperatures. The creation in the structure causes rearrangement of the clay particles to become closely packed together due to the reduction in the thickness of the absorbed water layer on the clay particle surface, which produces a new structure that promotes greater resistance against loading. It is considered that the new structure and higher stiffness

is due to aging on clay specimens which is caused by cementation (Tsuchida et al. 1991; Towhata et al. 1993).

In section 4.2.1 and 5.2.2, results of σ_p and temperature were presented. The results showed that saturated reconstituted Bank Station London Clay specimens subjected to temperature change at a constant vertical stress experienced a decrease in σ_p. The results are in line with other findings in the literature (e.g., Boudali 1994; Sultan et al. 2022; Marques et al. 2004; Cekerevac and Laloui 2004; Laloui et al. 2008; Hong et al. 2013; Jarad 2016; Kaddouri et al. 2019; Lahoori et al. 2021). The decrease in σ_p as temperature increases is linked to the reduction of the elastic domain due to the reduction in viscosity. At higher temperatures, the reduced viscosity increases the contact between the clay minerals (Shariatmadari and Saeidijam, 2011). Conversely, Mon et al. (2014) who studied the effect of temperature on ASP 100 clays found that an increase in temperature caused σ_p to increase. Additionally, Abuel-Naga et al. (2007) further found the relationship between temperature and σ_p to be independent. The difference in the behaviour between σ_p and temperature can be attributed to other studies containing higher initial void ratios and different testing techniques.

The compressibility parameters (C_c and C_s) show a slight variation as temperature increases. The influence of temperature on the compressibility parameters vary within the literature, with some studies showing a change as temperature increases (e.g., Kaddouri et al. 2019; Lahoori et al. 2021) and some studies finding negligible change (e.g., Campanella and Mitchell 1968; Tidfors and Sallfors 1989; Burghignoli et al. 2000; Cekerevac and Laloui 2004). The variation of C_c and C_s with temperature can be attributed to the loss of absorbed water as temperature increases (Paaswell, 1967) and weakening the inter- and intra-particle contacts within the clay cluster. These changes result in a decrease in stiffness and increased compressibility due to a denser packing of the soil skeleton. The viscous behaviour of the Bank Station London Clay specimens is further seen with the change in strain-rate as temperature increases. It is identified in section 5.2.2, that a variation in strain-rate and an

increase in temperature causes C_c to decrease linearly. This is caused by the specimens gaining ability to resist deformation and this effect becomes more prominent in slow strain-rates (e.g., SS-CRS-c) which is supported by the findings of Tsutsumi and Tanaka (2012).

6.2. Influence of Temperature on the 1D Creep and Stress Relaxation Behaviour

The influence of temperature on the time-dependent behaviour of saturated reconstituted Bank Station London Clay specimens has been studied in terms of creep and stress relaxation. In context of this study, it is assumed that creep begins at the end of primary consolidation and stress relaxation is initiated once zero axial displacement is applied to the specimen (as defined in Chapter 3). This assumption has also been proposed by other researchers (e.g., Ladd et al. 1977; Mersi and Godlewski 1997, Yin et al. 2014, Bagheri 2018).

The influence of temperature on $C_{\alpha e}$ and R_a can be identified in this study. The results show (in section 4.2.3) that an increase of temperature causes $C_{\alpha e}$ to peak at lower effective stresses with illustrates the dependency on temperature. The dependency of temperature at lower effective stresses is supported by the study of oedometer creep tests on Bryce Clay by Green (1969). Gupta (1964) found the increase in $C_{\alpha e}$ was related to the increase in temperature which activates a greater number of molecules in the medium, which leads to a weaking of the inter-particle bonds and an increase in compressibility. $C_{\alpha e}$ is also dependent of energy level, and therefore, increase the temperature is equivalent increasing the energy level (Eriksson, 1984; Tidfors and Sallfors, 1989). Therefore, as temperature increases, $C_{\alpha e}$ increases. Zhang et al. (2007) found the increase in $C_{\alpha e}$ as temperature increases being linked to the reduction in the pore-water viscosity and soil skeleton due to the decrease in shear resistance between the clay particles. Additionally, Towhata et al. (1993) illustrated the dependency of temperature on the creep behaviour and the deterioration of the soil skeleton. However, Li et al. (2018) found that the reconstituted Utby Clay specimens were temperature insensitive and revealed that

increasing temperature and stress did not provide concise evidence of creep behaviour. This is believed to be attributed to the pore sizes between the aggregates and the bonds between the solid particles.

Additionally, it can be identified in section 4.2.3 that an increase in stress and an increase in temperature cause a decrease in $C_{\alpha e}$. Conversely, Kaddouri et al. (2019) found compacted clayey soil would contain higher values of $C_{\alpha e}$ at higher stresses and temperature. It is believed that the reduction in $C_{\alpha e}$ as temperature and stress increase can be linked to the release of absorbed water films, which cause a decrease in $C_{\alpha e}$ due to the increase in stresses, as the resistance between the clay particles increase at higher temperatures (Zhang et al. 2007).

In section 5.2.3 and 5.3.2, it observed that temperature and strain-rate influences R_a. The resulted showed that with an increase of temperature and pre-relaxation loading rate, the curvature of stress relaxation curves is gradually faded resulting in almost a linear variation of relaxed stresses with logarithm of time (as seen in figure 5.5). This is supported by Yin et al. (2014) who reported a linear relationship between relaxed stresses and time. However, the results would disagree with Wang et al. (2017) and Bagheri et al. (2019) who found the stress relaxation process to involve three distinct phases. Additionally, Bank Station London Clay specimens that were subjected to an increase in temperature and decrease in strain-rate experienced an increase in R_a. The decrease in R_a could be attributed to the accumulation of less strain energy within the specimens during fast loading caused by weakening the bonds between the particles as temperature increases (Wang et al. 2011). On the other hand, prolonging the pre-relaxation loading stage may result in a portion of the absorbed thermal energy to be used for breaking the existing inter-particle bonds, and therefore, accumulation of less strain energy in the system. However, additional research is required to confirm to what extend strain-rate and temperature will affect the coefficient of stress relaxation.

6.3. Applications of Research Findings

The results presented in this study has highlighted the effect of temperature on the geomechanical behaviour of Bank Station London Clay. The findings of this study will enhance the understanding of the geotechnical community on the effect of temperature on the creep and stress relaxation behaviour of clays. Moreover, the results can be used to model or predict thermal triggered creep deformations during the construction of energy geo-structures (e.g., thermo-piles or ground source heating); as the temperature range (20 to 55°C) used within this study is the expected climatic conditions of London, UK, if net zero carbon emissions are not met. So, it is vital to understand how the increase in temperature affects the ground surrounding energy geo-structures. The consideration of the results from this study can have the potential to allow for companies to minimise their cost on maintaining infrastructure which have been affected by temperature induced ground movement. However, the results presented in this study have been obtained from reconstituted London Clay specimens and are not representative of all soils. The results from this study are relevant to a stress range 0 – 3500 kPa and temperature range of 20 to 55°C.

Chapter Severn – Summary

7.1. Conclusions

A series of 1D (incremental loading and CRS compression-relaxation) tests have been performed on reconstituted London Clay specimens obtained from Bank Station, London, UK. The tests have been performed across saturated and unsaturated (partially saturated) specimens at various initial water contents and under thermal conditions (only saturated specimens tested in thermal conditions due to COVID19 implications). The emphasis of the research study is to quantify the effect of temperature and soil suction on the time- and rate-dependent behaviour of stiff clays. The temperature range (20 - 55°C) studied in this work is representative of future prolonged climatic conditions the UK may see and is illustrative of temperatures surrounding geo-structures (e.g., thermo-piles).

The massive production of comparable samples using the reconstituted method, and the subsequent reconstruction of compression curves from an extensive experimental program, allows to obtain the data required to produce valuable findings to add depth & knowledge to the literature.

The consolidation behaviour of Bank Station London Clay specimens has proven to be sensitive to varying water contents, soil suction, temperature changes and strain rates. From the extensive experimental program, the 1D MSL tests illustrate that a reduction in water content (increase in soil suction) results in the compressibility of the specimens to decrease and shift upwards, which causes the compressibility parameters (C_c and C_s) to decrease. However, during the application of increased temperatures, it can be observed that the compressibility of the specimens were to increase and shift downwards. Though the compressibility parameters appear to be negligible to temperature change. Furthermore, the specimens during thermal CRS testing were sensitive to the coupled effect of temperature and strain-rate during the compressibility of the specimens. As the increase in temperature and decrease

in strain rate caused the compression curves to shift the left. Unlike the thermal 1D MLS tests, it can be observed that an increase in temperature and decrease in strain rate results in the compressibility parameters to decrease.

The apparent pre-consolidation stress (σ_p) during the 1D MSL and CRS tests is also influenced by decreasing water contents (increase in soil suction), increase in temperature and variations in strain rate. The results of the unsaturated 1D MSL oedometer tests illustrate that an increase in soil suction produces an increase in σ_p which can be termed 'suction hardening'. Conversely, the increase of temperature along with a decrease in strain rate produces a decrease in σ_p which can be known as 'thermal softening'. Both these findings would agree with results published in the literature.

The secondary consolidation ($C_{\alpha e}$) behaviour for the saturated, unsaturated and thermal saturated tested specimens proven to be very sensitive to soil suction and temperature change, with the largest effects found for stress levels close to the σ_p. However, there is no clear trend in the data, other than it appears that for most stress levels $C_{\alpha e}$ peaks at low initial soil suction prior to the σ_p before stresses increase before higher soil suction peaks are observed. Conversely, it is seen that the with an increase of temperature, $C_{\alpha e}$ peaks at temperatures between 35 - 55°C and at lower stresses. Similar to the unsaturated specimen's behaviour, there is no clear trend in the data to confirm whether temperature increases or decreases $C_{\alpha e}$ as temperature increases.

During the thermal 1D SS-CRS phase, the specimens underwent a stress relaxation phase which allowed for the $C_{\alpha e}$ to be derived by analysing the coefficient of stress relaxation (R_a). The saturated specimens proved to very sensitive to a change in temperature and strain rate when evaluating R_a, with the higher strain rates and increasing temperatures, R_a produced linearly decreasing values. However, with lower strain rates and increasing temperatures, R_a produced linearly increasing values. Therefore, geo-structures that were constructed during a single slow loading

rate would be subject to greater thermal creep deformations than single fast loading rate. It can be seen from the stress relaxation tests that the applicability of $R_a = \alpha$ which was suggested by Yin et al. (2014) for saturated soft clays appears, with an approximation, to be valid for saturated reconstituted Bank Station London Clay in the range of applied vertical stresses and temperatures considered in this study.

In addition to thermal 1D SS-CRS tests, thermal MSCRS tests were conducted to analyse the effect of R_a during multiple stress relaxation stages. These stages were to simulate the clays response to the construction of geo-structures during varying climatic conditions. The results show that at a constant temperature, an increase in the pre-relaxation strain rate by a factor of 5 was found to considerably affect the magnitude of relaxed stresses at each pre-relaxation strain level. Also, it was found that at a constant temperature, an increase in pre-relaxation strain level was to produce decreasing R_a values which contradicts the limited information seen in the literature. However, although the decrease of R_a, as pre-relaxation strain levels increase is positive for construction of geo-structures under varying temperature conditions. It is evident that thermal creep deformations still may occur and affect the construction of geo-structures.

In conclusion, it appears that the Bank Station London Clay specimens are affected by varying strain rates, temperatures and soil suction. These all play a major role in the construction and utilisation of energy geo-structures in stiff clays. As thermal triggered creep deformations will increase under future predicted temperatures within the UK. The increase in thermal creep deformations will only be seen during the construction of geo-structures with a slow single compression relaxation stage. To reduce the effect of thermal creep deformations, it would be advantageous to construct geo-structures across multiple compression relaxation stages. However, the limited information within this study and literature do not yet provide conclusive evidence on how temperature influences geo-structures that contain multiple stages of loading and relaxation.

7.2. Recommendations for Future Work

The research has made a marked contribution towards added significant and valuable data to the existing database on understanding the effect of temperature on time- and rate-dependent behaviour of stiff clays. It provided further information regarding the influence of soil suction on unsaturated clay specimens. However, from these findings, further investigations are needed to understand the behaviour of clays under varying temperatures and soil suction. The following recommendations for future studies are made:

- Further investigations and more test results over a broader range of stresses, temperatures and strain rates are required to validate the impact of temperature on the coefficient of stress relaxation under a single-stage stress compression-relaxation state.
- Further investigation and more test results of stresses, temperatures and strain rates are required to support the findings of this research program concerning the influence of pre-relaxation strain, strain rate, and temperature on the overall stress relaxation process in a multi-staged compression-relaxation state.
- Further research programs to investigate more complex tests, e.g., coupling the effects of suction and temperature with varied strain rates to understand the influence on the overall stress relaxation and creep process. Additionally, a research program to investigate the effect of heating and cooling cycles with varying strain rates to understand the influence on the overall stress relaxation process.
- Further research into the thermal mechanical behaviour of undisturbed, disturbed and reconstituted samples from different locations, depths and lithological units in the London Clay Formation is required to build a comprehensive database.

- A comprehensive study combining a laboratory program and numerically modelling is required to establish new models or functions which could predict the behaviour of London Clay in response to elevated temperatures.

References

ABUEL-NAGA, H., BERGADO, D., SORALUMP, S. & RUJIVIPAT, P. 2005. Thermal consolidation of soft Bangkok clay. Lowland Technology International, 7, 13-21.

ABUEL-NAGA, H. M., BERGADO, D., BOUAZZA, A. & RAMANA, G. 2007. Volume change behaviour of saturated clays under drained heating conditions: experimental results and constitutive modeling. Canadian Geotechnical Journal, 44, 942-956.

ALLENOU, C. 2003. Some characteristics of London clay. Characterisation and engineering properties of natural soils, 2, 851.

ARKELL, B. P. & DARCH, G. Impact of climate change on London's transport network. Proceedings of The Institution of Civil Engineers-Municipal Engineer, 2006. Thomas Telford Ltd, 231-237.

ASTM, I. 2003. Standard test method for measurement of soil potential (suction) using filter paper (Standard D5298-03), ASTM Internat.

ASTM-D4186-06 (2006). Standard test method for one-dimensional consolidation properties of saturated cohesive soils using controlled-strain loading. West Conshohoken, PA: ASTM International.

BAGHERI, M. 2018. Experimental investigation of the time-and rate-dependent behaviour of unsaturated clays. University of Nottingham. PhD Thesis.

BAGHERI, M., NEZHAD, M. M. & REZANIA, M. 2020. A CRS oedometer cell for unsaturated and non-isothermal tests, ASTM International.

BAGHERI, M., REZANIA, M. & MOUSAVI NEZHAD, M. 2018. Cavitation in high-capacity tensiometers: effect of water reservoir surface roughness. Geotechnical Research, 5, 81-95.

BAGHERI, M., REZANIA, M. & MOUSAVI NEZHAD, M. 2019. Rate dependency and stress relaxation of unsaturated Clays. International Journal of Geomechanics, 19, 04019128.

BALDI, G., HUECKEL, T. & PELLEGRINI, R. 1988. Thermal volume changes of the mineral–water system in low-porosity clay soils. Canadian geotechnical journal, 25, 807-825.

Benatti, J. B., Miguel, M. G., Rodrigues, R. A. & Vilar, O. M. 2010. Collapsibility study for tropical soil profile using oedometric tests with controlled suction. *Unsaturated Soils.* E.E. Alonso and A. Gens (eds), CRC Press, 1, 197-198.

BICALHO, K. V., CORREIA, A. G., FERREIRA, S. R., FLEUREAU, J.-M. & MARINHO, F. A. 2007. Filter paper method of soil suction measurement.

BOUDALI, M. Viscous behaviour of natural clays. Proc. 13th Int. Conf. on SMFE, 1994. 411-416.

BOURNE-WEBB, P., AMATYA, B., SOGA, K., AMIS, T., DAVIDSON, C. & PAYNE, P. 2009. Energy pile test at Lambeth College, London: geotechnical and thermodynamic aspects of pile response to heat cycles. Géotechnique, 59, 237-248.

BUISMAN, A. Results of long duration settlement tests. Proc. 1st ICSMFE, 1936. Cambridge, 103-107.

BULUT, R. & LEONG, E. C. 2008. Indirect measurement of suction. Laboratory and field testing of unsaturated soils. Springer.

BURGHIGNOLI, A., DESIDERI, A. & MILIZIANO, S. 1992. Deformability of clays under non isothermal conditions. Rivista italiana di Geotecnica, 26, 227-236.
BURGHIGNOLI, A., DESIDERI, A. & MILIZIANO, S. 2000. A laboratory study on the thermomechanical behaviour of clayey soils. Canadian Geotechnical Journal, 37, 764-780.
BURLAND, J. 1990. On the compressibility and shear strength of natural clays. Géotechnique, 40, 329-378.
CAMPANELLA, R. G. & MITCHELL, J. K. 1968. Influence of temperature variations on soil behavior. Journal of the Soil Mechanics and Foundations Division, 94, 709-734.
CASAGRANDE, A. The determination of pre-consolidation load and it's practical significance. Proc. Int. Conf. Soil Mech. Found. Eng. Cambridge, Mass., 1936, 1936. 60.
CASASSO, A. & SETHI, R., 2019. Assessment and minimization of potential environmental impacts of ground source heat pump (GSHP) systems. *Water*, *11*(8), p.1573.
CEKEREVAC, C. & LALOUI, L. 2004. Experimental study of thermal effects on the mechanical behaviour of a clay. International journal for numerical and analytical methods in geomechanics, 28, 209-228.
CEKEREVAC, C., LALOUI, L. & VULLIET, L. Dependency law for thermal evolution of preconsolidation pressure. Proceedings of the 8th International Symposium on Numerical Models in Geomechanics, Rome, Italy, Edited by GN Pande and S. Pietruszczak. AA Balkema, 2002. 687-692.
CHANDLER, R., CRILLY, M., SMITH, M., SMITH, M. & BRE. A low-cost method of assessing clay desiccation for low-rise buildings. Proceedings of the Institution of Civil Engineers-civil engineering, 1992. Thomas Telford-ICE Virtual Library, 82-89.
CHANDLER, R. & GUTIERREZ, C. 1986. The filter-paper method of suction measurement. Geotechnique, 36, 265-268.
CHENG, C.-M. & YIN, J.-H. 2005. Strain-Rate Dependent Stress--Strain Behavior of Undisturbed Hong Kong Marine Deposits under Oedometric and Triaxial Stress States. Marine Georesources and Geotechnology, 23, 61-92.
COLMENARES MONTANEZ, J. E. 2002. Suction and volume changes of compacted sand-bentonite mixtures. Imperial College London (University of London). PhD Thesis
COMMITTEE ON CLIMATE CHANGE. 'Net zero technical report' (2019).
CUI, D., WANG, S., CHEN, Q. & WU, W. 2021. Experimental Investigation on Loading-Relaxation Behaviors of Shear-Zone Soil. International Journal of Geomechanics, 21, 06021003.
CUI, Y.-J., LE, T. T., TANG, A. M., DELAGE, P. & LI, X.-L. 2009. Investigating the time-dependent behaviour of Boom clay under thermomechanical loading. Géotechnique, 59, 319-329.
CUISINIER, O. & LALOUI, L. 2004. Fabric evolution during hydromechanical loading of a compacted silt. International Journal for Numerical and Analytical Methods in Geomechanics, 28, 483-499.

DE BRUYN, D. & THIMUS, J.-F. 1996. The influence of temperature on mechanical characteristics of Boom clay: the results of an initial laboratory programme. Engineering Geology, 41, 117-126.
DEGAGO, S. Primary consolidation and creep of clays. The 2nd CREEP Workshop (CREBS IV) 2014, 2014.
DELAGE, P., SULTAN, N. & CUI, Y. J. 2000. On the thermal consolidation of Boom clay. Canadian Geotechnical Journal, 37, 343-354.
DI DONNA, A. & LALOUI, L. 2015. Response of soil subjected to thermal cyclic loading: experimental and constitutive study. Engineering Geology, 190, 65-76.
DINEEN, K. 1997. The influence of soil suction on compressibility and swelling. University of London.
ERIKSSON, L. Temperature effects on consolidation properties of sulphide clays. International Conference on Soil Mechanics and Foundation Engineering: 13/08/1989-18/08/1989, 1989. Balkema Publishers, AA/Taylor & Francis The Netherlands, 2087-2090.
ESFANDIARI, Z., AJDARI, M. & VAHEDIFARD, F. 2021. Time-dependent deformation characteristics of unsaturated sand–bentonite mixture under drying–wetting cycles. Journal of Geotechnical and Geoenvironmental Engineering, 147, 04020172.
FAVERO, V., FERRARI, A. AND LALOUI, L. 2016. Thermo-mechanical volume change behaviour of Opalinus Clay. International Journal of Rock Mechanics and Mining Sciences, pp 15-25.
GASPARRE, A. 2005. Advanced laboratory characterisation of London Clay. PhD Thesis.
GASPARRE, A. & COOP, M. 2008. Quantification of the effects of structure on the compression of a stiff clay. Canadian Geotechnical Journal, 45, 1324-1334.
GASPARRE, A., NISHIMURA, S., COOP, M. & JARDINE, R. The influence of structure on the behaviour of London Clay. Stiff Sedimentary Clays: Genesis and Engineering Behaviour: Géotechnique Symposium in Print 2007, 2011. Thomas Telford Ltd, 67-79.
GREEN, W. J. 1969. The influence of several factors on the rate of secondary compression of soil. MSc Thesis.
GUPTA, B. 1964. Creep of saturated soil at different temperatures. University of British Columbia. MSc Thesis. DOI: 10.14288/1.0050621
HAGHIGHI, A. 2011. Thermo-hydro-mechanical behaviour of Kaolin Clay. Heriot-Watt University. PhD Thesis
HAMILTON, J. & CRAWFORD, C. 1960. Improved determination of preconsolidation pressure of a sensitive clay. Special technical publication, 254-270.
HARRISON, A., PLIM, J., HARRISON, M., JONES, L. & CULSHAW, M. 2012. The relationship between shrink–swell occurrence and climate in south-east England. Proceedings of the Geologists' Association, 123, 556-575.
HARRISON, A., WHITE, J., JONES, L., ENTWISLE, D., HULBERT, A., LEE, K., MANSOUR, M. & WANG, L. 2020. User guide for the British Geological Survey GeoClimateUKCP09: clay shrink-swell dataset.
HEAD, K. H. 1992. Manual of soil laboratory testing. Volume 1. Soil classification and compaction tests.

HICHER, P.-Y. 1985. Comportement mécanique des argiles saturées sur divers chemins de sollicitations monotones et cycliques application à une modélisation élastoplastique et viscoplastique. These de doctoral d'etat es sciences physiques Paris6.
HIGHT, D., GASPARRE, A., NISHIMURA, S., JARDINE, R., COOP, M. & MINH, N. Characteristics of the London Clay from the Terminal 5 site at Heathrow Airport. Stiff Sedimentary Clays: Genesis and Engineering Behaviour: Géotechnique Symposium in Print 2007, 2011. Thomas Telford Ltd, 167-182.
HONG, P., PEREIRA, J.-M., TANG, A. M. & CUI, Y.-J. 2013. On some advanced thermo-mechanical models for saturated clays. International Journal for Numerical and Analytical Methods in Geomechanics, 37, 2952-2971.
HUECKEL, T., 2002. Reactive plasticity for clays during dehydration and rehydration. Part 1: concepts and options. *International Journal of Plasticity*, *18*(3), pp.281-312.
HUECKEL, T. & BALDI, G. 1990. Thermoplasticity of saturated clays: experimental constitutive study. Journal of geotechnical engineering, 116, 1778-1796.
HUECKEL, T. & BORSETTO, M. 1990. Thermoplasticity of saturated soils and shales: constitutive equations. Journal of geotechnical engineering, 116, 1765-1777.
HUECKEL, T. & PELLEGRINI, R. 1992. Effective stress and water pressure in saturated clays during heating–cooling cycles. Canadian Geotechnical Journal, 29, 1095-1102.
ILEME, O. C. M. 2017. Experimental study on thermo-hydro-mechanical behaviour of compacted kaolin clay. Heriot-Watt University. PhD Thesis.
JARAD, N. 2016. Temperature impact on the consolidation and creep behaviour of compacted clayey soils. Université de Lorraine.
JARAD, N., CUISINIER, O. & MASROURI, F. 2019. Effect of temperature and strain rate on the consolidation behaviour of compacted clayey soils. European Journal of Environmental and Civil Engineering, 23, 789-806.
KADDOURI, Z., CUISINIER, O. & MASROURI, F. 2019. Influence of effective stress and temperature on the creep behavior of a saturated compacted clayey soil. Geomechanics for Energy and the Environment, 17, 106-114.
KHALILI, N., ROMERO, E. & MARINHO, F. A. 2022. State of the Art Report. Advances in Unsaturated Soil Mechanics: Constitutive modelling, experimental investigation, and field instrumentation.
KIM, Y. T. & LEROUEIL, S. 2001. Modeling the viscoplastic behaviour of clays during consolidation: application to Berthierville clay in both laboratory and field conditions. Canadian Geotechnical Journal, 38, 484-497.
KING, C. 1981. The stratigraphy of the London Clay and associated deposits. Tertiary Research Special Paper. No. 6. DOI:10.1016/S0016-6995(82)80092-2
KOLIJI, A. 2008. Mechanical behaviour of unsaturated aggregated soils. EPFL.
LACERDA, W. 1973. Stress relaxation in soils. Proc. 8th ICSMFE, Moscow, 1973, 221-227.
LADD, C., FOOTT, R., ISHIHARA, K., SCHLOSSER, F. & POULOS, H. 1977. 'Stress Deformation and Strength Characteristic SOA Report,' Proceedings of the Ninth International Conference of Soil Mechanics and Foundation Engineering, Tokyo, Vol. 2, pp. 421-494.

LAHOORI, M., ROSIN-PAUMIER, S. & MASROURI, F. 2021. Effect of monotonic and cyclic temperature variations on the mechanical behavior of a compacted soil. Engineering Geology, 290, 106195.
LALOUI, L., LEROUEIL, S. & CHALINDAR, S. 2008. Modelling the combined effect of strain rate and temperature on one-dimensional compression of soils. Canadian Geotechnical Journal, 45, 1765-1777.
LEROUEIL, M. B. B. R. S. M. S. 1994. Viscous Behaviour of Natural Clays. 13th International Conference on Soil Mechanics and Foundation Engineering (New Delhi).
LEROUEIL, S. The Isotache approach. Where are we 50 years after its development by Professor Šuklje? 2006 Prof. Šuklje's Memorial Lecture. Proceedings of the XIII Danube-European Conference on Geotechnical Engineering, Ljubljana, Slovenia, 2006. 55-88.
LEROUEIL, S., KABBAJ, M., TAVENAS, F. & BOUCHARD, R. 1985. Stress–strain–strain rate relation for the compressibility of sensitive natural clays. Géotechnique, 35, 159-180.
LI, Y. 2019. On the impact of temperature perturbations on the creep of sensitive clay, Chalmers Tekniska Hogskola (Sweden). PhD Thesis.
LI, Y., DIJKSTRA, J. & KARSTUNEN, M. 2018. Thermomechanical creep in sensitive clays. Journal of Geotechnical and Geoenvironmental Engineering, 144, 04018085.
LOURENÇO, S., GALLIPOLI, D., TOLL, D. G., AUGARDE, C. E., EVANS, F. D. & MEDERO, G. M. 2008. Calibrations of a high-suction tensiometer. Géotechnique, 58, 659-668.
LOVERIDGE, F. & POWRIE, W. 2013. Pile heat exchangers: thermal behaviour and interactions. Proceedings of the Institution of Civil Engineers-Geotechnical Engineering, 166, 178-196.
LOWE, J. A., BERNIE, D., BETT, P., BRICHENO, L., BROWN, S., CALVERT, D., CLARK, R., EAGLE, K., EDWARDS, T. & FOSSER, G. 2018. UKCP18 science overview report. Met Office Hadley Centre: Exeter, UK.
MA, J., QIAN, M., YU, C. & YU, X. 2018. Compressibility evaluation of reconstituted clays with various initial water contents. Journal of Performance of Constructed Facilities, 32, 04018077.
MARINHO, F. A. & OLIVEIRA, O. M. 2006. The filter paper method revisited. Geotechnical Testing Journal, 29, 250-258.
MARQUES, M. E. S., LEROUEIL, S. & SOARES DE ALMEIDA, M. D. S. 2004. Viscous behaviour of St-Roch-de-l'Achigan clay, Quebec. Canadian Geotechnical Journal, 41, 25-38.
MARTINEZ CALONGE, D. 2017. Experimental investigation of the thermo-mechanical behaviour and thermal properties of London clay. PhD Thesis.
MAVROULIDOU, M., ZHANG, X., GUNN, M. J. & CABARKAPA, Z. 2013. Water retention and compressibility of a lime-treated, high plasticity clay. Geotechnical and Geological Engineering, 31, 1171-1185.
MESRI, G. 2003. Primary compression and secondary compression. Soil behavior and soft ground construction. DOI:10.1061/40659(2003)5.
MESRI, G. & CASTRO, A. 1987. C α/C c concept and K 0 during secondary compression. Journal of geotechnical engineering, 113, 230-247.

MESRI, G. & GODLEWSKI, P. M. 1977. Time-and stress-compressibility interrelationship. Journal of the Geotechnical Engineering Division, 103, 417-430.
MESRI, G., LO, D. O. K. & FENG, T. W. Settlement of embankments on soft clays. Proceedings of the Conference on Vertical and Horizontal Deformations of Foundations and Embankments. Part 2 (of 2), 1994. Publ by ASCE, 8-56.
MESRI, G. & VARDHANABHUTI, B. 2006. Closure to "Secondary Compression" by G. Mesri and B. Vardhanabhuti. Journal of Geotechnical and Geoenvironmental Engineering, 132, 817-818.
MITCHELL, J., BAXTER, C. & SOGA, K. Time effects on the stress-deformation behavior of soils. Proceedings of Professor Sakuro Murayama Memorial Symposium, 1997. Kyoto University, 1-64.
MON, E. E., HAMAMOTO, S., KAWAMOTO, K., KOMATSU, T. & MØLDRUP, P. 2014. Temperature effects on geotechnical properties of kaolin clay: simultaneous measurements of consolidation characteristics, shear stiffness, and permeability using a modified oedometer. GSTF Journal of Geological Sciences (JGS), 1.
MONROY, R. 2006. The influence of load and suction changes on the volumetric behaviour of compacted London Clay. Imperial College London (University of London).
MONROY, R., ZDRAVKOVIC, L. & RIDLEY, A. Volumetric behaviour of compacted London Clay during wetting and loading. Proc. 1st Eur. Conf. Unsaturated Soils, Durham, 2008. 315-320.
MORITZ, L. 1995. Geotechnical properties of clay at elevated temperatures. SGI Report, ISSN 0348-0755; 47
MURAYAMA, S. 1969. Effect of temperature on elasticity of clays. Highway research board special report.
MURPHY, J., SEXTON, D., JENKINS, G., BOORMAN, P., BOOTH, B., BROWN, K., CLARK, R., COLLINS, M., HARRIS, G. & KENDON, E. Climate change projections for the UK (UKCP09). AGU Fall Meeting Abstracts, 2010. GC31E-06.
NÄÄTÄNEN, A., VEPSÄLÄINEN, P. & LOJANDER, M. 1998. Finite element calculations on Haarajoki test embankment. Application of Numerical Methods to Geotechnical Problems. Springer.
NISHIMURA, S. 2006. Laboratory study on anisotropy of natural London Clay. Imperial College London (University of London). PhD Thesis.
NISHIMURA, S., JARDINE, R. & MINH, N. Shear strength anisotropy of natural London Clay. Stiff Sedimentary Clays: Genesis and Engineering Behaviour: Géotechnique Symposium in Print 2007, 2011. Thomas Telford Ltd, 97-110.
PAASWELL, R. E. (1967). Temperature effects on clay soil consolidation. *Journal of Soil Mechanics and Foundation Division, ASCE*, 93(3), pp. 9 – 22.
PEREIRA, J.-M. & DE GENNARO, V. On the time-dependent behaviour of unsaturated geomaterials. Unsaturated Soils-Proc. Fifth Int. Conf. on Unsaturated Soils, 2010. CRC press, 921-925.
PRIOL, G., GENNARO, V. D., DELAGE, P. & SERVANT, T. 2007. Experimental investigation on the time dependent behaviour of a multiphase chalk. Experimental Unsaturated Soil Mechanics. Springer.

REZANIA, M., BAGHERI, M. & MOUSAVI NEZHAD, M. 2020. Creep and consolidation of a stiff clay under saturated and unsaturated conditions. Canadian Geotechnical Journal, 57, 728-741.
RIDLEY, A. & BURLAND, J. 1993. A new instrument for the measurement of soil moisture suction. Géotechnique, 43, 321-324.
RIDLEY, A., DINEEN, K., BURLAND, J. & VAUGHAN, P. 2003. Soil matrix suction: some examples of its measurement and application in geotechnical engineering. Géotechnique, 53, 241-253.
Romero, E. (1999). Characterisation and hydro-mechanical-behaviour of unsaturated Boom clay: an experimental study. PhD Thesis.
SHARIATMADARI, N. & SAEIDIJAM, S. 2011. The effect of elevated temperature on compressibility and swelling of bentonite-sand mixtures. Electronic Journal of Geotechnical Engineering, 16, 137-146.
SHEAHAN, T. C., LADD, C. C. & GERMAINE, J. T. 1994. Time-dependent triaxial relaxation behavior of a resedimented clay. Geotechnical Testing Journal, 17, 444-452.
SINGH, A. & MITCHELL, J. K. Creep potential and creep rupture of soils. Soil Mech & Fdn Eng Conf Proc/Mexico/, 1969.
SIVAKUMAR, V. 1993. A critical state framework for unsaturated soil. University of Sheffield. PhD Thesis.
SMITH, R. E. & WAHLS, H. E. 1969. Consolidation under constant rates of strain. Journal of the Soil Mechanics and Foundations Division, 95, 519-539.
SORENSEN, K. K. 2006. Influence of viscosity and ageing on the behaviour of clays, University of London, University College London (United Kingdom).
SORENSEN, K. K., BAUDET, B. & SIMPSON, B. 2010. Influence of strain rate and acceleration on the behaviour of reconstituted clays at small strains. Géotechnique, 60, 751-763.
STANDARD, B. 1990a. BS1377: PART 5, 1990. Methods of tests of soils for civil engineering purposes-Compressibility, permeability and durability tests.
STANDARD, B. 1990b. BS 1377-2: 1990. Methods of test for soils for civil engineering purposes. Classification tests. British Standards Institution. London UK.
STANDING, J. & BURLAND, J. 2006. Unexpected tunnelling volume losses in the Westminster area, London. Géotechnique, 56, 11-26.
SULTAN, N., DELAGE, P. & CUI, Y. 2002. Temperature effects on the volume change behaviour of Boom clay. Engineering Geology, 64, 135-145.
TANAKA, N., GRAHAM, J. & CRILLY, T. 1997. Stress-strain behaviour of reconstituted illitic clay at different temperatures. Engineering Geology, 47, 339-350.
TARANTINO, A. & MONGIOVÌ, L. 2003. Calibration of tensiometer for direct measurement of matric suction. Géotechnique, 53, 137-141.
TAVENAS, F., LEROUEIL, S., ROCHELLE, P. L. & ROY, M. 1978. Creep behaviour of an undisturbed lightly overconsolidated clay. Canadian Geotechnical Journal, 15, 402-423.
TERZAGHI, K. 1936. A fundamental fallacy in earth pressure computations, Harvard University. PhD Thesis.
TIDFORS, M. & SÄLLFORS, G. 1989. Temperature effect on preconsolidation pressure. Geotechnical Testing Journal, 12, 93-97.

TOLL, D., LOURENÇO, S., MENDES, J., GALLIPOLI, D., EVANS, F., AUGARDE, C., CUI, Y.-J., TANG, A. M., ROJAS, J. & PAGANO, L. Soil suction monitoring for landslides and slopes. 2011. Geological Society of London.

TOWHATA, I., KUNTIWATTANAKU, P., SEKO, I. & OHISHI, K. 1993. Volume change of clays induced by heating as observed in consolidation tests. soils and foundations, 33, 170-183.

TRANI, L., BERGADO, D. AND ABUEL-NAGA, H., 2010. Thermo-mechanical behavior of normally consolidated soft Bangkok clay. International Journal of Geotechnical Engineering, pp.31-44.

TSUCHIDA, T., KOBAYASHI, M., MIZUKAMI, J., 1991. Effect of ageing of marine clay and its duplication by high temperature consolidation. Soils and Foundations 31 (4), 133–147.

TSUTSUMI, A. & TANAKA, H. 2012. Combined effects of strain rate and temperature on consolidation behavior of clayey soils. Soils and Foundations, 52, 207-215.

UK GOVERNMENT. 2020. The Ten Point Plan for a Green Industrial Revolution.

VAID, Y., ROBERTSON, P. & CAMPANELLA, R. 1979. Strain rate behaviour of Saint-Jean-Vianney clay. Canadian Geotechnical Journal, 16, 34-42.

VAID, Y. P. & CAMPANELLA, R. G. 1977. Time-dependent behavior of undisturbed clay. Journal of the Geotechnical Engineering Division, 103, 693-709.

WANG, M., XU, X., LI, J., SHEN, F. & LI, Y. 2017. An experiment study on stress relaxation of unsaturated lime-treated expansive clay. Environmental Earth Sciences, 76, 1-12.

WANG, S., QI, J. & YAO, X. 2011. Stress relaxation characteristics of warm frozen clay under triaxial conditions. Cold Regions Science and Technology, 69, 112-117.

WHEELER, S. & SIVAKUMAR, V. 1995. An elasto-plastic critical state framework for unsaturated soil. Géotechnique, 45, 35-53.

YASHIMA, A., LEROUEIL, S., OKA, F. & GUNTORO, I. 1998. Modelling temperature and strain rate dependent behavior of clays: one dimensional consolidation. Soils and Foundations, 38, 63-73.

YIN, J.-H. & GRAHAM, J. 1989. Viscous–elastic–plastic modelling of one-dimensional time-dependent behaviour of clays. Canadian geotechnical journal, 26, 199-209.

YIN, Z.-Y., ZHU, Q.-Y., YIN, J.-H. & NI, Q. 2014. Stress relaxation coefficient and formulation for soft soils. Géotechnique Letters, 4, 45-51.

ZHANG, C.-L., ROTHFUCHS, T., SU, K. & HOTEIT, N. 2007. Experimental study of the thermo-hydro-mechanical behaviour of indurated clays. Physics and Chemistry of the Earth, Parts A/B/C, 32, 957-965.